BREAKDOWN OF THE MuRA TETRAHEDRAL INTERMEDIATE

A COMPARATIVE STUDY OF THE ENZYMATIC AND NON-ENZYMATIC BREAKDOWNS OF THE TETRAHEDRAL INTERMEDIATE OF THE MurA REACTION

By

BARTOSZ BYCZYNSKI, B.Sc.

A Thesis Submitted to the School of Graduate Studies in Partial Fulfillment of the Requirements for the Degree of Master of Science

McMaster University

MASTER OF SCIENCE (2003)   McMaster University
(Chemistry)   Hamilton, Ontario

TITLE: A Comparative Study of the Enzymatic and Non-Enzymatic Breakdowns
of the Tetrahedral Intermediate of the MurA Reaction

AUTHOR: Bartosz Byczynski, B.Sc. (McMaster University)

SUPERVISOR: Professor Paul J. Berti

NUMBER OF PAGES: vii,127

Abstract

The mechanism of the non-enzymatic breakdown of the tetrahedral intermediate of MurA (a carboxyvinyl transferase) was determined in order to better understand the corresponding enzyme catalyzed reaction. The breakdown was general acid-catalyzed, with simultaneous C-O bond cleavage and protonation at the bridging oxygen of the phosphate leaving group. The carboxyl was shown to play an important role in the breakdown, with its pK_a of 3.2 appearing in the rate *versus* pH profile. The product distribution varied with pH. At pH 1, the products were predominantly UDP-GlcNAc, pyruvate and phosphate. Increasing proportions of MurA ketal arising from intramolecular attack of the 4'-OH, and EP-UDP-GlcNAc resulting from elimination were observed with higher pHs. The MurA ketal was structurally characterized, and shown to be analogous to the ketal formed by AroA, a related enzyme. pK_as corresponding to those expected of phosphate monoesters (1.6 and 6.2) were found in the product distribution *versus* pH profile. Observation of these pK_as supported the initial product of phosphate departure being an oxocarbenium ion-phosphate tight ion pair complex. A corresponding oxocarbenium ion intermediate in the enzymatic reaction could not be demonstrated.

Acknowledgements

Table of Contents

Table of Abbreviations

A_ND_N	concerted nucleophilic association and nucleophilic dissociation
AroA	S3P carboxyvinyl transferase
ATP	adenosine triphosphate
CMP	cytidine monophosphate
D_N+A_N	nucleophilic dissociation step followed by nucleophilic association step
EPSP	enolpyruvyl-S3P
EP-UDP-GlcNAc	enolpyruvyl-UDP-GlcNAc
G-1-P	glucose-1-phosphate
His-Tagged	protein fused to His_6 which binds Ni
IPTG	isopropyl-thiogalactoside
KDO	ketodeoxyoctonate
KIE	kinetic isotope effect
MurA	UDP-GlcNAc carboxyvinyl transferase
NeuAc	*N*-acetylneuraminic acid
PEP	phosphoenolpyruvate
PMSF	phenylmethylsulfonylfluoride
PPDK	pyruvate phosphate dikinase
S3P	shikimate-3-phosphate
SDKIE	solvent deuterium kinetic isotope effect
THI	tetrahedral intermediate
TS	transition state
UDP-GlcNAc	UDP-N-acetyl glucosamine
UDP-MurNAc	UDP-N-acetyl muramate

Chapter 1   Introduction

1.1   MurA and AroA are Good and Proven Biocidal Targets

1.1.1 The Bacterial Cell Wall, a Target of Choice

Ever since the discovery of penicillin, the bacterial cell wall has been the target of antibiotics. The bacterial cell wall maintains the shape and rigidity of the cell, and protects against lysis of the cell resulting from osmotic pressure.[1] Peptidoglycan, a highly cross-linked heteropolymer, serves as the rigid component of the bacterial cell wall. Peptidoglycan is essential for the function of the cell wall. Its synthesis is unique to bacteria; there are no homologues of peptidoglycan synthesis enzymes in higher organisms. Because peptidoglycan is unique and essential to eubacteria, agents which prevent proper formation of peptidoglycan, such as penicillin, are antibiotics.

Formation of peptidoglycan involves condensation of alternating UDP-GlcNAc and UDP-MurNAc-pentapeptide units (Figure 1.1-1). The chains of this heteropolymer are then cross-linked via the peptidyl moieties of the MurNAc-pentapeptide units. This cross-linking imparts the rigidity needed for the proper function of the peptidoglycan. Penicillin acts by irreversibly inactivating transpeptidase, the enzyme which catalyzes the cross-linking step. Preventing cross-linking is not the only method to

prevent proper peptidoglycan formation; inhibition the synthesis of peptidoglycan precursors is also an effective strategy.[2] Of the two precursors, UDP-GlcNAc and UDP-MurNAc-pentapeptide, only the latter is specific to peptidoglycan. UDP-MurNAc-pentapeptide synthesis starts from UDP-GlcNAc, and is a multistep process as shown in Figure 1.1-1.[3] The addition of the enolpyruvyl group to UDP-GlcNAc by MurA in the first step provides an essential linker between the carbohydrate and peptidyl moieties of UDP-MurNAc-pentapeptide.
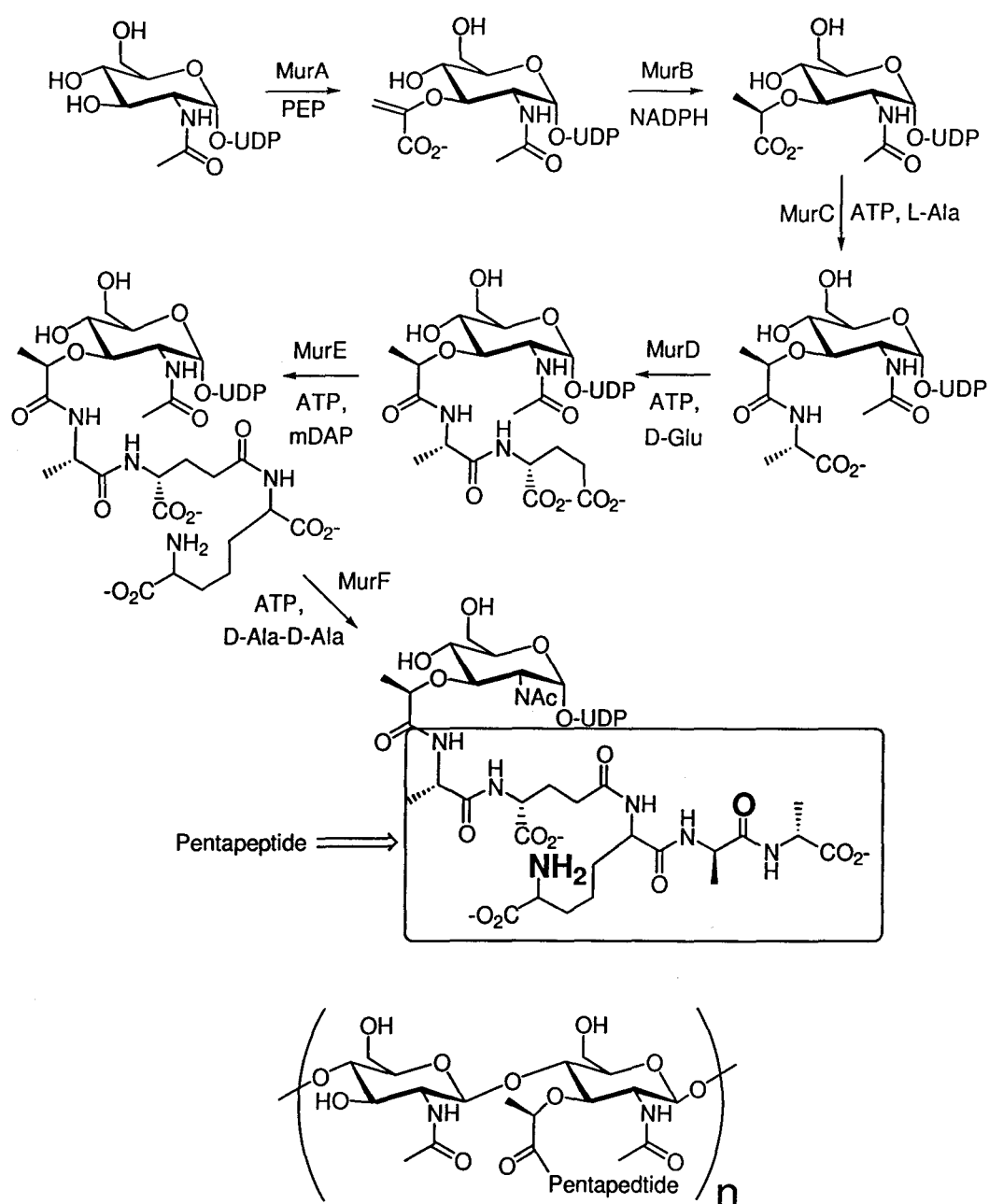
Figure 1.1-1 — (Above) UDP-MurNAc-pentapeptide synthesis. (Below) once a heteropolymer of alternating MurNAc-pentapeptide and GlcNAc unit is synthesized, cross linking occurs via a Gly$_5$ peptide linker forming amide bonds with the highlighted carbonyl in one polymer chain, and the highlighted amine in another polymer chain.

1.1.2 Unique Enzymes in Unique Pathways

UDP-N-acetylglucosamine enolpyruvyl transferase (MurA),

catalyses the transfer of the enolpyruvyl, or carboxyvinyl group, of

phosphoenol pyruvate (PEP) from phosphate to the 3'-hydroxyl of

UDP-N-acetylglucosamine (Figure 1.1-2). The reaction catalyzed by MurA

is not only found in a unique pathway, it also involves chemistry which is

very distinctive. In addition to MurA, carboxyvinyl transfer is catalyzed by

only two other enzymes, enol-pyruvyl shikimate-3-phosphate transferase

(AroA) and possibly NikO. AroA has been well characterized; it catalyzes

the penultimate step in the chorismate biosynthesis pathway (Figure

1.1-2). Chorismate is the precursor of aromatic amino acids and its

synthesis only occurs in plants and bacteria, making this pathway a good

target for herbicide (see below) as well as antibiotic development. NikO is

an enzyme involved in the synthesis of the antibiotic nikkomycin, and has

been proposed to catalyze carboxyvinyl transfer based on sequence

similarity to MurA and AroA.[4]
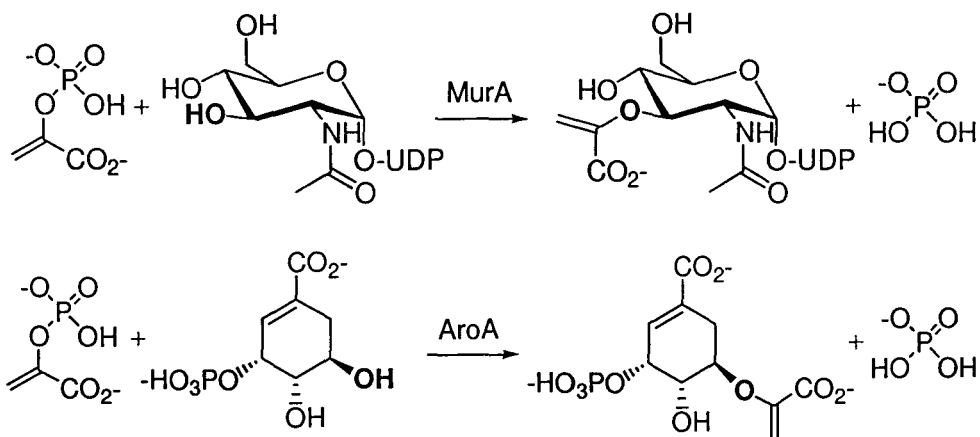
Figure 1.1-2 - Reactions catalyzed by MurA (above) and AroA (below). The enol-pyruvyl group and 3'-OH are highlighted

1.1.3 MurA and AroA are Good Antibiotic Targets

The unique chemistry of MurA and AroA, as well their existence in essential pathways not found in animals, makes them good antibiotic targets. MurA is a proven antibiotic target. It is susceptible to the antibiotic fosfomycin ((1R, 2S)-1, 2-epoxypropylphosphonic acid), produced by various strains of *Streptomyces*.[5] Fosfomycin is an irreversible inhibitor of MurA, covalently modifying Cys115[*] in the active site of the enzyme. This occurs via a nucleophilic attack of the thiolate of the cysteine, on the C2 of fosfomycin, opening the epoxide ring (Figure 1.1-3). Fosfomycin is a broad spectrum antibiotic, but fails in pathogenic organisms such as *M. tuberculosis, B. burgdorferi* (cause of Lyme disease) and the chlamydias. This intrinsic resistance is caused by the substitution of Asp for Cys115 in their MurAs.[6] The D115 MurA's are

---

[*] Cysteine number 115 is abbreviated Cys115 or C115. Aspartate number 115 is abbreviated Asp115 or D115. C115D is a mutant enzyme where cysteine has been replaced by aspartate. The structures of cysteine and aspartate are part of Figure 1.1-3.

capable of catalysis, but lack a strong enough active site nucleophile to

form a covalent adduct with fosfomycin.
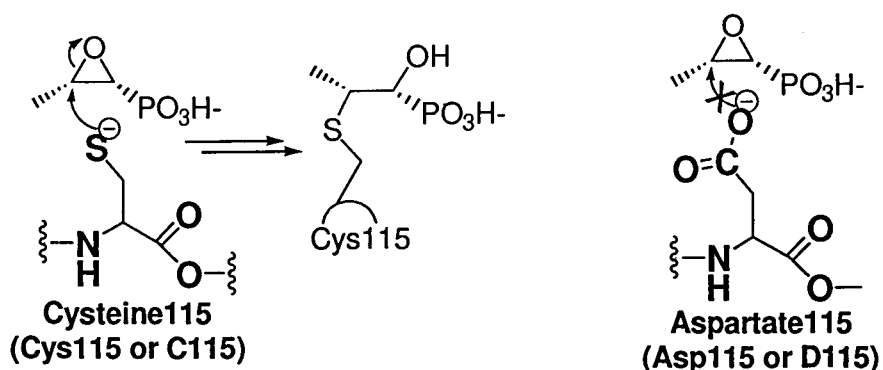
Figure 1.1-3 – (Left) Mechanism of MurA inactivation by fosfosmycin; (Right) Resistance of Asp115 MurA's results from reduced nucleophilicity of Asp relative to Cys. The amino acid structures are in bold.

Although AroA is not the target of any current antibiotics, it is the

target of the herbicide glyphosate. Glyphosate was once believed to be a

transition state mimic of a proposed oxocarbenium ion formed during the

AroA-catalyzed reaction (Figure 1.1-4). More recently, it has been shown

that although glyphosate inhibition is competitive with PEP, its site of

binding does not completely overlap with PEP.[7] Furthermore, glyphosate

can bind during the reverse reaction even when both substrates are in the

active site.[8] These results show that glyphosate is not a transition state

mimic, and inhibition by glyphosate results from adventitious allosteric

interactions, preventing PEP binding. Therefore, although glyphosate is

an effective herbicide, it is not a scaffold upon which new inhibitors, and

possible antibiotics could be designed. Attempts at modifying glyphosate

have not resulted in any inhibitors of AroA with lower K_d's than that of

glyphosate itself.[7]
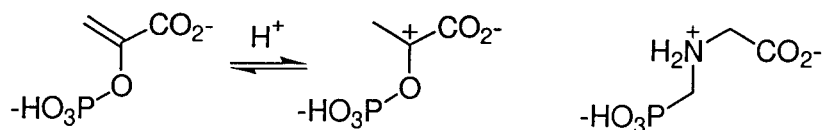
Figure 1.1-4 – (Left) Proposed oxocarbenium ion transition state/intermediate of which glyphosate was thought to be a mimic. (Right) Structure of glyphosate.

Neither fosfomycin nor glyphosate are transition state analogs.

Their inhibition results from adventitious interactions with MurA and AroA.

Design of new inhibitors based on these inhibitors is not possible using

any mechanistic information known about MurA and AroA enzymes. In

order to design new inhibitors, the mechanisms of MurA and AroA must be

determined in as much detail as possible. From this information inhibitors

can be designed that take advantage of the enzyme's own catalytic

machinery. Such inhibitors would serve as lead compounds in the design

of novel antibiotics. Microbial resistance to such antibiotics via mutations

of MurA and AroA would be difficult, as these modifications would also

affect catalysis.

1.2   Carboxyvinyl Transfer

1.2.1 Common Mechanism of Carboxyvinyl Transfer

MurA and AroA are among only a handful of PEP-utilizing enzymes

that catalyze C-O bond cleavage of PEP.[9] Most PEP utilizing enzymes

break the P-O bond. Carboxy-vinyl transfer is the first type of C-O bond

cleaving reaction, with the second being an aldol-type condensation

between the C3 of PEP and an aldehyde (Figure 1.2-1). This second

type of reaction is known to be catalyzed by two enzymes

3-deoxy-D-manno-2-octulosonate-8-phosphate synthase and

3-deoxy-D-arabino-heptulosonate-7-phosphate synthase.[10]
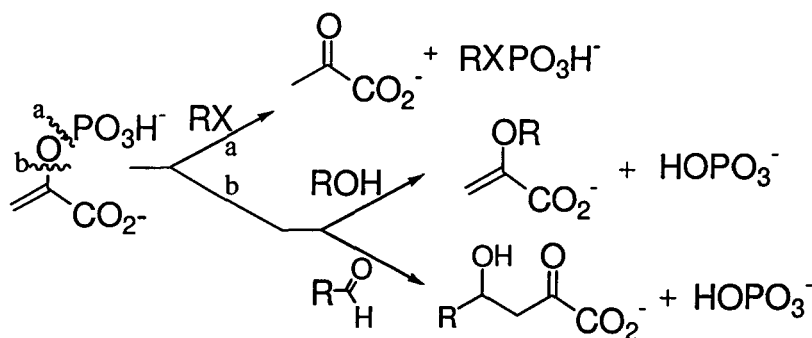
Figure 1.2-1 – Mechanisms of PEP-utilizing family. Most members of the family utilize P-O bond cleavage (path a). C-O bond cleavage (path b) occurs in two known reaction types; that of carboxyvinyl transfer (upper path b), and that of aldol condensation (lower path b) (Modified from refs. 9, 10).

The stereochemistry of carboxyl-vinyl transfer, in both MurA and

AroA is described in Figure 1.2-2. It involves first the addition of a proton

to C3 on the 2-si face of PEP,[11;12] accompanied by 2-re face attack at C2

by an alcohol (UDP-GlcNAc or S3P).[13] The result is anti addition with the

formation of a tetrahedral intermediate.[14;15] The THI then undergoes

elimination of the phosphate, and removal of a proton both from the 2-si

face,[11;12] resulting in syn elimination. Thus carboxyvinyl transfer occurs

with retention of configuration about the double bond.

8
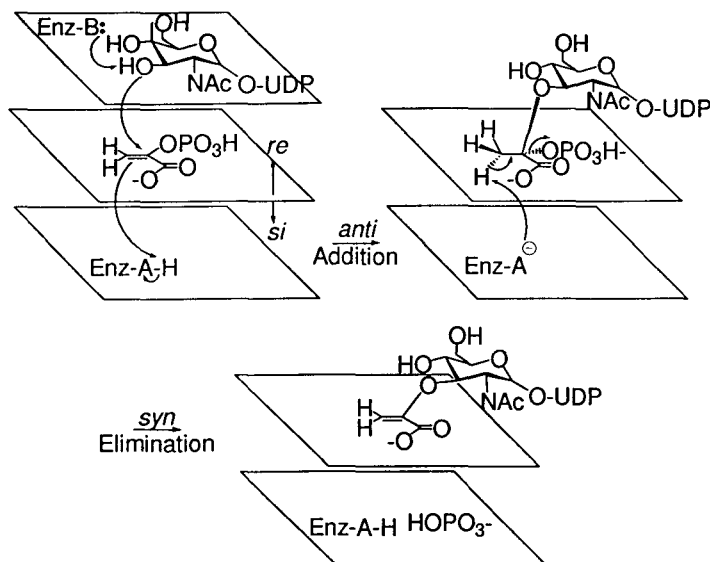
Figure 1.2-2 – Stereochemistry of the MurA catalyzed reaction showing *anti* addition and *syn* elimination. The stereochemistry of the AroA catalyzed reaction is similar (Modified from ref. 14).

1.2.2   Substrate Synergism and Conformational Change

Not only do MurA and AroA share similar chemical mechanisms,

their kinetic mechanisms are similar. The order of substrate binding is

random and highly synergistic.[16] That is, binding of one substrate

increases the enzyme's affinity for the other substrate. [14] Although PEP

can bind weakly to free enzyme, UDP-GlcNAc or S3P binding to free

MurA or AroA, occurs more readily. Once this binary complex is formed,

the affinity for PEP is greatly increased, with the resulting ternary complex

continuing on to form the THI and then products. In the reverse reaction,

initial enolpyruvyl UDP-GlcNAc (EP-UDP-GlcNAc) or enolpyruvyl S3P

(EPSP) binding to MurA or AroA, respectively, is kinetically preferred,

which increases the enzyme affinity for phosphate.

9

This substrate synergism and low affinity of PEP for free enzyme is believed to be the requirement for an enzyme conformational change.[2] Comparison of the crystal structures of MurA in the unbound (open) and bound (closed) states, shows that there is a flexible loop in the open structure that closes over the active site upon substrate binding.[17] Fluorescence and small angle x-ray scattering studies have confirmed that UDP-GlcNAc binding induces a conformational change in MurA, resulting in a more compact structure.[18] Similar observations have been made for AroA.[19]

1.2.3 Apparent Nucleophilic Catalysis by MurA

The flexible loop in MurA that closes over the active site contains Cys115. Cys115 is the site of covalent attachment of fosfomycin.[17] Given the apparent importance of this loop in the initiation of catalysis, the role of Cys115 has been the subject of a number of studies. Cys115 forms a covalent phospholactoyl-enzyme adduct (Enz-PEP) with PEP (Figure 1.2-3). This enzyme adduct has been characterized by NMR and shown to contain PEP bound to an enzyme nucleophile.[16] Although conclusive evidence has not identified Cys115 as this nucleophile, Enz-PEP has been show to protect against MurA inactivation by fosfomycin and thiol-modifying agents.[20]
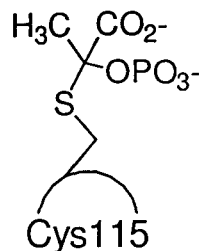
Figure 1.2-3 – Structure proposed for the phosphothiolactyl enzyme adduct (Enz-PEP)

The Enz-PEP adduct has been shown to be kinetically competent[†]. Upon addition of UDP-GlcNAc, the adduct reacts with a rate consistent with the rate of appearance of products. In the absence of UDP-GlcNAc the second-order rate of formation of Enz-PEP (1.5×10^7 $M^{-1}s^{-1}$) is 60-fold slower than k_{cat}/K_m, presumably because of the reduced binding affinity of PEP for free enzyme. The rate of Enz-PEP formation is increased in the presence of UDP-GlcNAc. Using rapid chemical quench studies, under single turnover conditions, it was shown that Enz-PEP formed with a rate of 5×10^7 $M^{-1}s^{-1}$, consistent with the overall rate of catalysis.[16]

The identification of Enz-PEP as a kinetically competent intermediate, combined with its ability to form THI upon the addition of UDP-GlcNAc, was believed to show that formation of Enz-PEP precedes the THI during normal catalysis. Pre-steady state kinetics studies using the normal substrates have been unable to show whether Enz-PEP precedes the THI.[16] The rates of appearance of both intermediates are

---

[†]   An intermediate is kinetically competent when its rates of formation and breakdown are as fast or faster than the overall rate of the reaction.

very similar, and fast enough to be near the limit of detection using current rapid-mixing techniques.

It was possible to use (Z)-fluoro-PEP as a PEP analog to form the corresponding fluoro analogs of Enz-PEP and the THI at rates which are retarded by ~10^4-fold relative to the normal reaction. The reduced rates allowed measurement of an initial 5-fold kinetic preference for formation of the fluoro-THI relative to the fluoro-Enz-PEP. The two intermediates then slowly interconvert, until at equilibrium, there are about equal amounts of the two intermediates. Thus, fluoro-THI formation does not require prior fluoro-Enz-PEP formation.[9] Assuming that the reaction with PEP as a substrate proceeds with a similar mechanism, formation of Enz-PEP is likely off the main catalytic pathway, resulting in a branched mechanism (Figure 1.2-4).
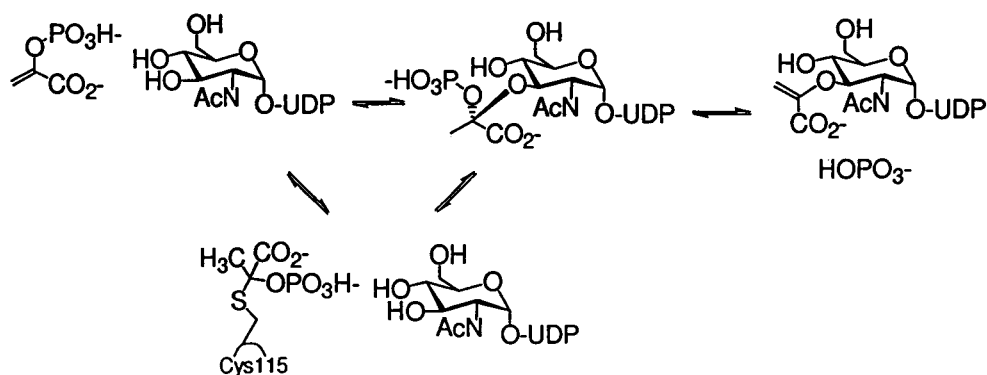
Figure 1.2-4 – Branching mechanism of MurA showing Enz-PEP to be off the main catalytic pathway. Its formation is not required for the formation of THI.

1.2.4 General Acid/Base Catalysis – A New Role for Cys115

Given that formation of Enz-PEP is off the main catalytic pathway, the importance of nucleophillic catalysis by Cys115 came into question. The C115D and C115E mutants of MurA are active, but the C115A and C115S are not.[6] Thus, as long as amino acid 115 is an ionizable group, MurA retains activity. The C115D mutant has been kinetically characterized, showing differences from wild-type in the pH dependence of k_{cat}. There is a shift in the pK_a in the basic limb from 9.4 in the wild-type to ~6 in the C115D mutant. Given the expected pK_a of an active site cysteine (8 to 11) and aspartate (2 to 6), the shift in the pH dependence seems to be due to the change in amino acid 115. This would suggest the role of Cys115 in the wild-type enzyme as a general acid that catalyzes the formation of the THI by protonating at C3. Upon formation of the THI, Cys115 could then remove the C3 proton during the elimination to form products. However, it should be noted that the shift in pH-dependence could be due to a change in the rate limiting step in the C115D-catalyzed reaction. Therefore, further evidence is needed to support Cys115 as general acid/base catalyst.[6]

The X-ray structure of fosfomycin-inactivated MurA, with bound UDP-GlcNAc, shows Cys115 in the correct position to protonate the 2-*si* face of PEP (Figure 1.2-2).[21] However, in another structure of C115A MurA with fluoro-THI bound, the Ala115 C-β is not close enough to C3 to

13

imply acid-catalysis by Cys115 in the wild-type enzyme.[13] This may be a consequence of the flexibility of the loop containing the Ala115, or the C115A mutation may remove the interactions that keep Cys115 in a position to carry out acid-catalysis. The C115A fluoro-THI structure also shows one of the phosphate bridging oxygens positioned 2.5 Å from C3, making it possible that intramolecular base catalysis by the phosphate could be occuring.[13] However, recent evidence with AroA has shown that phosphate cannot be performing intramolecular base catalysis during the AroA elimination. Instead, Glu341 has been proposed to act as a general acid/base catalyst, via protonation/deprotonation at C3. Given that superposition of MurA and AroA structures shows that Cys115 in MurA and Glu341 in AroA occupy the same position in space, this supports a common function for both residues (*i.e.* general acid/base catalysts).[22]

1.2.5 Evidence for Oxocarbenium Ion Intermediates

Although there is good evidence for general acid/base catalysis during carboxyvinyl transfer, it still unclear whether proton transfer in the addition is concerted with nucleophillic attack or if these steps occur separately. Similarly, elimination could occur with proton abstraction and leaving group departure being either concerted or stepwise.

Stepwise mechanisms would result in the formation of oxocarbenium intermediates (Figure 1.2-5) (This assumes protonation occurs first in addition and phosphate departs first, otherwise anionic

intermediates are formed). It would not be possible to isolate and

structurally characterize an oxocarbenium ion intermediate, because it

would undergo attack by water at near-diffusion-controlled rates, resulting

in breakdown to predominately pyruvate, phosphate, and UDP-GlcNAc or

S3P.[23;24] Though direct observation of such intermediates would be

impossible, there have been several lines of evidence which suggest their

existence.
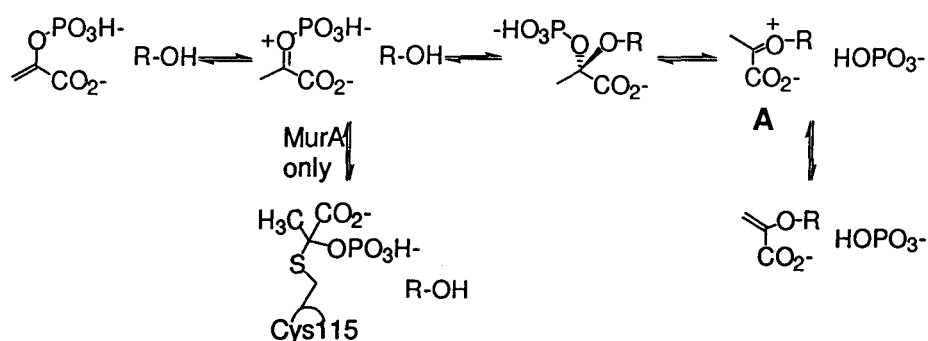
Figure 1.2-5 – Mechanism of carboxyvinyl transfer showing proposed oxocarbenium ion intermediate (**A**)for the addition and elimination steps. (The Enz-PEP only form in the MurA catalyzed reaction)

Using (Z)-fluoro-PEP as a PEP substrate analog showed that MurA

was unable to eliminate phosphate from fluoro-THI to yield products. The

rate was decreased by at least 10^6-fold relative to the normal reaction,

with the rate of the addition being reduced by ~10^4-fold. The rate of

non-enzymatic breakdown of the fluoro-THI was reduced 6×10^3-fold

relative to THI.[6] The non-enzymatic breakdown of THI goes through the

same oxocarbenium ion that would occur in the elimination step with a

stepwise mechanism,[24] thus reduction in the rates of the enzymatic

formation and breakdown of fluoro-THI can be accounted for by the

destabilization of the presumed oxocarbenium intermediates, with

inductive withdrawal of electron density from C2 by fluorine.

If the mechanism of the addition and elimination steps in the

enzymatic reaction is associative and concerted, the effect of fluorine

would be expected to be smaller as there would be less positive charge

buildup at C2. However, if the elimination is concerted but dissociative, a

large degree of positive charge at C2 could still build up (Figure 1.2-6),

and the reaction would be significantly slowed by fluorine substitution.

Thus, these results imply that there is significant positive charge buildup at

C2 in the addition and elimination steps, but whether this is at the

transition states of concerted addition/eliminations or in intermediates in

stepwise addition/eliminations is not clear.
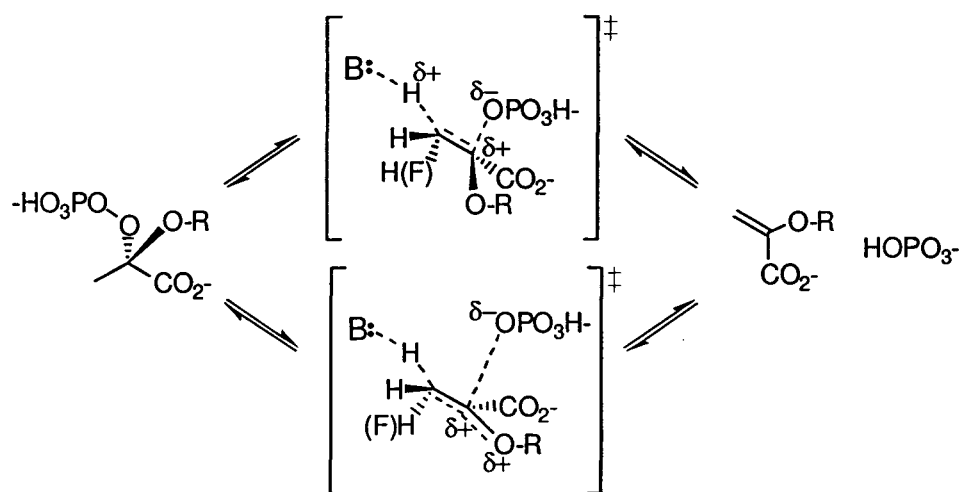
Figure 1.2-6 – Elimination from the THI to form products could be highly concerted (top) or dissociative (bottom) transition state. Since in the dissociative mechanism the removal of the proton lags behind phosphate departure, there is significant positive charge build up at C2.

Studies using fluoro-PEP as a substrate analog with AroA showed similar extents of retardation for the addition and elimination steps. The K_d's for the fluoro-THI and fluoro-EPSP have been measured as 600 pM and 17 µM, respectively (K_d for EPSP is 4 µM). These show tight binding of the fluoro-THI, and binding of fluoro-EPSP which is only 4-fold weaker than that of EPSP. Therefore, the reduction in rates is not due to significant steric hindrance by fluorine.[25]

1.3   Non-Enzymatic Breakdown of the THI

1.3.1 MurA and AroA THIs – Previous Work

The chemistry of breakdown of the MurA THI (**1**), the related AroA

THI (**5**) or other α-carboxyketal phosphates,[26;27] have not been previously

studied in detail. One study of **5**, reported it to have a half-life of 45 min at

pH 7 and greater than 48 h at pH 12. The products of **5** breakdown at pH

4 were reported to be S3P (**6**), phosphate and pyruvate. At pH 7 in

addition to these products, EPSP (**7**) and AroA ketal (**8**) were observed

(Figure 1.3-1).[28] MurA THI has reported half lives of 2.1 h at pH 8 and 39

s at pH 5.[9] At both pH values UDP-GlcNAc (**2**), phosphate and pyruvate

were the only reported products. These results are insufficient to draw

any mechanistic conclusions about the breakdowns of **1** and **5**. Thus, our

objective was to gain a better understanding of the chemistry of **1** and **5** by

obtaining more direct experimental evidence, together with application of

what is understood about related systems.
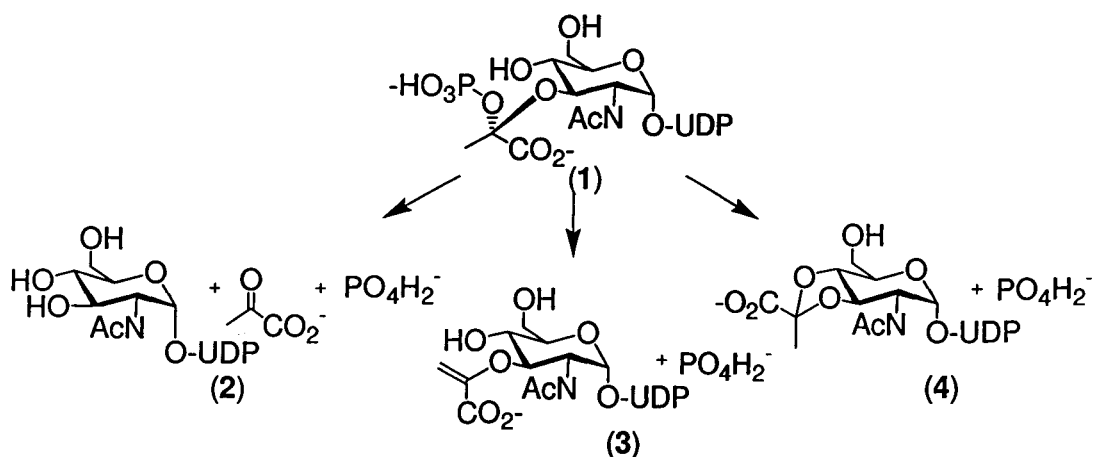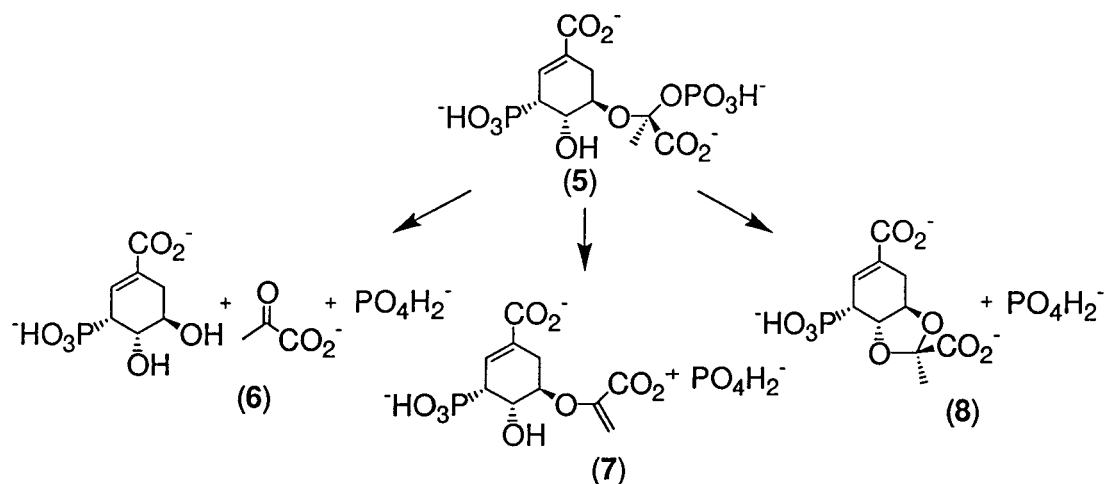
Figure 1.3-1 – Products of breakdown of the AroA THI (**5**)(below) and the corresponding potential products of the MurA THI (**1**)(above). (left) Products of Hydrolysis: UDP-GlcNAc (**2**)/S3P (**6**), pyruvate, phosphate. (center) Products of elimination: EP-UDP-GlcNAc (**3**)/EPSP (**7**), phosphate. (right) Products of intramolecular nucleophillic attack: MurA ketal (**4**)/AroA ketal (**8**) and phosphate.

1.3.2 Acetal[‡] Hydrolysis

The THIs contain α-carboxyketal phosphate functionalities and it is therefore informative to examine mechanistic aspects of hydrolysis of simpler acetals. Acetal hydrolysis, except in what have been deemed "special cases", occurs via a specific acid-catalyzed mechanism, or A1 mechanism.[29] Without the explicit inclusion of the protonation steps, the mechanism of acetal hydrolysis involves C-O bond cleavage to form an oxocarbenium ion intermediate. This intermediate reacts with water to form a hemiacetal, which subsequently undergoes a second C-O bond cleavage resulting in aldehyde or ketone formation (upper route, Figure 1.3-2). Cases where hydrolysis occurs with the formation of a carbonium

---

[‡]   The term acetal when used generally will encompass both acetals and ketals. When referring to a specific compounds, acetal will refer to compounds which result from aldehydes and ketal will refer to compounds which result form ketones

ion intermediate are rare (lower route, Figure 1.3-2), and normally only

occur when an exceedingly stable carbonium ion is formed. However,

such is the case for alkaline hydrolysis of acetal phosphates (see

below).[30;31]
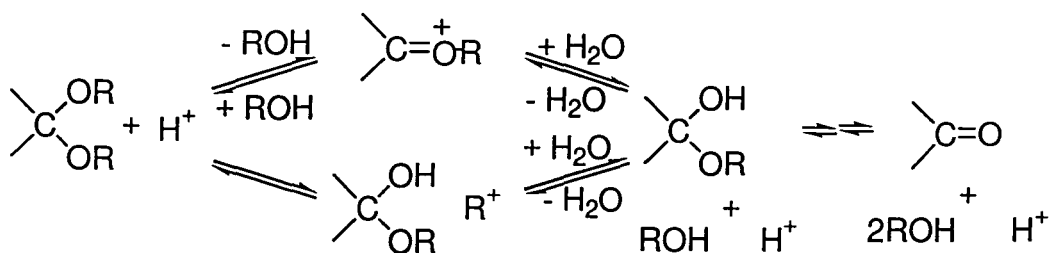
Figure 1.3-2 – General Mechanism for acetal hydrolysis involving the formation of an oxocarbenium ion intermediate (upper route). Hydrolysis via carbonium ion formation (lower route).

Oxocarbenium ions react with solvent at near diffusion-controlled

rates.[32;33] Therefore, reaction of the oxocarbenium with water to be the

rate-limiting step could only occur for very reactive acetals. An at least

partially rate-limiting breakdown of hemiacetal can also be envisioned,

especially given that acetal and hemiacetal hydrolysis are expected to be

mechanistically similar. However, Cordes[34] has argued that if the

hemiacetal hydrolysis were rate-limiting, a large build-up of the hemiacetal

would be expected over the course of the reaction, since the equilibrium in

water greatly favours the hemiacetal over the acetal. When the hydrolysis

of the dimethyl ketal of acetone was followed by NMR, the rate of

disappearance of the ketal correlates with appearance of the acetone and

methanol, showing that breakdown of the hemiacetal cannot be

rate-limiting.[35] This conclusion has been generalized to other acetals, however in the case of mixed acetals where the two substituent alcohol's leaving groups abilities are significantly different it may not hold. Such is the case for the acylal[§] α-methoxybenzyl propionate (9). Because propionate is much better as a leaving group than methanol, the hydrolysis of the acylal is sped up relative to the hemiacetal. This results in non-first order disappearance of the acylal and a transient build-up of the hemiacetal.[36] Even with a difference of approximately 12 in the pK_a's of the leaving groups, the breakdown of the hemiacetal is only partially rate limiting. Thus for the hemiacetal hydrolysis to be completely rate limiting a much larger difference in leaving group pK_a's would be needed.

(9)
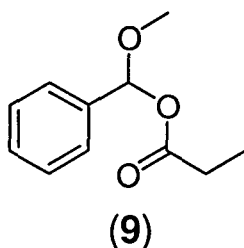
The remaining candidate for the rate-limiting step of acetal hydrolysis is the conversion of the acetal into the oxocarbenium ion. This conversion, however, can be made up of several sub-steps including protonation of the leaving group, breaking of the C-O bond and the diffusion apart of any ion-molecule pair or ion-pair intermediates. Although the separation of ion-molecule pairs[37-39] or ion-pairs[40;41] has

---

[§]   An acylal is an acetal where one of the alcohol substituents is replaced by a carboxylate

been shown to occur after the rate limiting step for most acetals, there are cases, such as the hydrolysis of CMP-NeuAc,[33] where this is not the case (Section 1.3.4). The relative rates and order of protonation and C-O bond breaking steps have been shown to be important in determining the nature of the rate-determining step of acetal hydrolysis.

There are three distinct possibilities for acetal hydrolysis, (1) specific acid-catalysis, where the C-O bond breakage is rate-limiting and protonation occurs as a fast pre-equilibrium, (2) pH-independent hydrolysis, where the C-O bond cleavage occurs without prior protonation of the substrate, and (3) general acid-catalysis, where the protonation and C-O bond cleavage are both partially rate-limiting, and occur within a single step.[29]

The most common mechanism of acetal hydrolysis is through specific acid-catalysis[42] (Figure 1.3-3).[29;34] Protonation of the leaving group in a prequilibrium step results in a better leaving group. This makes C-O bond cleavage easier in the subsequent rate-limiting step. The importance of oxocarbenium ion stability, leaving group ability and substrate basicity has been probed with secondary deuterium KIEs and substituent effect studies. β-secondary deuterium KIEs on specific acid acetal hydrolysis fall in the range of k_H/k_D 1.1 to 1.25.[29] The rate of hydrolysis has been shown to be sensitive to polar substituents in the carbonyl moiety (R_1), with electron donating substituents increasing rates.

Electron donating groups in the alcohol substituent which does not leave (R_2), also increase the rate of hydrolysis.[29] The KIE and substituent effects are consistent with significant oxocarbenium ion character in the transition state.

$$R_1 \underset{R_1}{\overset{OR_3}{\underset{\diagdown}{\overset{\diagup}{C}}}}OR_2 \quad \underset{-H^+}{\overset{+H^+}{\rightleftharpoons}} \quad R_1 \underset{R_1}{\overset{H}{\underset{\diagdown}{\overset{\overset{O}{\diagup}R_3}{C^+}}}}OR_2 \quad \longrightarrow \quad R_1 \underset{R_1}{\overset{+}{\diagdown}}C=OR_2 + R_3OH$$

$$K_{H_2O}/K_{D_2O} = 0.43 \quad K_{H_2O}/K_{D_2O} = 0.29$$
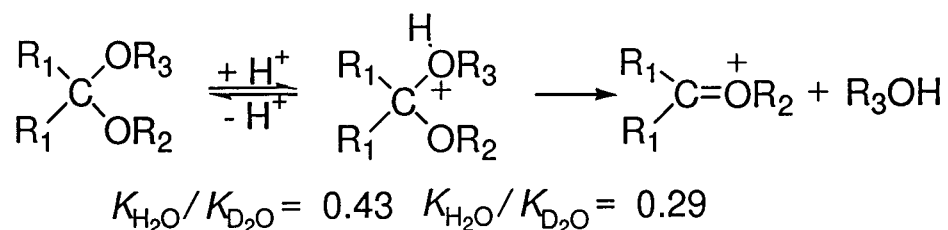
Figure 1.3-3 – Specific acid-catalyzed hydrolysis of acetals to form the oxocarbenium ion intermediate. Calculated EIEs for each step are also shown

Substituent effects in the leaving group (R_3) have shown only a small preference for electron donating groups.[29] Electron donating groups favour protonation of the substrate in the first step but retard the breaking of the C-O bond in the second step. Thus, for the specific acid-catalyzed mechanism, substrate protonation is more important than C-O cleavage. Solvent EIEs for both steps have been calculated by Schowen to be 0.43 and 0.29, respectively.[43] Given that the isotope effect of the proton from solvent in the second step is a secondary one, the expected SDKIE should range between 0.43 and 0.29, with lower values expected as C-O bond cleavage increases in the transition state. Observed SDKIEs range between 0.30 and 0.40,[29] consistent with the expected range, showing various degrees of C-O bond cleavage in the transition state.

The second general mechanism of acetal hydrolysis is observed with leaving groups that form particularly stable anions. For such acetals the rate of hydrolysis is independent of pH in a certain region of the pH profile. Within this region, substituent effects show electron donation in the carbonyl moiety and electron withdrawing groups in the leaving group increase the rate of hydrolysis.[29] Thus, the substituent effects support a mechanism involving unimolecular dissociation (Figure 1.3-4). SDKIEs for the pH-independent hydrolysis are small and inverse, consistent with IEs calculated for such a mechanism (0.9).[43]

$$ \underset{R_1}{\overset{R_1}{>}}C\overset{OR_3}{\underset{OR_2}{<}} \longrightarrow \underset{R_1}{\overset{R_1}{>}}C=\overset{+}{O}R_2 + R_3O^- \underset{-H^+}{\overset{+H^+}{\rightleftharpoons}} \underset{R_1}{\overset{R_1}{>}}C=\overset{+}{O}R_2 + R_3OH $$
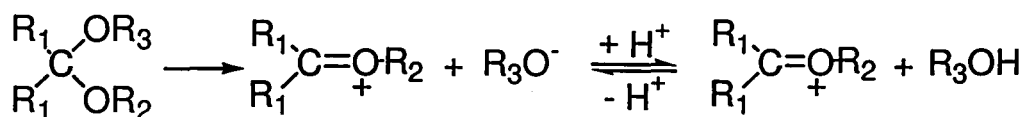
Figure 1.3-4 – pH Independent hydrolysis of acetals involving rate limiting unimolecular dissociation, followed by protonation of the leaving group.

The first two general mechanisms for acetal hydrolysis display two extremes with respect to the ease of C-O bond cleavage. In specific acid-catalyzed hydrolysis, protonation is sufficiently easy and occurs in a fast pre-equilibrium step that is required for C-O cleavage. The reaction space for the specific acid-catalyzed mechanism can be drawn as in Figure 1.3-5-left. In pH-independent acetal hydrolysis, lowering the leaving group pK_a facilitates C-O cleavage, but consequently decreases the pK_a of the acetal conjugate acid making protonation more difficult (Figure 1.3-5-right). The transition from the specific acid-catalyzed mechanism to the pH-independent mechanism is not abrupt. Acetals

24

where protonation and C-O bond cleavage are both partially rate-limiting

hydrolyse by the third general mechanism, namely general acid-catalysis

(Figure 1.3-5-centre). General acid-catalysis involves concerted

protonation and C-O cleavage within a single rate-limiting step (Figure

1.3-6).[34]
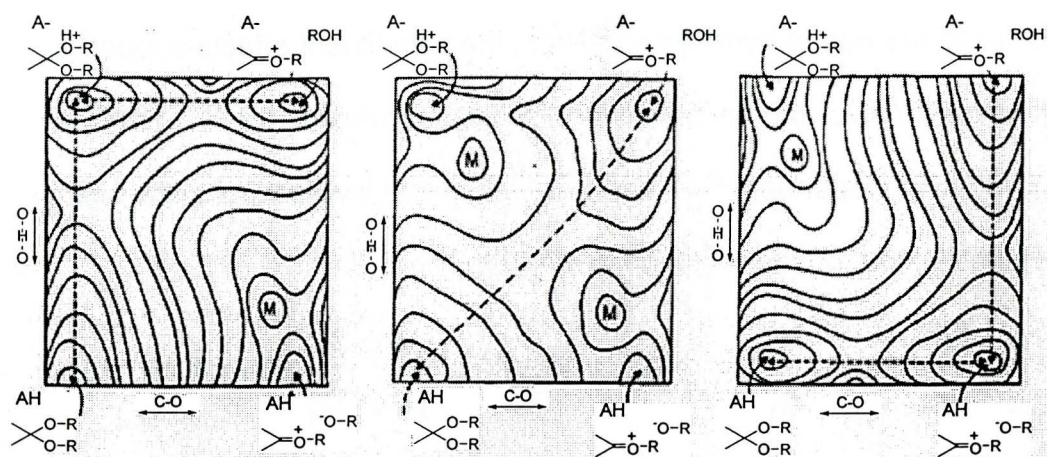
Figure 1.3-5 - Contour diagrams showing reaction space for proton and C-O bond cleavage steps of acetal hydrolysis. Regions marked with "M" are energy maxima. (left) Specific acid-catalyzed mechanism. (centre) General acid-catalyzed mechanism. (right) pH independent hydrolysis. (modified from ref.29)
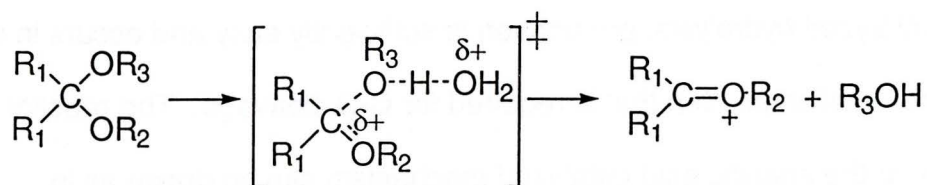
Figure 1.3-6 – Rate-limiting step of general acid-catalyzed acetal hydrolysis.

General acid-catalysis of acetal hydrolysis occurs for three general

types of acetals. (i) Acetals that have relatively good leaving groups and

relatively stable product oxocarbenium ions, such as 2-(*p*-nitrophenoxy)

tetrahydropyran (**10**). (ii) Acetals with poor leaving groups but exceedingly

stable product oxocarbeniums ions, such as tropone diethyl ketal (**11**). (iii)

Acetals such as benzaldehyde di-*tert*-butyl acetal (**12**), which do not fit the

first two requirements, but have significant reactant steric destabilization

also undergo general acid-catalysis. Relief of steric strain in the transition

state facilitates C-O cleavage.[42]

(10)   **(11)**   **(12)**
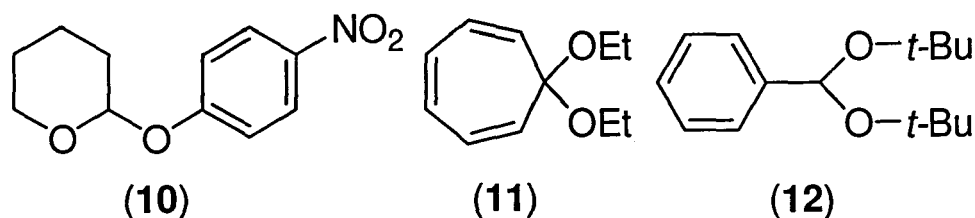
The common feature of each of these types of acetals is that C-O

cleavage is relatively easy. Jencks proposed that C-O bond cleavage

facilitates protonation such that only acetals that undergo large changes in

pK_a from reactant to the transition state show general acid-catalysis.[42]

Furthermore, protonation changes from being unfavourable in the reactant

to being favourable in the transition state.

The importance of facile C-O cleavage is further illustrated through

substituent effect studies.[42] Substituent effects in the carbonyl moiety and

the non-departing alcohol moiety are similar to those for specific

acid-catalysis. In the leaving group however, substituent effects are

opposite to specific acid-catalysis, showing increased rate with electron

withdrawing groups. Electron withdrawal favours C-O cleavage, but

hinders protonation, showing the former to be more important.[29]

The observation of general acid-catalysis has lead certain groups to explore the possibility of having an intramolecular source for this proton. Such work has primarily focused on intramolecular catalysis by carboxyl groups due to the observation of "intramolecular" catalysis by Asp 52 of lysozyme in the hydrolysis of glycosides. Intramolecular general acid-catalysis by a carboxyl has been sought, but not observed, for a number of acetals where the mechanism of hydrolysis is specific acid-catalyzed in the absence of the carboxyl. A study of the hydrolysis of o-carboxyphenyl alkyl acetals (13), showed that carboxylic acid (R_1 = H) containing acetals hydrolyse up to 1000-fold faster than the corresponding methyl ester (R_1 = Me).[29] A general acid-catalyzed mechanism of the hydrolysis of the acid would have a different degree of oxocarbenium ion character than the corresponding specific acid-catalyzed mechanism of the ester. This would lead to substituent effects at R_2 in the same direction, but different magnitude, if the mechanism changed from specific to general acid-catalyzed. The fact that substituent effects in R_2 did not change on going from the acid to the ester, did not support a change in the type of acid-catalysis for the two compounds. The rate acceleration due to the carboxylic acid was attributed to electrostatic stabilization of the developing oxocarbenium ion by the carboxylate, within a specific acid-catalyzed mechanism.
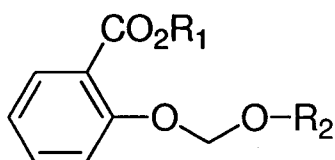
(13)

Intramolecular general acid-catalyzed hydrolysis by a carboxylic

acid group has been observed for acetals which normally undergo

intermolecular general acid-catalyzed hydrolysis in the absence of the

acid. Acetals such as 2-(o-carboxyphenyl)tetrahydropyranyl (**14**) and

benzaldehyde methyl o-carboxyphenyl acetals (**15**) hydrolyse 10^4-10^6

times faster than the corresponding carboxyl-lacking acetal.[44] Such rate

acceleration is greater than expected for electrostatic acceleration of

hydrolysis and thus attributed to intramolecular general acid-catalysis. To

be able to confidently invoke intramolecular general acid-catalysis the

effect on rate must be larger than that from simply bringing together the

acid and the acetal.
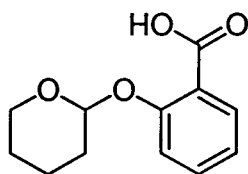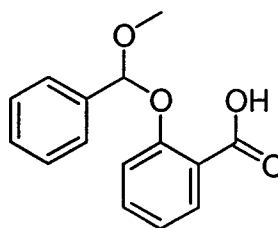
(14)   **(15)**

1.3.3 Monoalkyl Phosphate Hydrolysis

At first glance, one would expect that the hydroysis of the THI

would be exactly analogous to acetal hydrolysis, with phosphate simply

28

substituting as the leaving group. However, phosphate differs in two important ways from the typical leaving group in acetal hydroysis. First, it has three additional oxygens that may be protonated. Such protonation can result in changes in leaving group ability of up to 10^{16}-fold[**]. Second, hydrolysis can occur via P-O or C-O bond cleavage. Methyl[45;46], ethyl, isopropyl[47] and t-butyl[48] phosphate monoesters hydrolyze via two distinct mechanisms. At high pH, hydrolysis involves the monoanion and occurs via P-O bond cleavage. At low pH, hydrolysis involving the neutral or the conjugate acid occurs via C-O bond cleavage. Whereas the nature of the alkyl group has very little effect on the rate and mechanism of P-O bond cleavage, both the rate and mechanism of C-O bond cleavage show strong dependencies on the alkyl group structure.[47]

The pH profiles for methyl and isopropyl phosphate show rate maxima at pH $\approx$ 4, and an increase in rate proportional to proton concentration at pH < 1 (Figure 1.3-7). The pK_a's for the first and second ionizations of the phosphate are about 2 and 7.[47] Thus, at the rate maximum at pH 4 the monoanion is the major species, whereas at pH < 1 the neutral species is most abundant. Hydrolysis of the monoalkyl phosphates at pH 5 in $H_2^{18}O$ results in incorporation of ^{18}O-label into

---

[**]   Based on a difference of ~16 in the pK_as of the conjugate acids of the best leaving group H_3PO_4 (acid-catalyzed hydrolysis of RH_2PO_4) and the worst PO_4^{3-} (uncatalyzed hydrolysis of RPO_4^{2-}).[29;95]

phosphate.[45;47;48] This indicates hydrolysis via P-O bond cleavage for

methyl, ethyl and isopropyl phosphate.
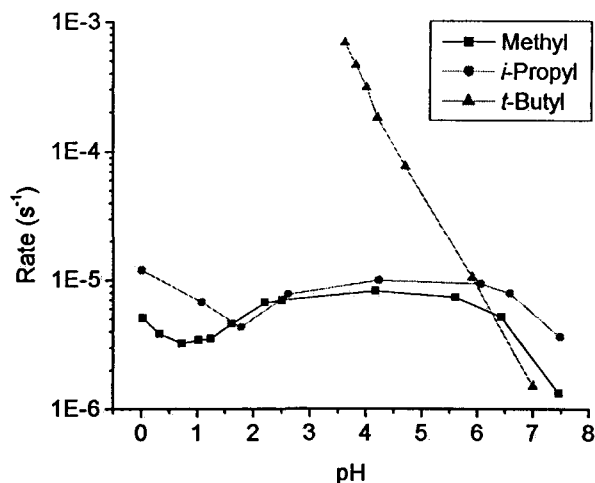
Figure 1.3-7 — Rate vs. pH profiles for methyl[45], isopropyl[47] and t-butyl[48] phosphate monoesters. Methyl and isopropyl phosphates rates are a 100°C and t-butyl phosphate rates are at 73.9°C

This cleavage was first proposed to occur via spontaneous

hydrolysis of the monoanion.[45] Intramolecular general acid-catalysis by

transfer of a proton from a non-bridging oxygen to the bridging oxygen,

directly, or through an intervening water molecule, was believed to be

synchronous with P-O bond cleavage. This resulted in a dissociative

mechanism with the formation of a metaphosphate ion intermediate

(Figure 1.3-8). The existence of a metaphosphate ion intermediate and

the importance of intramolecular catalysis to monoanion hydrolysis have

both come into question. More recent evidence has shown that although

free metaphosphate intermediates can occur during solvolysis in certain

solvents, such as sterically hindered alcohols like t-butanol, they do not

30

exist in water.[49] Metaphosphate formed in aqueous solution does not

escape its initial solvation shell before reacting. Hydrolysis of monoalkyl

phosphates in water leads to inversion of stereochemistry at phosphorus,

consistent with dissociative or associative S_N2 mechanisms. Direct

experimental evidence to distinguish between these possibilities has not

been shown. However, recent computational studies demonstrate that the

dissociative S_N2 mechanism is preferred.[50;51]
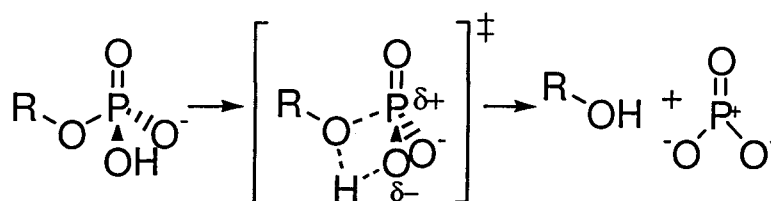
Figure 1.3-8 – P-O bond cleavage of alkyl phosphate via intramolecular proton transfer and formation of metaphosphate intermediate

Alternatively, intermolecular specific acid-catalyzed hydrolysis of

the dianion has been proposed. This mechanism involves fast equilibrium

pre-protonation of the dianion at the bridging oxygen, making the alcohol a

better leaving group in the rate-determining cleavage of the P-O bond

(Figure 1.3-9).[52] Similar mechanisms have been proposed in the

hydrolysis of alkyl sulphates[53;54] and phosphoramidates,[55;56] where bridge

oxygen/nitrogen protonation promotes subsequent S-O or P-N bond

cleavage.

For methyl phosphate such a mechanism requires that at pH 4,

where P-O cleavage is maximal, an anionic zwitterion with an estimated

pK_a of -4 is formed. Given that the concentration of such a species would be minute, it would have to react rapidly to account for the observed rate of 8.23×10^{-6} s^{-1}. Based on the observed rate of hydrolysis at pH 4 and the estimated concentration of the anionic zwitterion, this rate would be 2×10^6 s^{-1}. Such a rate is within the limits of a diffusion-limited proton transfer at pH 4, and thus possible. This mechanism has been further supported by experimental studies involving substituents effects[46] and solvent IEs[30;52] and computational studies[50;57].
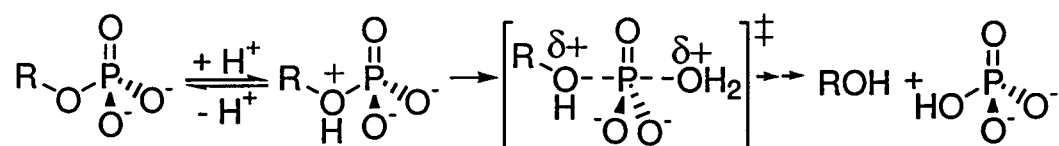
Figure 1.3-9 – P-O bond cleavage mechanism from anionic zwitterion, involving concerted transfer of metaphosphate to water

The dianion undergoes acid-catalyzed P-O bond cleavage most readily because it results in the most stable, monoanionic metaphosphate, transition state. Specific acid-catalyzed hydrolysis of the monoanion or neutral monoalkyl phosphate would be expected to go through less stable neutral or cationic metaphosphate transition states, respectively. Thus, at low pH where P-O cleavage is slowed, mechanisms involving C-O bond cleavage become favourable. At 100°C, in 4M perchloric acid, the amount of P-O bond cleavage is reduced to 27%, 48%, 1% and 0% for methyl, ethyl, isopropyl and t-butyl (in 1M perchloric acid) phosphates, respectively.[47] Under these conditions the rates of hydrolysis for methyl,

ethyl and isopropyl phosphate are 1.5×10^{-5}, 9.9×10^{-6} and 1.1×10^{-3} s^{-1},

respectively. Hydrolysis of t-butyl phosphate is much faster, 2.3×10^{-3} s^{-1} at

10°C in 2.5 M perchloric acid. Whereas, the entropies of activation for

isopropyl and t-butyl in acid are positive, corresponding to a unimolecular

reaction, they are negative for methyl and ethyl phosphate. This supports

a bimolecular, $A_N D_N$ hydrolysis for methyl and ethyl phosphate.[47] With

neopentyl phosphate, $A_N D_N$ attack is slowed due to increased steric

hindrance (Figure 1.3-10), which results in only P-O bond cleavage.[58]

This further supports an $A_N D_N$ attack by water in primary monoalkyl

phosphates and explains the increased rate with methyl versus ethyl

phosphate.
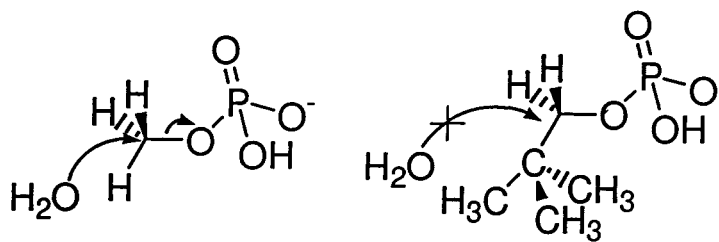
Figure 1.3-10 – (Left) $S_N 2$ mechanism of C-O cleavage of methyl phosphate. (Right) The $S_N 2$ mechanism is slowed in the case of neopentyl phosphate due to increase steric hindrance.

This $A_N D_N$ process is slow compared to the $D_N + A_N$ mechanism of

isopropyl and t-butyl phosphate hydrolysis. In the case of t-butyl

phosphate, the $D_N + A_N$ C-O bond cleavage mechanism is nearly as fast as

P-O bond cleavage from the dianion at pH > 6. Thus the pH profile shows

only a small inflection at around pH 6 where the population of the dianion

begins to increase (Figure 1.3-7). The mechanisms of C-O bond cleavage

for the *t*-butyl phosphate monoanion, neutral and conjugate acid have

been proposed to be spontaneous dissociation of phosphate (Figure

1.3-11). Acid-catalysis observed in the pH profile would arise then from

specific acid-catalysis at the non-bridging oxygens.[48]
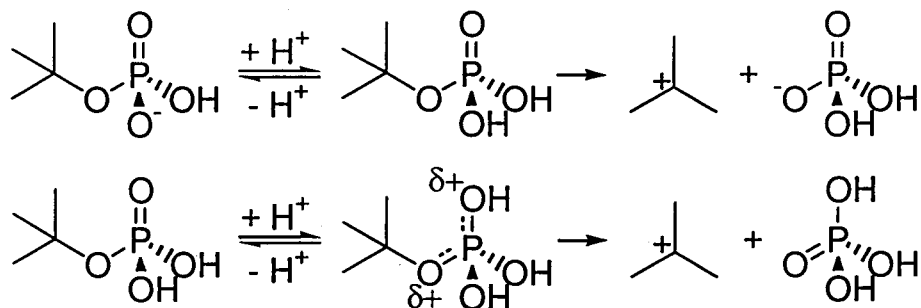
Figure 1.3-11 – Specific acid-catalysis of monoanion (upper) and neutral (lower) butyl phosphate hydrolysis via non-bridging oxygen protonation

A second mechanism involving specific acid-catalysis at the

bridging oxygen can also be proposed (Figure 1.3-12). For the

acid-catalyzed hydrolysis of the monoanion, such bridging oxygen

protonation would make C-O bond cleavage step much faster than the

corresponding catalysis via non-bridging oxygen protonation. However,

the protonation itself would be more difficult given that the pK_a of the

bridging oxygen is about 6 pH units lower. Thus, it is difficult to tell if the

acceleration of the C-O cleavage would be enough to overcome the

10^6-fold lower steady-state concentration of the zwitterionic form of the

neutral. The principle of microscopic reversibility becomes useful in

distinguishing between mechanisms. Since reverse reaction of the

non-bridging monoanion pathway involves attack of an anion on the

carbocation (Figure 1.3-11, upper), it is expected to be faster than the corresponding attack of a neutral on the carbocation as takes place in the bridging monoanion pathway (Figure 1.3-12, upper).[59] Thus for t-butyl phosphate the non-bridging pathway would seem to be favoured. This may change if the hydrolysis is carried out in a solvent were the carbocation lifetime is very short and thus little preference for the nature of the nucleophile exists.[60] Also, in solvents where the desolvation of the nucleophile is slow, attack of the more solvated anion may be significantly slowed relative to the less solvated neutral.[61]
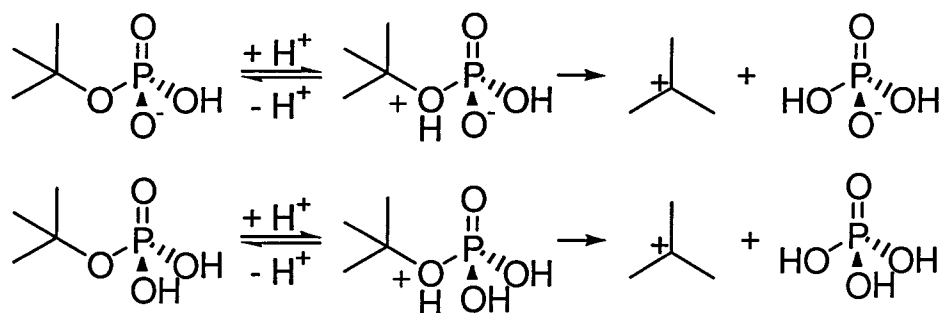
Figure 1.3-12 - Specific acid-catalysis of monoanion (upper) and neutral (lower) butyl phosphate hydrolysis via bridging oxygen protonation

1.3.4 Acetal Phosphate Hydrolysis

One major group of acetal phosphates that has been studied are glycosyl phosphates, with most work focussed on α-glucose-1-phosphate (**16a**). The pH-profile of the hydrolysis of **16a** shows that its susceptibility to C-O cleavage is between that of isopropyl and t-butyl phosphate. As with t-butyl phosphate, C-O bond cleavage occurs exclusively at low pH and P-O cleavage at high pH.[30] Thus **16a** hydrolysis is typical of an alkyl

phosphate with a reasonably stable product carbocation in the C-O cleavage mechanism. This having been said, the lifetime of the glucosyl oxocarbenium has been estimated to be 10^{-12} s in water,[62] only one order of magnitude greater than a bond vibration. In the presence of anionic nucleophiles such as azide, the glucosyl oxocarbenium does not have a finite lifetime in solution, and the mechanism becomes dissociative S_N2.[63]
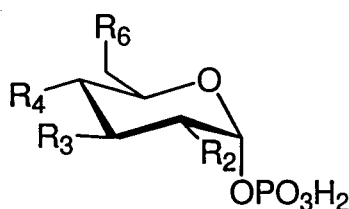
16a: $R_2=R_3=R_4=R_6=$ OH   16f: $R_2=$ H, $R_3=R_4=R_6=$ OH
16b: $R_2=$ F, $R_3=R_4=R_6=$ OH   16g: $R_3=$ H, $R_2=R_4=R_6=$ OH
16c: $R_3=$ F, $R_2=R_4=R_6=$ OH   16h: $R_4=$ H, $R_2=R_3=R_6=$ OH
16d: $R_4=$ F, $R_2=R_3=R_6=$ OH   16i: $R_6=$ H, $R_2=R_3=R_4=$ OH
16e: $R_6=$ F, $R_2=R_3=R_4=$ OH
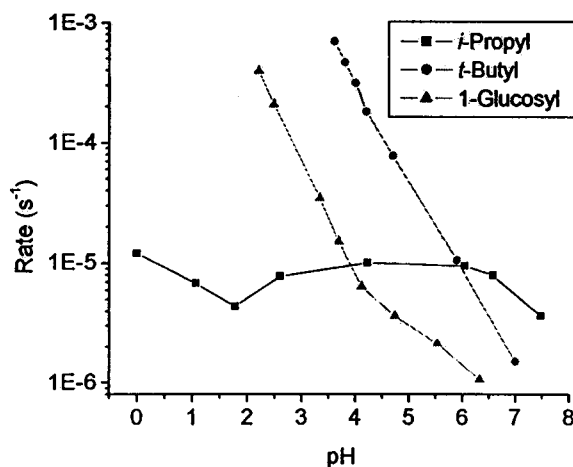
Figure 1.3-13 - Rate vs. pH profiles for hydrolysis isopropyl[47], t-butyl[48], α-1-glucosyl (16a)[30] phosphates. The rates were measured at 100°C, 73.9°C and 82.0°C, respectively.

Other studies have examined other glycosyl phosphates and the effects of structure on the rate of hydrolysis, including deoxy-fluoro and deoxy analogs of **16a**. The relative rates of hydrolysis of fluoro-substituted glucose-1-phosphates were determined to be 1:7:4:16:60 for 2-F (**16b**), 3-F (**16c**), 4-F (**16d**), 6-F (**16e**) and unsubstituted glucose-1-phosphate (**16a**), respectively at 25°C in 1M $HClO_4$.[64] Under the same conditions, the relative rates for 2-deoxy (**16f**), 3-deoxy (**16g**), 4-deoxy (**16h**), 6-deoxy (**16i**) and glucose-1-phosphate were 2700:8:27:5:1, respectively.[65] The effects of substitution at the 2-position are the most pronounced due to their proximity to the site of the positive charge in the oxocarbenium ion. Fluorine substitution inductively withdraws electron density from the developing oxocarbenium ion, while the substitution of hydrogen for the 2-hydroxyl greatly stabilizes the developing oxocarbenium ion via an inductive effect, as well as hyperconjugation, and has the greatest effect on the rate. The effects of the other substitutions, although smaller, show that these more remote sites can also affect the rate. As fluorines slow the rate relative to the hydroxyls and the hydrogens accelerate it, field effects have been proposed to govern the change in rates.[65] There is increasing dipole-charge destabilization of the developing oxocarbenium ion as the substituents become more electronegative.

The effect of changing the stereochemistry of the phosphate and hydroxyls has also been studied by comparing the rate of hydrolysis of

both the α and β anomers of mannose-1-phosphate (**17**),

galactose-1-phosphate (**18**) and glucose-1-phosphate (**19**). At pH 1 and

82°C the relative rates of the β and α anomers are 1.3, 2.1 and 1.6 for

mannose-1-phosphate, galactose-1-phosphate and G-1-P, respectively.[66]

Thus, the stereochemistry of the leaving group has a small effect. The

change in stereochemistry of the 2- and 4-hydroxyls also has a small

effect, with α-mannose and α-glucose hydrolysing at a similar rate, and

α-galactose hydrolyzing 1.9 times as fast as α-glucose.[66] Thus for

glycosyl phosphate hydrolysis, changes other than at the 2-position, can

affect the rate, but these rate effects are no larger than 1.5 orders of

magnitude.

α: R_1 = phosphate, R_2 = H
β: R_1 = H, R_2 = phosphate
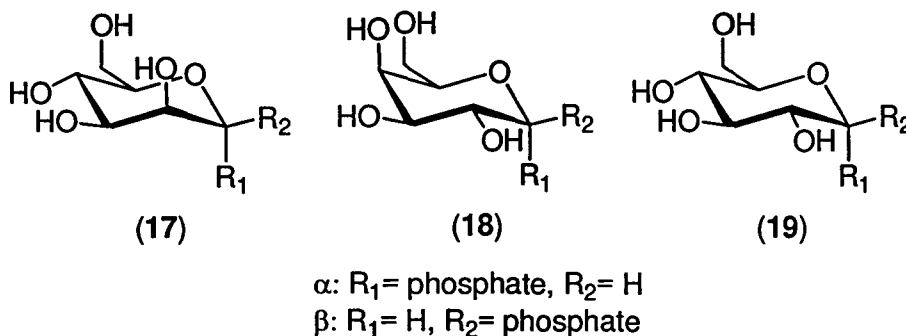
1.3.5 Vinyl Ether Hydrolysis

A major challenge in applying the understanding of hydrolysis of

acetals, alkyl phosphates and acetal phosphates, to α-carboxyketal

phosphate (**20**) hydrolysis, is determining the role of the carboxlyate.

Substitution of an α-carboxyl in place of the α-hydrogen of acetal

phosphates could have a number of effects. (i) The carboxyl is much

larger and thus could sterically destabilize the reactant. [67-69] (ii) In the

ionized form, the carboxylate's negative charge could destabilize the

reactant by electrostatic repulsion of the negative phosphate leaving

group. The reverse effect, reactant electrostatic stabilization of a positive

pyridinium leaving group, is observed with N-glycosides (21).[70] (iii) The

carboxyl will produce a substituent effect, the nature of which will depend

on the carboxyl protonation state. As the carboxylic acid, it is strongly

electron withdrawing, but weakly electron withdrawing as the carboxylate.

Thus, the carboxylate will stabilize the oxocarbenium relative to the

carboxylic acid.[71] As well, the carboxyl could play a role in catalysis by

acting as (iv) an intramolecular general acid,[72;73] (v) a nucleophile,[33;74] or

(vi) by electrostatic stabilization[75] of the developing oxocarbenium ion.

$$R_1-O \diagup OPO_3H^-$$
$$R_2 \diagdown COO^-$$

(20)

(21)
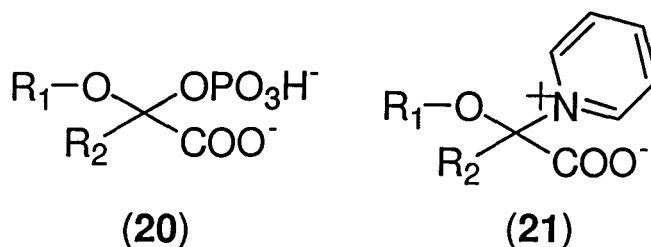
Such a large number of possible roles for the carboxyl makes

discerning its role(s) in any given system difficult. However, one can look

at related systems where a smaller number of roles are possible. One

such system is that of vinyl-ether hydrolysis (Figure 1.3-14), which shares

with acetal hydrolysis a common oxocarbenium ion intermediate. The

rate-limiting step in vinyl ether hydrolysis is the initial protonation of the

39

double bond. As the geometry around the carbon that becomes positively

charged does not change between reactant and transition state, steric

destabilization of the reactant is no longer relevant. Also, electrostatic

effects on the reactant are not relevant because it is not charged.
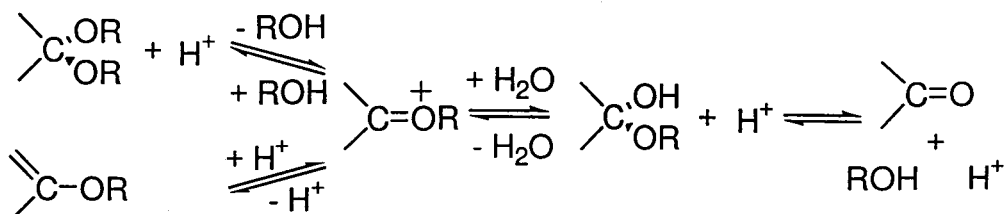
Figure 1.3-14 — Similar mechanisms of hydrolysis for acetals and vinyl-ethers.

A series of vinyl ethers, which form oxocarbenium ion intermediates

closely resembling that of the THI hydrolysis were studied by Kresge *et*

al.[76] The rates of the acid-catalyzed hydrolysis of α-methoxyacrylic acid

(24) and methyl α-methoxyacrylate (25) show significantly slower rates of

hydrolysis than α-methoxyacrylate (23) (Figure 1.3-15). However,

α-methoxyacrylate still hydrolyses 16-fold more slowly than the

corresponding vinyl-ether where the α-carboxylate is replaced by an

α-hydrogen (22). The rates of hydrolysis are consistent with the expected

substituent effects of the various carboxyl forms. This supports a role for

the carboxylate and carboxylic acid as simple electron-withdrawing

substituents, without any role involving intramolecular general acid or

electrostatic catalysis.

(22)   **(23)**   **(24)**   **(25)**

Relative Rates: 81000   5100   4   1
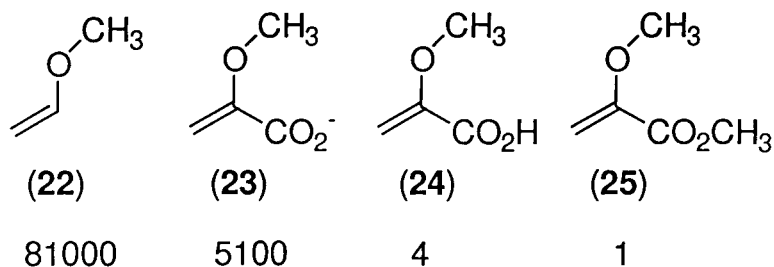
Figure 1.3-15 - Effects of α-carboxylate, α-carboxylic acid and α-carboxyl ester substitutions on the rate of acid-catalyzed vinyl ether hydrolysis.

In the hydrolysis of E-1-methoxy-2-(2-carboxyphenyl)ethylene (**26**), the role of the carboxyl extends beyond a substituent effect to general acid-catalysis. Spontaneous hydrolysis of the neutral form is 2-3 orders of magnitude greater than that of the corresponding vinyl ether where the carboxyl is replaced by a hydrogen.[77;78] The catalytic role of the carboxylate could be via intramolecular general acid or electrostatic catalysis. However, whereas the methyl ester of **26** is subject to buffer catalysis, the free acid is not. This is consistent with intramolecular general acid-catalysis, where buffer acids cannot compete with the intramolecular reaction (Figure 1.3-16).

(26)
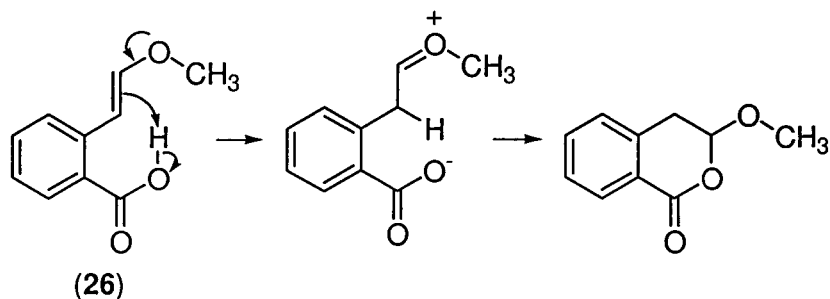
Figure 1.3-16 — Mechanism of hydrolysis of E-1-methoxy-2-(2-carboxyphenyl)ethylene (**26**) via intramolecular general acid-catalysis. The capture of the oxocarbenium ion by the carboxylate occurs after the rate-determining step.

41

1.3.6 α-Carboxy Acetal/Acetal Phosphate Hydrolysis

Although the role of an α-carboxyl has been determined in several systems involving vinyl ether hydrolysis, the role of an α-carboxyl is more complicated in acetal hydrolysis (Section 1.3.4) and no study has focussed on exploring its effect. The closest relevant study is that of the hydrolysis of NeuAc pyridinium salts (27). The hydrolysis is spontaneous (*i.e.* no acid-catalysis), and occurs only 3-fold faster in the carboxylate form than the carboxylic acid form.[70] The carboxylic acid form hydrolyses 60-fold faster than isoquinilonium 2-deoxyglucose (28).[79] As both protonation states of 27 are of similar reactivity, the increase in their rates of hydrolysis over 28 can be attributed to steric destabilization of the ground state.

(27)   (28)
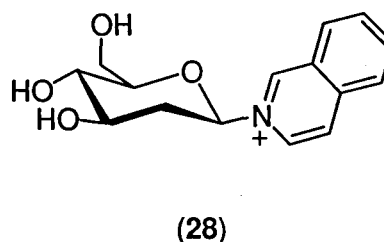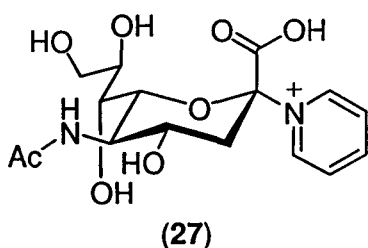
Studies on the hydrolyses of α-carboxy acetals and α-carboxy acetal phosphates have not examined the role of the carboxyl in detail, but did investigate the role of acid-catalysis and the importance of ion pairs. Hydrolysis of α-*p*-nitrophenyl NeuAc (29) has four different mechanisms across the pH range (Figure 1.3-17).[80] Hydrolysis is base-catalyzed at high pH, a feature which seems unique to NeuAc-based glycosides.

Hydrolysis becomes uncatalyzed at intermediate pH, with leaving group

substituent effects and SDKIEs consistent with a unimolecular dissocation

mechanism, similar to that of acetals where C-O bond cleavage is facile

(Figure 1.3-4).[29] At low pH the hydrolysis is acid-catalyzed, with an

inflection near the pKa of the carboxylate. Therefore, both the carboxylate

and carboxylic acid forms undergo acid-catalyzed hydrolysis. The leaving

group substituent effects are small and the SDKIEs are both near 1.3,

supporting general acid-catalysis (Figure 1.3-6). This is further supported

by the fact that acetals where C-O bond cleavage is facile also show

general acid-catalysis.[29;42]
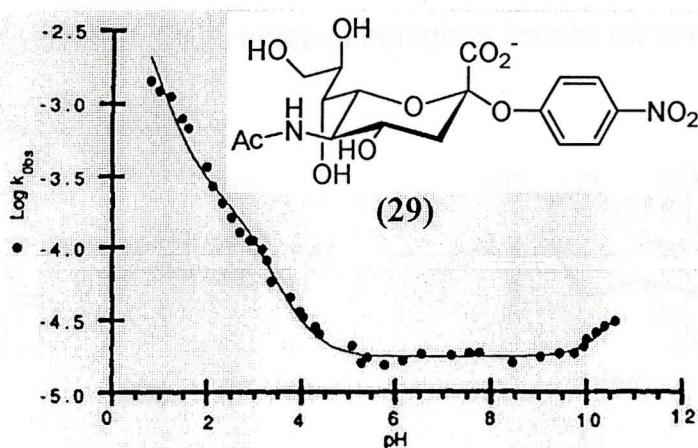
Figure 1.3-17 – Rate vs. pH profile (from ref. 80) and structure of α-p-nitrophenyl NeuAc.

For α-carboxy acetal phosphates the dependence of rate on pH has

not been as extensively studied. Hydrolysis of the α-carboxy acetal

phosphodiester β-CMP-KDO (**30a**) shows only a 3-fold change in rate

between pH 7 and 9.[81] Similarly, β-CMP-NeuAc (**31**) hydrolyzes at the

same rate at pH 8 and 10.[82] At more acidic pHs, where the reaction is

acid-catalyzed, the rate *versus* pH profile shows an inflection near the pK_a

of the carboxylate of β-CMP-NeuAc.[83] Thus, α-carboxy acetal

phosphodiesters show pH-independent and acid-catalyzed regions similar

to **29**. Rate versus pH profiles have been measured for

KDO-β-2-phosphate (**30b**) and KDO-α-2-phosphate (**30c**) between pH 0

and 5.3. No corresponding pH independent region is seen, although the

profile does not extend into the basic region where it is observed for **29**

and **31**. The profiles do show an inflection near the expected pK_a of the

carboxylate, with rate levelling out below this pH.[27]
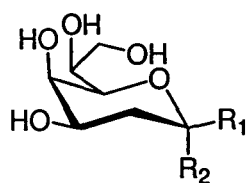
30a: R_1= CMP, R_2= CO_2H
30b: R_1= phosphate, R_2= CO_2H
30c: R_1= CO_2H, R_2= phosphate
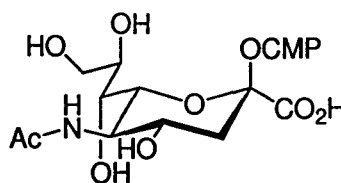
(31)

Insight into the type of acid-catalysis operative for the hydrolysis of

α-carboxy acetal phosphates has been obtained primarily through the

measurement of SDKIEs. **30b** shows a SDKIE of 1.10 at pH 0, consistent

with general acid-catalysis.[27] For **30a**, a SDKIE of 2.7 and buffer catalysis

have been reported at pH 7.5.[81] These measurements are in the

pH-independent region and thus do not give any information about the

type of acid-catalysis, as the authors claim. The SDKIE for **31** hydrolysis

at pH 5 is 0.45.[33] This inverse SDKIE is typical of specific acid-catalysis.

However, the interpretation of this SDKIE may be clouded by kinetic

complexity as described in Figure 1.3-18. If the formation of the tight-ion

pair is reversible, the SDKIE will approach the EIE on step 1, which is

inverse. Thus, even if step 1 is general acid-catalyzed, with an expected

isotope effect > 1, a net inverse isotope effect will be observed. Such

kinetic complexity is supported by increase in the overall rate and increase

in the SDKIE, from 0.45 to 0.66 in the presence of azide. The former

SDKIE is consistent with equilibrium formation of the tight ion pair

complex($\|31\|$). The latter is consistent with azide being an efficient trap

of the ion pair complex (k_3), shifting the observed SDKIE toward the

intrinsic IE on k_1.[33]
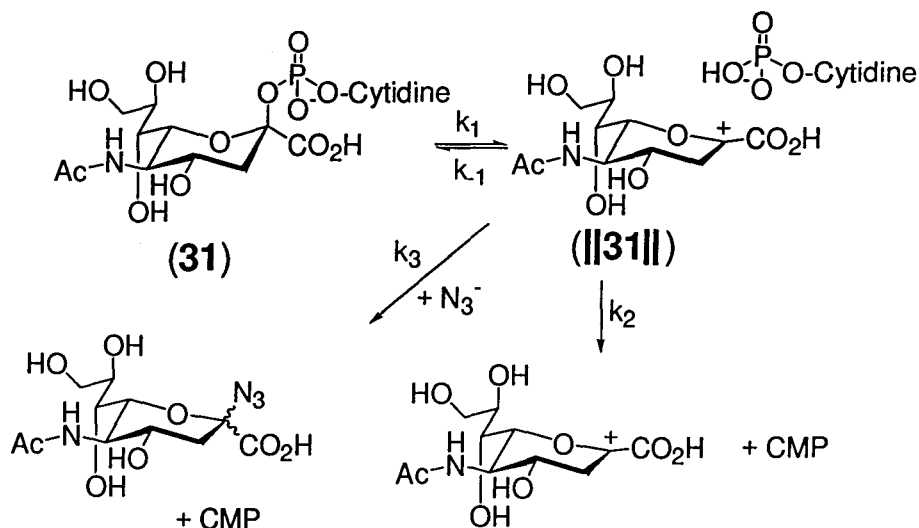
Figure 1.3-18 – Reaction scheme showing possible origin of kinetic complexity in the SDKIEs observed for **31**. The first, reversible, step is dissociation of **31** to form a tight ion pair complex($\|31\|$). Diffussional separation of the complex is the first irreversible step of the reaction. If $k_{-1} \gg k_2$ and $k_1 \gg k_3$ the observed SDKIE will be the EIE on the first step, calculated to be 0.32. If $k_{-1} \ll k_2$ or $k_{-1} \ll k_3$ the observed SDKIE will be the isotope effect on k_1.

1.4 Objectives: Understanding the Chemistry of the MurA THI

Significant mechanistic questions remain regarding the mechanisms of MurA and AroA. Previous study of the breakdowns of MurA and AroA THIs did not allow for any mechanistic conclusions to be drawn. We have therefore studied the non-enzymatic breakdown of the MurA THI in more detail and gained a better understanding of the inherent reactivity of this unstable molecule. What we have learned about the MurA THI's reactivity, together with application of what is understood about related systems, has helped to better define effective catalytic strategies that MurA may be using in promoting catalysis.

Chapter 2   Materials and Methods

2.1   General

UDP-GlcNAc, PEP and fosfomycin were purchased from Sigma.

UV/Vis spectroscopy was performed using quartz cuvettes and a Cary

100Bio spectrophotometer.   Protein purification was performed at 4 °C on

an FPLC chromatographic system (Amersham Biosciences).

Mini-PROTEAN 3 (Bio-Rad) was used for sodium dodecyl sulphate

polyacrylamide gel electrophoresis (SDS-PAGE) (4% stacking gel and a

10% resolving gel) with electrode running buffer (25 mM Tris, 192 mM

glycine, and 0.1% sodium dodecyl sulphate (SDS)) and SDS reducing

buffer ($\leq$ 42 mM Tris-HCl, pH 6.8, $\leq$ 17% glycerol, $\leq$ 0.7% SDS, $\leq$ 0.07%

bromophenol blue, and $\leq$ 3% β-mercaptoethanol).   Preparative and

analytical HPLC were performed on Waters 616 or 626 LC systems

equipped with dual wavelength UV detectors.   All liquid scintillation

counting was done using Liquiscint scintillation fluid (National Diagnostics)

and a Beckman LS 6500 liquid scintillation counter.   Aqueous solutions

were freeze dried using a Centrivap Concentrator (Labconco Corporation).

NMR spectra were acquired on a Bruker AV 200, AV 500, or AV

600 spectrometers.   NMR spectra obtained using the Bruker AV 500 or AV

600 were acquired by Dr. Don Hughes of the Nuclear Magnetic

Resonance Facility at McMaster University (unless otherwise noted).

Mass spectral electrospray ionization data was obtained by the staff at the

McMaster Regional Centre for Mass Spectrometry using a Micromass

Quattro-LC Triple Quadrupole Mass Spectrometer.

2.2   E. coli MurA Subcloning and Expression

E. coli MurA was subcloned from a plasmid expressing E. coli

MurA which was His-tagged, this was a gift from Dr. Martin Pavelka

(University of Rochester). The plasmid from this cell line was used as a

template for the PCR. The primers used were EC_MurA_For_BB–

5'-GAACAAACCATATGGATAAATTTCGTGTTC-3' and

EC_MurA_Rev_BB–5'-CTCTCGGATCCTTACTCGCCTTTCACAC GC-3'

and contained NdeI and BamHI restriction sites, respectively. Once

subcloned into the kanamycin resistant pET41a (Novagen), ECMurA was

expressed as the native protein in BL21 (DE3) cells and more recently in

BL21 *(DE3) cells (Invitrogen).

2.3   E. coli MurA Purification

E. coli MurA was overexpressed using the pET41a expression

plasmid construct in BL21 STAR(DE3). The following purification is for

cells coming from 6L of growth medium. LB broth, containing 30 μg/mL

kanamycin, was inoculated with 60 mL saturated overnight culture and

grown at 37 °C until an OD_{600} of 0.6 was reached. Expression of the MurA

was then induced using 1 mM IPTG, and the cells were incubated at 37 °C

for 4 hours. The cells were then harvested by centrifugation at 5000 × g for 10 min, yielding typically 12-15 g of cells. The bacterial pellet was resuspended in 50 mL of Buffer A (50 mM Tris, pH 7.5, 1 mM EDTA, 1 mM PMSF, 1 mM benzamidine), at which point it was either frozen or used immediately in the purification.

The cells were lysed using 2 passes through a French press. Just before lysis, 100 μg/mL DNase and RNase were added to the resupended cells. After lysis, cell debris was removed by centrifugation at 10000 × g for 10 min. Ammonium sulphate was added to 70% saturation, and the precipitated protein was collected by centrifugation at 50000 × g for 10 min. The protein was redissolved for 1 hour, with mixing, in Buffer B (Buffer A with 1 M $(NH_4)_2SO_4$). Insoluble debris was removed by centrifugation at 50000 × g for 10 min.

Hydrophobic interaction chromatography was used with the supernatant applied at 10 mL/min to a 40 mL column containing Phenyl-Sepharose High-Sub media (Amersham Biosciences) equilibrated in Buffer B. After the absorbance had returned to baseline, the flow rate was reduced to 5 mL/min and a gradient from Buffer B to Buffer A was run over 40 min (200 mL). Fractions (5mL) were collected, and selected fractions were run on SDS-PAGE. Fractions containing MurA were pooled and the $(NH_4)_2SO_4$ in the collected fractions was then exchanged. This was done by concentrating the protein using a 200 mL Amicon

concentrator with a YM-10 membrane. Once the volume was reduced to less than 10 mL, the concentrate was diluted to 200 mL with Buffer A and reconcentrated to 50 mL.

Anion-exchange chromatography was then used, with concentrate applied at 10 mL/min to a 40 mL column containing Q-Sepharose FF media (Amersham Biosciences) equilibrated in Buffer A. Once the sample was applied and the absorbance had returned to baseline, the flow rate was reduced to 5 mL/min and a gradient from Buffer A to Buffer C (Buffer A plus 1M KCl) was run over 40 min (200 mL) collecting 5 mL fractions. Fractions were again assayed for the presence of MurA using SDS-PAGE. MurA was collected and concentrated using the 200 mL protein concentrator to the desired concentration, usually 50-150 mg/mL (1-3 mM). MurA aliquots were then frozen in liquid nitrogen and stored at -80 °C. The typical yield was 250-450 mg per 6 L of initial bacterial culture as judged by the Biorad Protein Assay.

The active concentration of MurA was determined from kinetic assays at 25 °C, containing varying amounts of the irreversible inhibitor fosfomycin. Assay reactions (2 mL) containing ~100 nM MurA, 100 μM UDP-GlcNAc, 50 mM Tris, pH 7.5, and 0, 10, 30, 100, 300, 1000 nM fosfomycin were incubated for 30 min. 100 μM PEP was added and 5 timepoints (375 μL each) were taken at 1, 2, 3, 4, 5 min. The timepoints

were added to 375 μL 2X Malachite Green Reagent[tt] to stop the reaction.

The amount of phosphate produced at each timepoint was quantitated by

measuring the A_{660} and referencing to a phosphate standard curve. The

rate of the MurA reaction for each of the fosfomycin concentrations was

determined by linear fitting of the phosphate versus time data. A plot of

rate-*versus*-fosfomycin concentration was then plotted and linear fitting

gave the active concentration of MurA from the x-intercept (where

[fosfomycin] = [MurA]).

2.4   His –Tagged E. coli MurA Purification

His-Tagged E. coli MurA (His-MurA) was overexpressed using a

pTRCHISB expression plasmid (Novagen) in BL21 STAR(DE3). The

following purification was designed for cells coming from 6L of growth

medium. LB broth, containing 50 μg/mL ampicillin, was inoculated with

60mL saturated overnight culture and grown at 37°C until an OD_{600} of 0.6

was reached. Expression of the His-MurA was then induced using 1 mM

IPTG, and the cells were incubated at 37 °C for 4 hours. The cells were

then harvested by centrifugation at 5000 × g for 10 min, yielding typically

12-15 g of cells. The bacterial pellet was resuspended in 50 mL of Buffer

D (50 mM Tris, pH 7.5, 20 mM imidazole, 300 mM NaCl, 1 mM PMSF,

---

[tt]   This reagent is the same as that used by Lanzetta *et al.,* [87] but twice as
concentrated.

1 mM benzamidine), at which point it was frozen or used immediately in the purification.

The cells were lysed using 2 passes through a French press. Just before lysis, 100 μg/mL DNase and RNase were added to the resupended cells. After lysis, cell debris was removed by centrifugation at 10000 × g for 10 min. Ammonium sulphate was then added to the supernatant to 70% saturation, and the precipitated protein collected by centrifugation at 50000 × g for 10 min. The protein was redissolved in Buffer D for 1 hour with mixing. Insoluble debris was then removed by centrifugation at 50000 × g for 10 min.

The supernatant was applied at 2 mL/min onto a 40 mL column containing Ni-charged Chelating-Sepharose media (Amersham Biosciences), equilibrated in Buffer D. The column was washed thoroughly with Buffer D, then His-MurA was eluted by stepping up to Buffer D but with 500 mM imidazole. The eluted protein was concentrated to 5 mL or less, and then diluted to 200 mL with Buffer A. This was followed by reconcentration of His-MurA typically to 50 mg/mL or about 1 mM. MurA aliquots were then frozen in liquid nitrogen and stored at -80 °C. The typical yield was 50-75 mg per 6 L of initial bacterial culture.

2.5   [^{33}P] PEP Synthesis and Purification

[^{33}P] PEP was synthesized from [γ-^{33}P] ATP (Amersham Biosciences) using the pyruvate kinase exchange reaction.[84] In a reaction

containing pyruvate 2 μM kinase, 1 μM PEP was incubated with 10 μM

pyruvate and $[\gamma\text{-}^{33}P]$ ATP (0.1 μM, 25 μCi). Because the equilibrium

constant for the reaction is 6.6×10^{-5}, only a small amount of ADP is

produced and the concentrations of the other components remain

essentially constant. The label exchanges between the ATP and PEP,

and given the ten-fold excess of PEP, 91% of the label should end up in

the PEP. This would give ideally PEP which was 9.1% labelled.
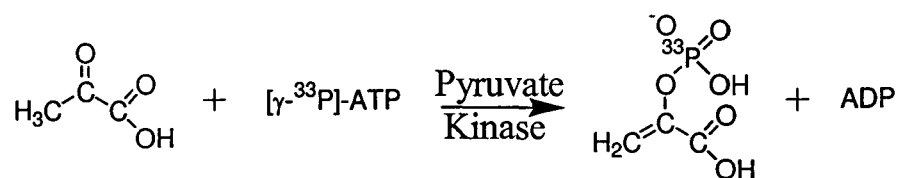
Figure 2.5-1 - Synthesis of $[^{33}P]$ PEP using pyruvate kinase.

PEP was purified in two steps. The concentrations of the reaction

components were too low to detect by UV, therefore standards were run

prior to the purifications, with A_{240} and A_{260} detection, to determine elution

times of each component. First, ATP was separated from PEP and

pyruvate using a C_{18} reverse phase column (YMC-Pack ODS-A 250 X4.6

mm I.D.), with PEP and pyruvate eluting in 50 mM triethylammonium

acetate, pH 6.0, at 1 mL/min then stepping up to 50 mM triethylammonium

acetate (TEAA), pH 6.0, with 20% methanol to elute the ATP. The PEP

fraction was then purified using a 1 mL Hitrap-Q anion exchange column

(Amersham Biosciences) using a gradient from 100 to 500 mM NH_4HCO_3,

pH 10, over 20 min at 1 mL/min. The collected PEP was freeze-dried,

with water added repeatedly until all the NH_4HCO_3 was removed.

2.6   [1-^{14}C] and [^{13}C$_3$] PEP Synthesis and Purification

[1-^{14}C] and [^{13}C$_3$] labelled PEPs were synthesized from [1-^{14}C] and

[^{13}C$_3$] pyruvates (Amersham Biosciences and Cambridge Isotope

Laboratories, respectively) using the enzymatic reaction of pyruvate

phosphate dikinase (PPDK) (a generous gift from Prof. D. Dunaway-

Mariano) (Figure 2.6-1).[85] Labelled pyruvate (10 mM) was incubated

overnight with 15 mM ATP, 10 mM phosphate, 10 U of inorganic

pyrophosphatase, and 10 μL of 2 mg/mL stock of PPDK. The reaction

was monitored using a 1 mL Mono-Q anion exchange column (Amersham

Biosciences) using a gradient from 100 to 500 mM NH_4HCO_3, pH 10, over

30 min at 1 mL/min flow rate with A_{240} and A_{260} detection. Once the

reaction was determined to be complete by HPLC, 10 mM glucose and

1 U hexokinase were added to convert the remaining ATP to ADP. This

was done because ADP was more easily resolved from the PEP than was

ATP. The PEP was then purified by HPLC from the reaction using a

20 mL column, packed with Q-Sepharose HP media (Amersham

Biosciences), using a gradient from 100 to 500 mM NH_4HCO_3, pH 10, with

A_{240} and A_{260} detection. The collected PEP was freeze dried with water

added repeatedly until all the NH_4HCO_3 was removed.
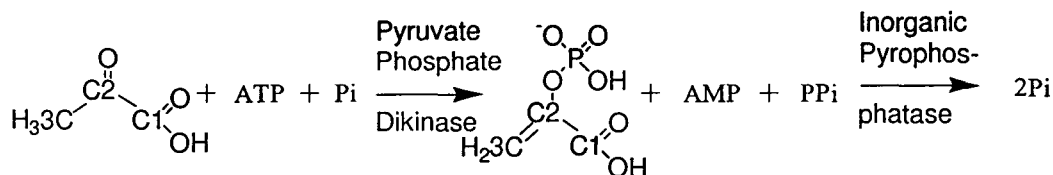
Figure 2.6-1 - Carbon-labelled PEP synthesis from carbon-labelled pyruvates using pyruvate Pi dikinase.

$$\text{Glucose} + \text{ATP} \xrightarrow{\text{Hexokinase}} \text{Glucose-6-Phosphate} + \text{ADP}$$

Figure 2.6-2 - Reaction catalyzed by hexokinase, used to remove excess ATP.

2.7 THI Synthesis and Purification

Reaction mixtures containing 2 mM MurA, 2 mM UDP-GlcNAc, 200 µM PEP, 50 mM potassium phosphate, pH 7.5, were prepared and quenched after 5 s with KOH to 200 mM. The quenched reaction was extracted repeatedly with chloroform to remove the protein. Vigorous mixing using a vortexer for 2 min (with each extraction step) was needed to precipitate and remove all the protein. For the characterization of the THI and its breakdown products, the THI was purified on a 1 mL Mono-Q anion exchange column with a gradient of 100 to 500 mM NH_4HCO_3, pH 10, over 30 min at 0.5 mL/min and A_{260} and A_{280} detection. After collection of the THI, it was freeze-dried with repeated addition of dilute NH_4OH until all the NH_4HCO_3 was removed.

For kinetic studies of the breakdown of the THI, THI was purified on the 1 mL Mono-Q anion exchange column with a gradient of 100 to 500 mM KCl in 10 mM NH_4Cl, pH 10, over 30 min at 0.5 mL/min with A_{240} and A_{260} detection. The syntheses and purifications of $[^{13}C_3]THI$, $[^{14}C]THI$,

[^{33}P]THI were as above, but with the appropriately labelled PEP. For the radiolabeled THIs 0.25-0.5 μCi [^{14}C]PEP or [^{33}P]PEP was used per reaction.

2.8   Characterization of the THI and its Breakdown Products

The THI was characterized by electrospray-mass spectrometry. The radioactive products of the breakdowns of [^{14}C]THI and [^{33}P]THI and were purified by HPLC and the characterized using liquid scintillation counting. [^{13}C$_3$]THI was characterized by ^{31}P and ^{13}C NMR on the AV 600 (acquired by Jason Lee). [^{13}C$_3$]THI was broken down in NH$_4$HCO$_3$ at pH 7.5 overnight and the [^{13}C$_3$]ketal product (25 nmol) was repurified and characterized by NMR. One dimensional ^{1}H, ^{13}C, and 2-dimensional HMBC spectra were collected using the AV 600. The HMBC spectrum was collected in 128 increments with 256 scans per increment and a delay time of 1 s between scans. The data were linear-predicted in F$_1$ to 1024 points before Fourier transformation. The spectra were collected without ^{13}C decoupling, so correlations are seen to the ^{13}C satellites of the methyl signal in the ^{1}H spectrum.

2.9   Kinetic Studies of Non-Enzymatic THI Breakdown

2.9.1 pH Dependence of Rate and Product Distribution

The THI was allowed to breakdown at 25 °C over a range of pH

from 1-12. The rate of breakdown and distribution of products was

monitored by HPLC. As purified THI contained ~300 mM KCl and 10 mM

NH_4Cl, it was diluted 10-fold into the breakdown reactions to minimize salt

effects from KCl, and buffering from NH_4Cl. The breakdown reactions

contained, per timepoint, 50 μL THI (1 to 2 nmol), diluted with 450 μL

buffer (50 mM final concentration, except for HCl[‡‡]) at the desired pH. In

general, 5 to 7 timepoints were used at each pH, resulting in total reaction

mixture of 2.5-3.5 mL. The buffers used were: pH < 2, HCl; pH 2.5 to 3.5,

glycine; pH 4.0 to 5.5, acetate; pH 6.0 to 9.5, Bis-Tris propane; pH 7.5 to

8.5, Tris; pH 9.5 to 10.5, glycine; pH 12, KOH. For each reaction, a test

mixture consisting of 100 μL of 10 mM NH_4Cl and 900 μL 56mM buffer

was made, and the pH measured and recorded as the pH of the

breakdown reaction. At pH $\geq$ 9, KOH traps were used to prevent

atmospheric CO_2 from entering the solution and lowering the pH. Without

KOH traps the breakdown of the THI was not first order, but instead

accelerated as the pH dropped over time.

[‡‡]   When using HCl to control the pH of the breakdown reactions, the final
concentration of HCl was about 100 mM, 33 mM, 10 mM in the pH 1, 1.5, 2 reactions,
respectively.

All reaction timepoints were stopped by adding KOH to pH 12, as judged by pH paper (with a pH range from 10-12), bringing the volume to 1 mL. After stopping the reaction timepoints, they were stored at 4 °C for no more than 16 h before analysis by HPLC. The HPLC method used for analysis of the reaction timepoints was similar to the purification of the THI. A 1mL Mono-Q anion exchange column with a gradient of 100 to 500 mM KCl in 10mM NH_4Cl, pH 10, was used. However, the length of the gradient was 15 min and the flow rate was 1 mL/min. A_{240} and A_{260} detection was used, but only the 260 nm channel, where absorbance is due only to the uridine ring, was used to quantitate UDP-GlcNAc, MurA ketal, EP-UDP-GlcNAc and THI peaks. Percentages of each of the four compounds present, in each timepoint, were calculated from the area of the peak for the given compound, divided by the total area of the peaks for all four compounds. The rate of THI breakdown was then determined by fitting a percent degradation versus time graph to a first order curve using Grafit (Erithacus Software Ltd.). From this rate and the ratios of the products formed (in the final timepoint), the rates of the formations for the products was calculated using:

$$k_A = k_{THI} Xf_A \qquad (1)$$

where k_A is the rate of formation of product A, k_{THI} is the rate of THI breakdown, and f_A is the fraction of product A produced. To better determine the fraction of MurA ketal and EP-UDP-GlcNAc products at pH

$\leq$ 4, 2 mL reactions containing 200 μL of purified THI were allowed to breakdown completely, were brought to pH 12 with a minimal volume of KOH and the product distribution determined by HPLC as above.

2.9.2 Data analysis

The rate of disappearance (k) of the THI was determined by fitting to (2) using Grafit. Where A_t is the amount of THI at time t, and A_∞ is the amount of THI at infinite time.

$$A_t = A_\infty(1-e^{-kt}) \qquad (2)$$

pK$_a$ values for rates and product distributions were fitted by non-linear regression to equations for single (3) or double ionizations (4), with proportional weighting of data points, using Grafit. For k *versus* pH profiles, y = k_i, the rate constant at pH = i, $Limit_1$ to $Limit_3$ were k_{max}, k_{mid}, and k_{min} at the extremes of pH, and pK_j = pK_{a2}, pK_k = pK_{a4}. For product *versus* pH profiles, y = $f(X)_i$, the fraction of product X formed at pH = i, $Limit_1$ to $Limit_3$ were $f(X)_{low}$, $f(X)_{mid}$, and $f(X)_{high}$ at the extremes of pH, and pK_j = pK_{a1}, pK_k = pK_{a3}.

$$y = \frac{Limit_1 + Limit_2 \bullet 10^{(pH-pK_j)}}{10^{(pH-pK_j)}+1} \qquad (3)$$

$$y = \frac{Limit_1 + Limit_2 \bullet 10^{(pH-pK_j)}}{10^{(pH-pK_j)}+1} - \frac{(Limit_2 - Limit_3) \bullet 10^{(pH-pK_k)}}{10^{(pH-pK_k)}+1} \qquad (4)$$

For some fitted curves for product distributions, the limits at extrema were fixed, *i.e.* $f(3)_{low}$ = 1.0, $f(4)_{low}$ = 0, and $f(5)_{low}$ = 0. Fixing

these values in the fitted curves gave greater consistency in pK_as. When not fixed the fitted values of $f(X)_{low}$ were within 0.004 of the fixed values.

2.9.3 Solvent Deuterium Isotope Effect

The solvent deuterium KIE was measured at pL 2.0, at 25 °C. Except for the inclusion of D_2O, the rate of breakdown was measured with the same protocol as was used for the pH dependence study (Section 2.9.1). Buffers used for the reactions in D_2O were adjusted to pL 2.0 using concentrated HCl and a pH meter. The amount of H_2O introduced from the concentrated HCl was negligible, with the final buffer solution being approximately 99.9% D_2O. The pH meter reading was adjusted using (5),[86]

$$pL = pH(meter\ reading) + 0.3314n + 0.0766n^2 \qquad (5)$$

where n is the atom fraction of deuterium. In the reaction mixtures them selves the 50 μL of purified THI (in H_2O), was mixed with 450 μL D_2O buffer. Thus the resultant reaction mixtures were 90% D_2O.

2.9.4 Breakdown of [33P]THI in Aqueous Methanol

[33P]THI was allowed to breakdown in 50% (v/v) methanol to determine if methyl [33P]phosphate would be produced. Under the conditions used, methyl [33P]phosphate production would only occur if P-O bond breakage was occurring in the hydrolysis of the THI. Reaction conditions were identical to those for the pH dependence study (Section

2.9.1), except for the inclusion of 50% methanol. The breakdown reactions were allowed to go to completion at pH 2, 8, 9, 10 and compared to reactions at the same pH, without methanol. The concentration of THI used did not allow for detection of phosphate and methyl phosphate by absorbance. Therefore, immediately before loading on the HPLC, 5 µmol methyl phosphate and 0.5 µmol phosphate were added to the reactions. The products were separated on a 1 mL Mono-Q column with a gradient of 20 to 500 mM KCl in 10 mM KOH, pH 12, over 15 min at a flow rate of 1.0 mL/min.

Fractions (0.33 mL) were collected and the Malachite Green assay was used to detect phosphate.[87] Because methyl phosphate was not detectable by the Malachite Green assay. It was first treated with alkaline phosphatase (Sigma) to liberate phosphate. Fractions which only reacted with Malachite Green after treatment with alkaline phosphatase were deemed to contain methyl phosphate. After fractions containing phosphate and methyl phosphate were identified, the amount of radioactivity in the fractions was determined using liquid scintillation counting. To ensure that methyl phosphate was produced and could be detected if P-O bond cleavage was occurring, [γ-^{33}P]ATP was broken down at pH 7 in 50% methanol in the presence of 10 mM Ca^{2+} at 25 °C overnight. Under these conditions P-O bond cleavage with the release of the γ-phosphate of ATP is known to occur[88].[89]

2.10   Enzymatic Reaction Intermediate Studies

2.10.1   Search for the Enzymatic MurA Ketal

AroA ketal has been shown to form from incubation of the AroA reaction at equilibrium.[90] The corresponding experiment with the MurA reaction was done, with HPLC used to monitor the production of MurA ketal. A reaction containing 38 mM UDP-GlcNAc, 75 mM PEP, 100 mM phosphate, pH 7.6, and 0.3 mM MurA was prepared and monitored over 15 days at 25 °C. Samples from the reaction were analyzed by anion exchange chromatography using a 1 mL Mono-Q column with a gradient of 100 to 500 mM NH_4HCO_3, pH 10, over 30 min at 0.5 mL/min flow rate with A_{240} and A_{260} detection.

Experiments were also performed to investigate whether denaturation of MurA, from a reaction at equilibrium, would release any oxocarbenium ion intermediate, which would partially degrade to the MurA ketal. The MurA reaction was quenched with base, so that the THI was stable, and thus any MurA ketal produced would have to come from the release of an oxocarbenium ion intermediate. A reaction containing 100 μM [1-^{14}C] PEP (0.25 μCi), 2 mM UDPGlcNAc, 50 mM phosphate, pH 7.6, and 500 μM MurA was prepared. It was quenched <5 s after addition of enzyme to 167 mM KOH. The reaction mixture was separated on a Mono-Q column using a gradient from 100 to 500 mM NH_4HCO_3, pH 10, over 30 min at 0.5 mL/min flow rate with A_{240} and A_{260} detection. Fractions

(0.2 min) were collected between PEP and EP-UDP-GlcNAc, and the radioactivity in the fractions was determined by liquid scintillation counting. The PEP peak trailed significantly. In order to determine whether the MurA ketal peak was present, hidden under the PEP peak, eluate between the PEP and EP-UDP-GlcNAc peaks was collected, re-injected and the fractions collected and counted as before.

2.10.2   NMR of the MurA Reaction at Equilibrium

The AroA reaction at equilibrium, using [2-^{13}C] PEP as a substrate, has been investigated using NMR. In the NMR spectrum, signals from PEP and EPSP have been identified as well as those for the THI and ketal.[91] The same experiment with MurA could potentially give signals for the MurA bound THI as well as any other enzyme bound intermediates. The NMR spectra of oxocarbenium ions have been reported for stable aromatic oxocarbenium ions. These studies have shown that the cationic carbon can have a range of chemical shifts, from 170-220 ppm.[92]

To determine if any intermediate in addition to the THI could be seen by NMR, a MurA reaction was prepared containing 2 mM [^{13}C$_3$]PEP, 2 mM UDP-GlcNAc, 50 mM phosphate, pH 7.6, and 2.6 mM MurA. An overnight 1D-^{13}C-NMR spectrum was acquired on the AV 500, with a spectral width from 0-220 ppm. A 2D-INADEQUATE experiment was also performed on the AV 500. 2D-INADEQUATE detects carbon-carbon coupling, which could potentially detect the C2 carbon of the

oxocarbenium ion intermediate via coupling to unassigned carbons in the 1D-^{13}C-NMR spectrum.

2.10.3   Enzymatic Partitioning of THI

Experiments with AroA have shown that purified AroA THI can be added back to AroA resulting in partitioning of the THI to S3P and EPSP.[22;28] At pH 7.5, partitioning results in 3:1 EPSP to S3P. The reaction of the AroA THI to occurs with an almost diffusion controlled rate. The corresponding experiment with MurA is made more difficult by the existence of the covalent phospholactoyl-enzyme adduct,[16] which would prevent reaction of MurA with the THI. Thus, partitioning experiments were with MurA to which a 2-fold excess of UDP-GlcNAc was added. Reactions containing varying concentrations of MurA and UDP-GlcNAc, 50 mM Tris, pH 7.5, and 2000 cpm [^{14}C]THI were stopped at various times by bringing the pH to 12 with KOH. The products of the partitioning experiments were determined using HPLC with a 1 mL Mono-Q anion exchange column with a gradient of 100 to 500 mM NH_4HCO_3, pH 10, over 30 min at 0.5 mL/min flow rate with A_{240} and A_{260} detection.

The pyruvate (indicative of non-enzymatic breakdown), PEP, EP-UDPGlcNAc and THI peaks were collected and the radioactivity present in the peaks determined using liquid scintillation counting. The partitioning ratio was determined from the ratio of PEP to EP-UDPGlcNAc. The second order rate constant for reaction of THI with MurA was

determined from the pseudo first-order rate of breakdown of the THI divided by the enzyme concentration. This pseudo first-order rate was determined by calculating the approximate half-life of the THI from the percentage THI broken down and the length of time the reaction was incubated before quenching.

Chapter 3   Results

3.1   E. coli MurA Purification

The purification of MurA involved first lysing the cells using a

French press. Two passes through French press were found to give

efficient lysis. Addition of DNase and RNase before lysis was essential in

order to keep the lysate from forming clumps. Overall it was found that

using buffers, at every step, which contained the protease inhibitors

PMSF, benzamidine and EDTA, increased protein yield and gave MurA

with a higher specific activity.

Both the hydrophobic interaction chromatography and

anion-exchange steps were capable of handling up to 250 mg of MurA per

run. During the hydrophobic interaction chromatography MurA came off in

a broad peak in the middle of the gradient (Figure 3.1-1). During the

anion-exchange chromatography MurA eluted in the first of two peaks

(Figure 3.1-2). The second peak contained no protein, and is believed to

results from the products of DNA and RNA hydrolysis. The MurA

collected could be concentrated to 50-150 mg/mL or 1-3 mM. Attempts at

concentrating the protein further led to the formation of a thick gel. The

typical yield was 250-500 mg per 6 L of initial bacterial culture.
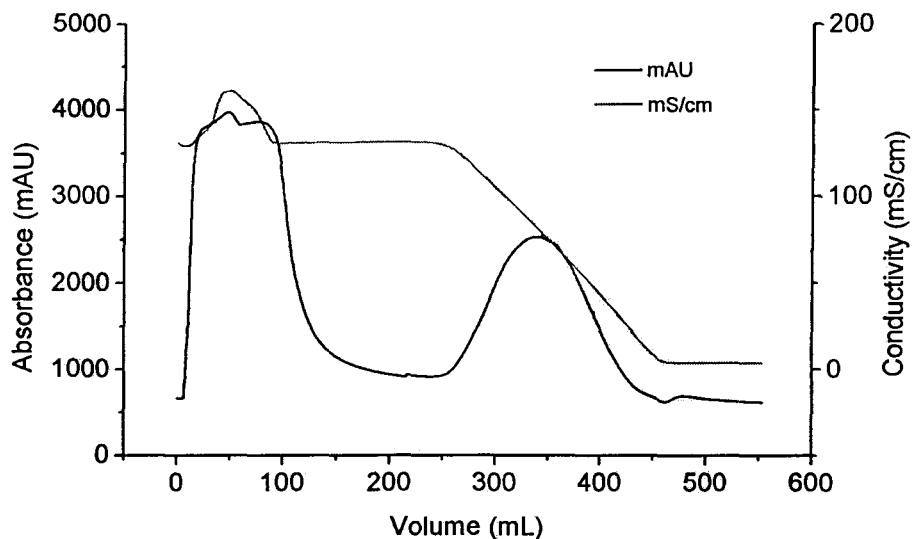
Figure 3.1-1 – Chromatogram from MurA purification on a 40 mL column containing Phenyl-Sepharose High-Sub media. MurA eluted in the 330 mL peak.
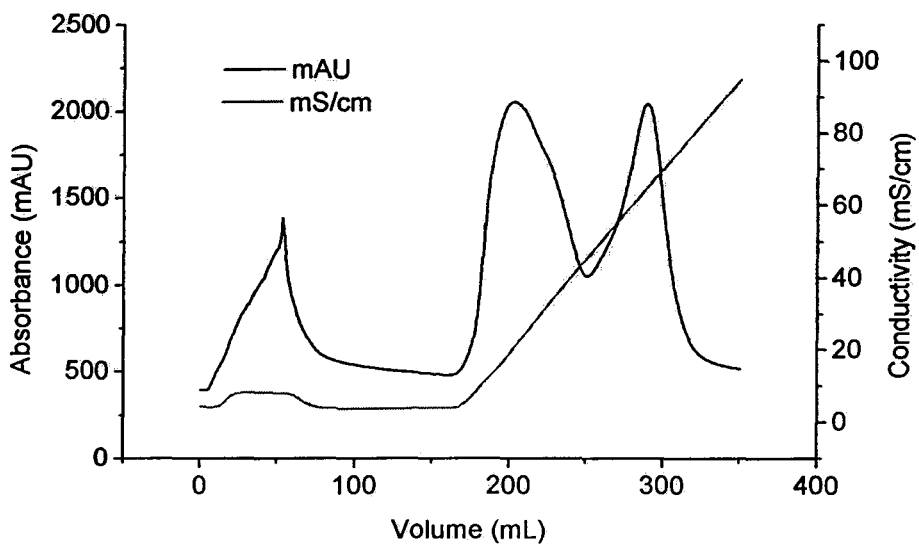
Figure 3.1-2 – Chromatogram from the purification of MurA on a 40 mL column containing Q-Sepharose FF media. MurA eluted in the 200 mL peak.

Purified MurA was generally >95% pure (data not shown). The

concentration of active MurA, which was determined using the fosfomycin

titration, closely paralleled the concentration by absorbance at 276 nm using an ε_{276} of 13000 $M^{-1}cm^{-1}$ (determined by the method of Edelhoch).[93] The Biorad assay gave similar results when the bovine gamma globulin standard curve was used as a reference.

3.2   His –Tagged E. coli MurA Purification

As with MurA, His-MurA was purified in the presence of the protease inhibitors PMSF and benzamidine, but EDTA was not used because it interfered with the subsequent chromatographic step. The Ni-affinity chromatography had a capacity of up to 200 mg of His-MurA per run. After washing the protein on the column, and stepping the imidazole concentration to 500 mM, His-MurA eluted in a single peak (Figure 3.2-1). Difficulty was encountered during concentration of His-MurA, as precipitation of His-MurA occurred as the concentration approached 1 mM.
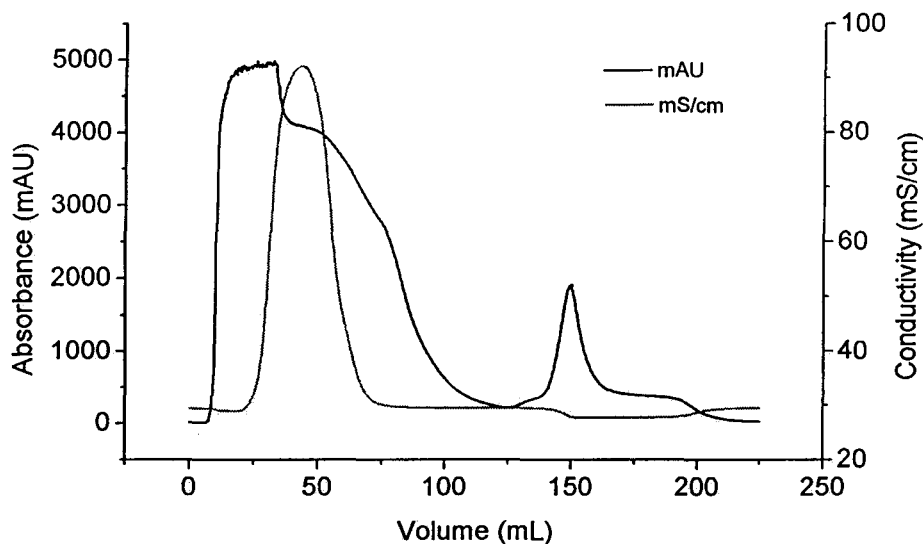
Figure 3.2-1 — Ni-affinity chromatogram of His-MurA on a 40 mL. MurA eluted in the 150 mL peak.

Several attempts at determining the concentration of His-MurA

using the fosfomycin titration failed, as it seemed to take a significantly

longer time for fosfomycin to react with the enzyme. Measurement of the

His-MurA concentration by absorbance at 276 nm or using the Biorad

assay gave results which seemed to be 2-5 times higher than the activity

of the protein implied. The typical yield was 50-100 mg per 6L of initial

bacterial culture. The purity of the His-MurA was >90% as judged by

SDS-PAGE.

3.3   [^{33}P] PEP Synthesis and Purification

The reverse phase chromatography step effectively separated

[γ-^{33}P] ATP (20.0 min) from PEP (4 min) (Figure 3.3-1). The

anion-exchange which was meant to separate PEP (17 min) from cold

impurities, also showed a second, unexpected, radioactive peak from

phosphate (6 min) (Figure 3.3-1). The nature of the method used for [^{33}P]

PEP synthesis gave a large excess of cold PEP in the stock [^{33}P] PEP.

During the purification the fraction of radioactivity in the PEP was

monitored, allowing an approximate total PEP concentration in the [^{33}P]

PEP stock of 87nM to be determined. Based on the specific activity of

2500 Ci/mmol of the [γ-^{33}P] ATP stock, the concentration of [^{33}P] PEP was

calculated to be 0.7 nM. This indicates a percent labelling of only 0.8%,

some ten-fold lower than expected.
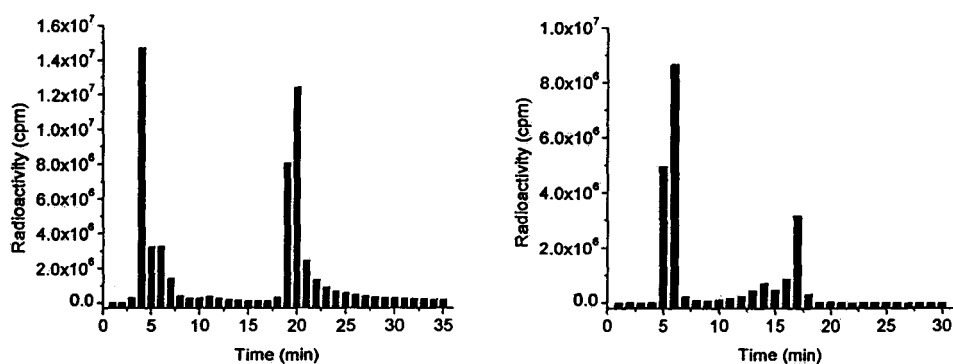
Figure 3.3-1 – (Left) Reverse phase purification of [^{33}P] PEP synthesis. Phosphate (4 min) and PEP (6 min) separated from ATP (20min). Fractions 4-7 were pooled (Right) Hitrap-Q anion exchange purification of fraction 4-7 of reverse phase. PEP (17 min) is separated from pyruvate (contains no radioactivity) and P$_i$ (6 min) using a gradient from 100-500mM NH$_4$HCO$_3$ over 20 min. Fractions at 16-18min were collected as PEP.

3.4   [1-^{14}C] and [^{13}C$_3$] PEP Synthesis and Purification

Monitoring of the reaction was simplified by a 1.5-fold excess of

ATP relative to the labelled pyruvate. The reaction was deemed complete

when the AMP absorbance at 260 nm peak was twice the size of the ATP

peak using the 1 mL Mono-Q anion exchange column chromatrography.

Up to 10 μmol was purified, per run, using the 20 mL column, packed with

Q-Sepharose HP media. The PEP (17 min) was the final peak to come

elute. Less than 5% of the ADP remained in PEP collected after

purification, with greater than 90% of the PEP being recovered. The

structure of the [$^{13}C_3$] PEP was confirmed using ^{13}C NMR (Appendix A -

Figure A-4, Table 3.4-1). The chemical shifts of the [$^{13}C_3$] PEP matched

those of unlabelled PEP(data not shown).

Table 3.4-1 - ^{13}C NMR chemical shifts and coupling constants for the [$^{13}C_3$]PEP.

	δ (ppm)	^1J (Hz)
C1	172.5	76.2 (C2)
C2	149.8	76.2 (C1), 80.2 (C3)
C3	100.5	80.2 (C2)
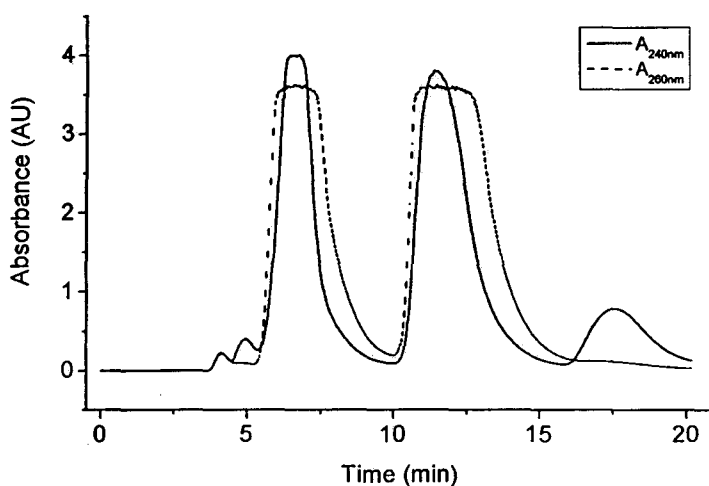
Figure 3.4-1 – HPLC chromatogram from purification of PEP on 20mL Q-Sepharose HP column. Elution times: AMP (6.5min), ADP (11min) and PEP (17min).

3.5   THI Synthesis and Purification

Optimal yields of THI were achieved with reaction mixtures containing 2 mM MurA, 2 mM UDP-GlcNAc, 200 μM PEP, 50 mM potassium phosphate, pH 7.5. Use of MurA which was >90% active was important for good THI yield. Also, concentrations of PEP higher than 200 μM gave reduced yields. The speed with which the reactions were quenched with 200 mM KOH did not affect the yield greatly. However, quenching immediately (<5 s) did give slightly better yields. THI yields of 3-10% of the MurA concentration were typical.

Efficient extraction of MurA from the quenched reaction was important to prevent contamination of the Mono-Q column. For small scale reactions (<1 mL), repeated extraction with 0.5 volumes of chloroform was effective. For larger reactions 1 volume of chloroform was used to prevent the precipitating MurA from forming a thick gel. After each extraction, it was also necessary to back extract the precipitated MurA with chloroform to prevent the loss of aqueous phase caught up in the precipitate. Purification of the THI on the 1 mL Mono-Q, whether with the NH_4HCO_3 or KCl/NH_4Cl buffer systems, resulted in THI eluting as the final peak (Figure 3.5-1). Both buffer systems also routinely gave THI that was >98% pure.
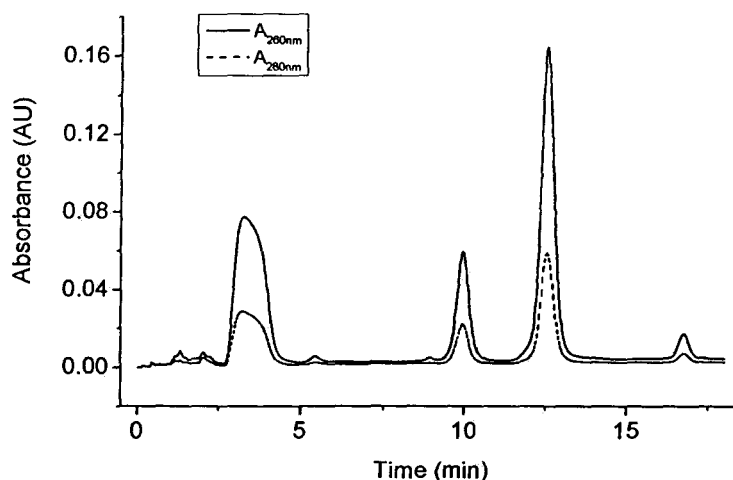
Figure 3.5-1 - HPLC chromatogram of THI synthesis reaction on a Mono-Q column. Elution times: UDP-GlcNAc (3 min), UDP-MurNAc (10 min), EP-UDP-GlcNAc (12.5 min) and THI (17 min).

One surprising observation from the THI purification was the peak at 10 min (Figure 3.5-1). This peak was collected and identified by 1H NMR. The 1D-spectrum was similar to that of UDP-GlcNAc except for a doublet (1.35 ppm) integrated to 3 protons, and a quartet (4.29 ppm) integrated to 1 proton (spectrum not shown). Coupling between these peaks was confirmed using a 1D-TOCSY experiment on the same sample. In this experiment irradiation of the signal at 1.35 ppm resulted in magnetization transfer to the signal at 4.29 ppm (Figure A-5). They correspond to the expected $-CH-CH_3$ group in UDP-MurNAc, confirming its identity. Both KOH and HCl quench of MurA without substrates showed that UDP-MurNAc is present within the enzyme preparation. The importance of UDP-MurNAc binding to MurA is currently being studied by our group.

3.6   Characterization of the THI and its Breakdown Products

Characterization of the THI previously showed incorporation of ^{14}C or ^{32}P into the THI when the corresponding labelled PEP was used.[15] As well, the ^1H, ^{13}C and ^{31}P NMR spectra of [2-^{13}C] THI were acquired.[15] Our characterization of the THI involved first similar experiments showing incorporation of ^{14}C and ^{33}P into the THI. The ^{31}P and ^{13}C NMR spectra of [$^{13}C_3$] THI were acquired. The ^{31}P NMR spectrum was similar to the published spectrum (Appendix A - Figure A-6 and Table 3.6-1). The ^{13}C NMR spectrum (Appendix A - Figure A-7 and Table 3.6-1) gave the chemical shift and coupling constant of the three carbons in the lactoyl group (Figure 3.6-1). An electrospray-mass spectrum of the THI in the anion mode also showed the expected m/z of 774.2 for the THI monoanion (Appendix A - Figure A-1).
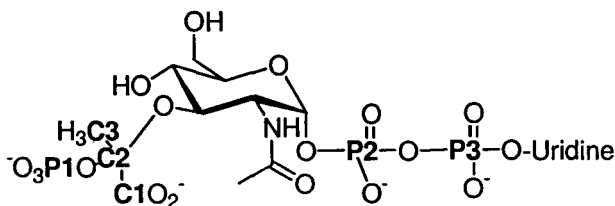
Figure 3.6-1 — Structure of the THI, showing the three phosphate groups and numbering of the carbons originating from PEP.

Table 3.6-1 — ^{13}C and ^{31}P NMR chemical shifts and coupling constants for the THI

	δ (ppm)		δ (ppm)	^1J (Hz)	^2J (Hz)
P1	-3.5	C1	175.4	71.3 (C2)	10.6 (C3)
P2	-13.5	C2	100.7	71.3 (C1), 45.2 (C3)	7.5 (P1)
P3	-15.5	C3	24.5	45.2 (C3)	10.6 (C1)

The products of the THI breakdown were previously reported to be only UDP-GlcNAc, pyruvate and phosphate.[9] We have confirmed these products via incorporation of ^{14}C and ^{33}P into pyruvate (Figure 3.6-2) and phosphate (Figure 3.7-5), respectively, when the appropriately labelled THI was used. The identity of UDP-GlcNAc was confirmed via co-elution with a known standard (data not shown). In addition two other products have been identified as EP-UDP-GlcNAc and the MurA ketal (Figure 3.6-3). These products are formed when the breakdown of the THI occurs under alkaline conditions. [14]C is incorporated into both products when [^{14}C] THI is broken down (Figure 3.6-2). EP-UDP-GlcNAc was confirmed via co-elution with a standard prepared from reaction of PEP and UDP-GlcNAc in the presence of MurA (data not shown).
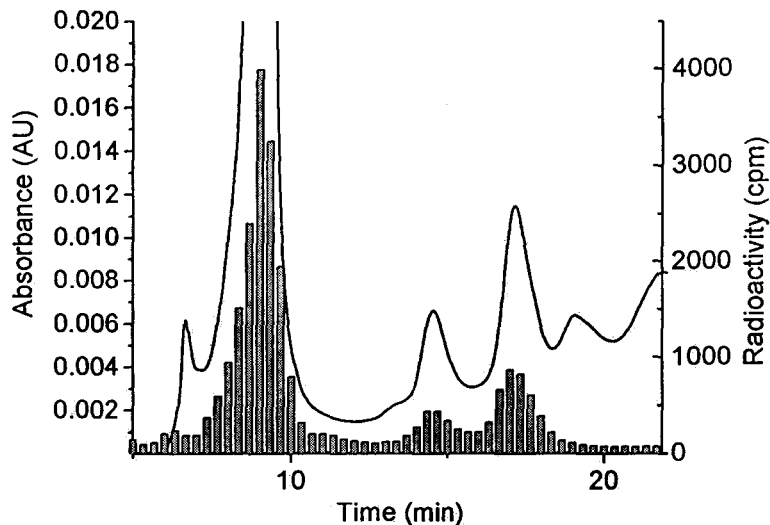
Figure 3.6-2 - - Mono-Q HPLC chromatogram of [^{14}C] THI (100 000 cpm), which was broken down at pH 7 overnight. Elution times: UDP-GlcNAc (8 min), MurA ketal (14.5 min) and EP-UDP-GlcNAc (17 min). The large radioactivity peak is pyruvate, the other two correspond to the MurA ketal and EP-UDP-GlcNAc peaks.

No standard existed for the MurA ketal. Thus [^{13}C$_3$]THI (1.7 µmol) was broken down at pH 7.5 and the MurA ketal was purified from the breakdown products. This resulted in 25 nmol of the MurA ketal, which was only about 25% pure, having approximately 1 eq of EP-UDP-GlcNAc and 2 eq of UDP-GlcNAc present as contaminants. These contaminants prevented full characterization of the MurA ketal by ^{1}H NMR. However, a doublet with a chemical shift characteristic of a methyl was distinguished from signals expected from the contaminants (Appendix A - Figure A-11 and Table 3.6-2). ^{13}C NMR showed a signal at the expected chemical shifts, and having the expected coupling constants, for the MurA ketal C1 and C3. In addition, the same spectrum showed signals for all three

carboxyvinyl carbons of EP-UDP-GlcNAc (Appendix A - Figure A-8 and

Table 3.6-2).
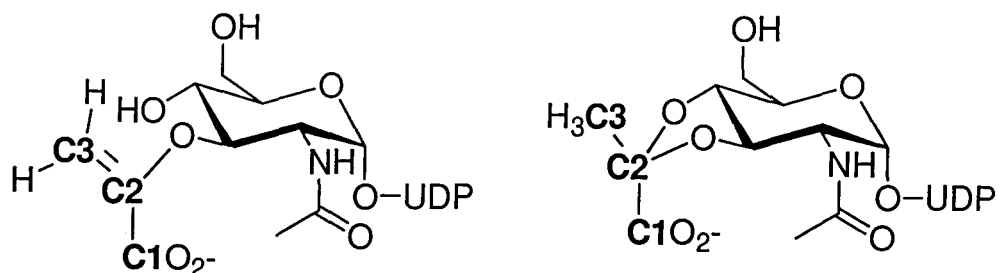
Figure 3.6-3 - Structures of EP-UDP-GlcNAc and the MurA ketal, showing numbering of the carbons originating from PEP.

Table 3.6-2 – ^{13}C and ^1H NMR chemical shifts and coupling constants for EP-UDP-GlcNAc and the MurA ketal.

		δ (ppm)	^1J (Hz)	Comments
MurA ketal	C1	176.4	67.3 (C2)	weak
	C2	107.8	67.3 (C1), 43.6 (C3)	
	C3	22.0	43.6 (C2)	weak
	H-3	1.54	128.5 (C3)	
EP-UDP-GlcNAc	C1	170.1	74.1 (C2)	
	C2	155.2	74.1 (C1), 80.7 (C3)	
	C3	94.1	80.7 (C2)	

Identification of the expected signal between 90 and 110 ppm for

the MurA ketal C2 was made difficult by a broad signal resulting from the

spectrometer probe glue (Appendix A - Figure A-8). Removal of this

signal was made possible using trapezoidal multiplication to cut off the first

2.5 msec of the FID. The resulted in a spectrum where the broad signal

was diminished (Appendix A - Figure A-9). From this spectrum expansion

of the region from 105-110 ppm showed a weak signal (107.8 ppm) which

had the expected chemical shift, multiplicity and coupling constant as that

expected of the MurA ketal. However, this signal was too weak to be

conclusive. An HMBC spectrum of the same sample showed a correlation

between the MurA ketal methyl (H-3, 1.54 ppm) and C3 (22.0 ppm) and

the signal at 107.8 ppm which was thus assigned to C2 (Appendix A -

Figure A-11).

3.7   Kinetic Studies of Non-Enzymatic THI Breakdown

3.7.1 pH Dependence of Rate and Product Distribution

The KCl/NH_4Cl buffer system was used in preference to NH_4CO_3

for anion exchange on Mono-Q columns, during the kinetic study due to

minimal background absorbance over the course of the gradient. This

allowed measurement of the minor product, EP-UDP-GlcNAc, down to

0.2% of the total products, from an initial 1 to 2 nmol of THI. Below 0.2%

the EP-UDP-GlcNAc peak was visible but not quantiatable.

Disappearance of the THI peak was accompanied by appropriate

increases of the product peaks (Figure 3.7-1). The disappearance of the

THI could be fit to a first order curve (Figure 3.7-2). During later

experiments the preparation of the THI resulted in an unknown impurity,

which could not be resolved from the THI by HPLC. This impurity did not

degrade over the duration of the experiments, and thus the area of the

impurity and the THI peaks were summed at each timepoint. Fitting of the

summed disappearance over time still gave a first order decay, with

comparable rates to assays where the impurity was absent (data not

shown).
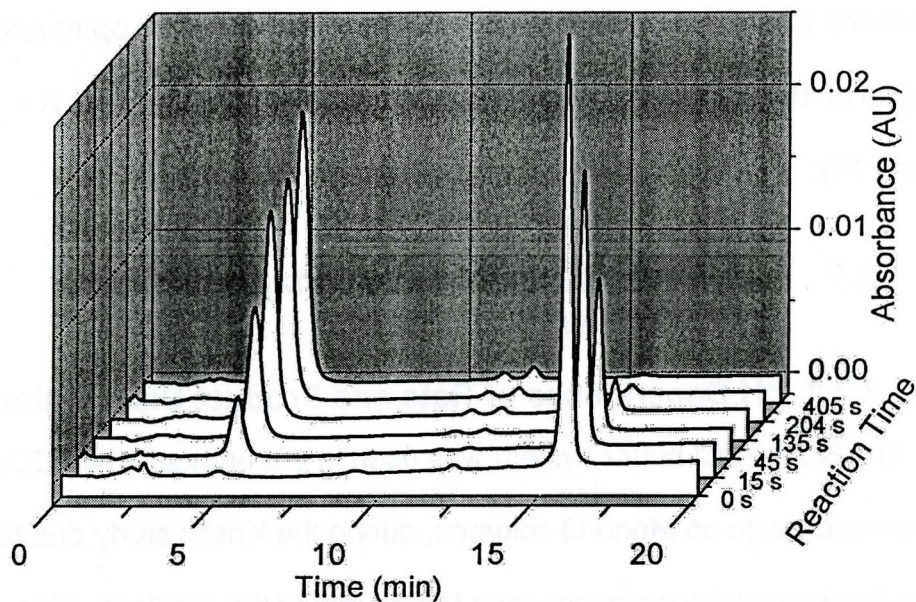
Figure 3.7-1 - Overlay of HPLC chromatograms for the different timepoints in the
breakdown of the THI at pH 5. Each sample contains material from initially 1 to 2 nmol
THI. Elution times: UDP-GlcNAc (4.9 min), MurA ketal (11.5 min), EP-UDP-GlcNAc
(12.3 min) and THI (15.7 min).
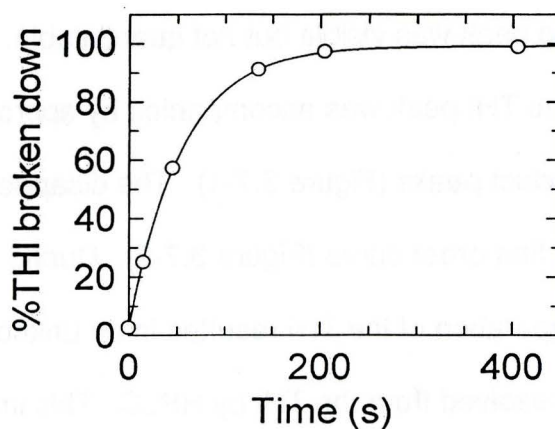
Figure 3.7-2 - THI breakdown at pH 5 is plotted as a percent disappearance, and fitted to
equation 2. The data is from the chromatograms in Figure 3.7-1.

The rate of the THI breakdown, in general, increased towards acidic pH. The rate versus pH profile was fit to two ionizations (equation 4), with $pK_{a2} = 3.2 \pm 0.1$ and pK_{a4} 8.9 ± 0.3. Below pK_{a2} the rate was pH independent. Above pK_{a2} the reaction showed acid-catalysis, with a slope of -1 on the log k vs. pH plot. Above pK_{a4} the acid-catalyzed rate was 6-fold higher (Figure 3.7-3 and Appendix B - Table B-1, Table B-2).
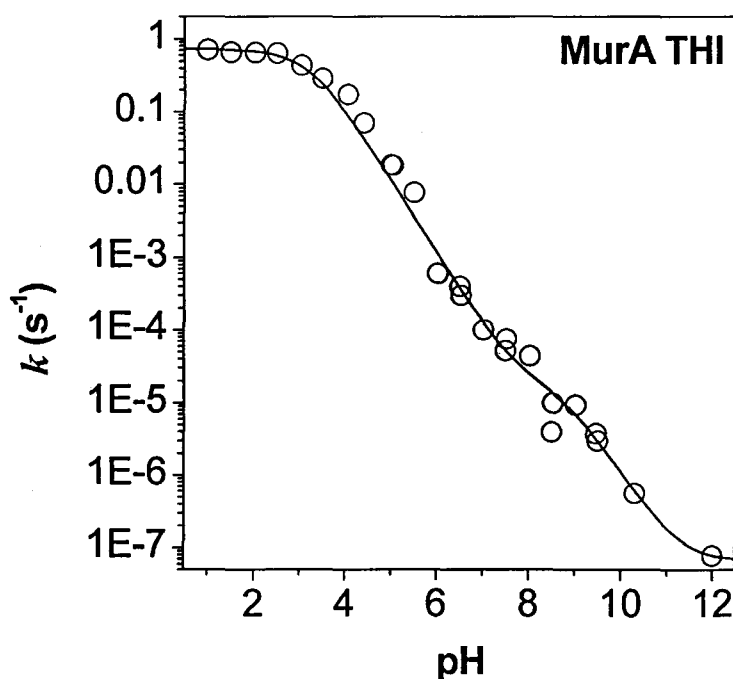
Figure 3.7-3 – Rate vs. pH profile for the breakdown of the THI. Line fitting was as in Section 2.9.2, and showed pKa's of 3.2 ± 0.1 and 8.9 ± 0.3.

The product distribution showed an increase in EP-UDP-GlcNAc and MurA ketal products as the pH was increased. The fraction of UDP-GlcNAc decreased from 1 to 0.907 with increasing pH, with pK_{a1} = 1.7 and pK_{a3} = 6.2. MurA ketal produced showed similar pK_a's, increasing from a fraction 0 to 0.062 with pK_{a1} = 1.5 and pK_{a3} = 6.1. The

proportion of EP-UDP-GlcNAc also increased with pH from a fraction of 0

to 0.030. No EP-UDP-GlcNAc was quantitatable at pH < 3, thus only the

pK_{a3} = 6.2 was fitted (Figure 3.7-4 and Appendix B - Table B-1, Table

B-2).
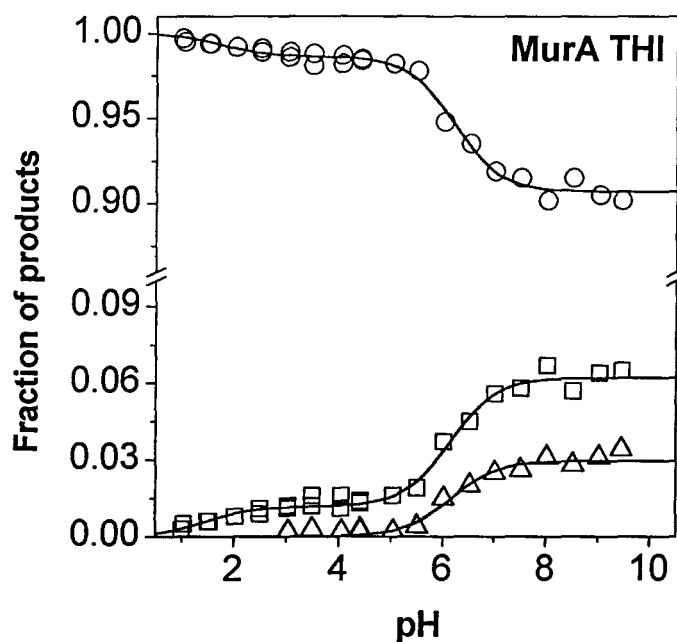
Figure 3.7-4 – Variation of product distribution with pH for the breakdown of the THI.
Legend: o – UDP-GlcNAc, pyruvate and phosphate; △ - EP-UDPGlcNAc and phosphate;
□ – MurA ketal and phosphate.

3.7.2 Solvent Deuterium Isotope Effect

The SDKIE at pL 2.0 was measured by comparison of the average

of 5 rates measured at pH 2.0 (in H_2O) and 4 rates measured at pD 2.0 (in

90% D_2O) (Appendix B - Table B-1). In calculating the SDKIE, the ratio of

the rates was divided by 0.9 to account for the fact that the experiment

was run in 90% D_2O. The resulting SDKIE was 1.3 ± 0.4.

3.7.3 Breakdown of [^{33}P]THI in Aqueous Methanol

In order to determine if the mechanism of UDP-GlcNAc formation

involves C-O or P-O bond cleavage, [^{33}P]THI was broken down in 50%

methanol. The products of the breakdown were analyzed by HPLC and

showed no methyl [^{33}P]phosphate at pH 1, 8, 9, or 10 (Figure 3.7-5). The

limit of detection for P-O bond cleavage was estimated at 3% based on

the molar fraction of methanol, 0.31, and amounts of [^{33}P]phosphate

detected.
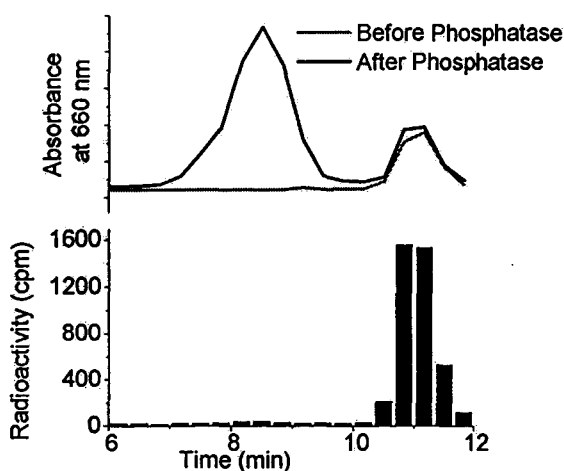
Figure 3.7-5 - Chromatogram of [^{33}P]THI which was allowed to break down in 50% (v/v) methanol and 50 mM glycine, pH 10.0. The sample was chromatographed on a 1 mL Mono-Q column. (Top) Malachite Green assay on the fractions (0.33 mL) collected. Phosphate was detectable before treating the fractions with alkaline phosphatase. Whereas, only after treatment with alkaline phosphatase was signal from fractions containing methyl phosphate detected.

In a control reaction, [γ-^{33}P]ATP was hydrolyzed in 50% methanol

under conditions where P-O bond cleavage is known to occur. Similar

HPLC analysis showed that P-O bond cleavage in ATP hydrolysis could

be detected by methyl [^{33}P]phosphate production (Figure 3.7-6). To verify

that there was no significant change in mechanism in 50% methanol, unlabeled MurA THI was degraded in 50% methanol at pH 7.0. The rate constant of this degradation was 1.4×10^{-4} s^{-1}, similar to that in water, 1.3 $\times 10^{-4}$ s^{-1}. There was an apparent increase in proportion of ketal to 24%, likely due to the methyl ketal product arising from methanol attack on the cationic intermediate co-eluting with the intramolecular ketal product. The proportion of EP-UDP-GlcNAc was unchanged (2.5%).
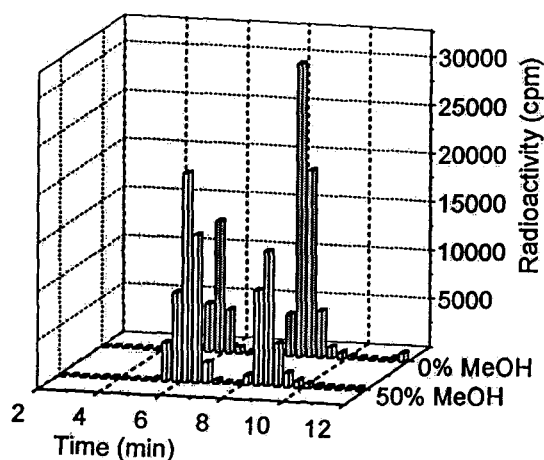
Figure 3.7-6 - Overlay of chromatograms of [γ-^{33}P]ATP broken down in 50 mM Tris, pH 7, and 10 mM Ca^{2+} in the presence and absence of 50% methanol. Radioactivity in fractions (0.33 mL) collected was determined using liquid scintillation counting. The known peaks are methyl phosphate (6.2 min) and phosphate (8.5 min). There is also an unknown radioactive impurity (5.8 min), present in the [γ-^{33}P]ATP, which is unresolved from methyl phosphate.

3.8   Enzymatic Reaction Intermediate Studies

3.8.1 Search for the Enzymatic MurA Ketal

Incubation of the MurA reaction at equilibrium for 15 days did not produce any observable MurA ketal. If the MurA ketal is produced at all,

its rate of appearance is much slower than the production of the AroA

ketal under similar conditions. After 10 days of incubation of the AroA

reaction, the AroA ketal is the only shikimate containing species present.[90]

In another experiment the MurA reaction was base quenched to

see if MurA ketal would be produced. The reaction conditions were similar

to the THI synthesis, but with [1-^{14}C]PEP. From the THI breakdown

characterization, it is known that MurA ketal elutes between the PEP and

EP-UDP-GlcNAc. Direct detection of MurA ketal from the quenched

reaction by HPLC followed by scintillation counting was not possible,

because of tailing of the PEP peak, into the area where the MurA ketal

was expected to elute.

Therefore, eluate between the PEP and EP-UDP-GlcNAc peaks

from the injected quenched reaction was collected and pooled. In a

second HPLC run, this collected eluate was reinjected and the

radioactivity in fractions collected between the PEP and EP-UDP-GlcNAc,

was counted (Figure 3.8-1). The results where overlaid with a

chromatogram from the breakdown of [^{14}C]THI, where [^{14}C]MurA ketal is

known to be present. Two radioactive peaks were present between the

PEP and EP-UDP-GlcNAc, but neither corresponded to the retention time

of the MurA ketal. These peaks were shown to be impurities in the

[1-^{14}C]PEP used in the enzymatic quench reaction.
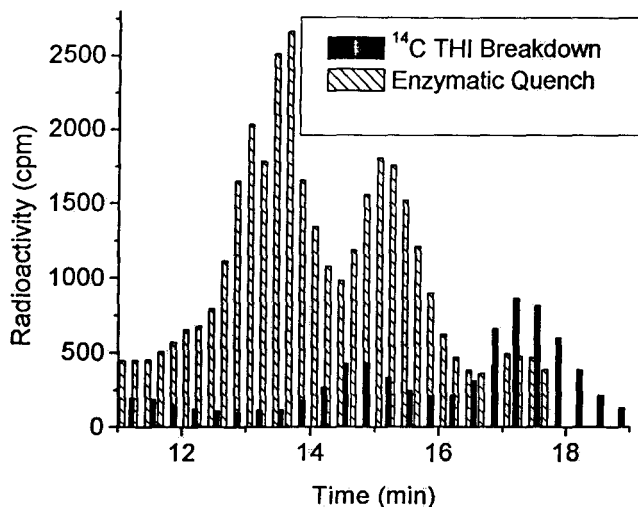
Figure 3.8-1 – (Black) Broken down (pH 7.5) purified [^{14}C] THI chromatogram (Same as Figure 3.6-2). Overlaid (gray) is the chromatogram resulting from reinjection of the products from a [^{14}C] THI synthesis, which elute between PEP and EP-UDP-GlcNAc. Both samples were run under identical conditions on HPLC. Fractions were collected in the area of the chromatograms shown, and the radioactivity in the fractions was determined by liquid scintillation counting. The known peak present in both chromatogram is EP-UDP-GlcNAc (17.2 min). The other known peak in the [^{14}C] THI breakdown chromatogram is the MurA ketal (14.7 min). The peaks in the enzymatic quench chromatogram do not correspond to any known peaks.

3.8.2 NMR of the MurA Reaction at Equilibrium

Direct detection of an oxocarbenium ion intermediate in the MurA reaction was attempted using ^{13}C-NMR. An overnight ^{13}C-NMR spectrum, of the MurA reaction at equilibrium with [^{13}C$_3$]PEP included as a substrate, was acquired (59519 scans) (Figure A-12). As expected signals for PEP, EP-UDP-GlcNAc, and the THI were observed. In addition signals assigned to pyruvate and UDP-MurNAc were also observed.

Table 3.8-1 - [13]C chemical shifts of identified peak from MurA reaction at equilibrium, with [[13]C₃]PEP included as a substrate.

		δ (ppm)	[1]J (Hz)	[2]J (Hz)
THI	C1	179.8	61.2 (C2)	
	C2	96.2	61.2 (C1), 43.3 (C3)	
	C3	24.6	43.3 (C3)	
PEP	C1	171.8	75.3 (C2)	
	C2	149.9	75.3 (C1), 77.7 (C3)	7.2 (P1)
	C3	100.3	77.7 (C3)	
EP-UDP-GlcNAc	C3	95.0	79.6 (C2)	
MurNAc	C1	178.8	53.4 (C2)	
	C2	50.8	53.4 (C1), 34.9 (C3)	
	C3	16.4	34.9 (C3)	
pyruvate	C1	170.3	62.3 (C2)	13.4 (C3)
	C2	205.2	62.3 (C1), 39.7 (C3)	
	C3	26.6	39.7 (C3)	13.4 (C1)

There was no triplet at a chemical shift of 170-220 ppm as would be expected of the C2 of an oxocarbenium ion intermediate. There were however weak doublets which were unassigned in the methyl (25.4 and 22.6 ppm) and carboxyl (176.4ppm) range of chemical shifts. These could be signals from the C1 and C3 of the oxocarbenium ion intermediate. 2D-INADEQUATE, which detects carbon-carbon coupling was therefore used to try detect the C2 carbon of the oxocarbenium ion intermediate via coupling to these unassigned carbons. The same sample as in the previous experiment was used to run the INADEQUATE experiment,

however by time the sample was run all the substrates had been converted to UDP-MurNAc. Nonetheless, carbon-carbon coupling could not be detected from the UDP-MurNAc by the INADEQUATE experiment. Therefore, it would not have detected coupling from the weak unassigned C1 and C3 signals even if a fresh sample had been run.

3.8.3 Enzymatic Partitioning of THI

All partitioning experiment showed no evidence of pyruvate production. Thus under the conditions used, non-enzymatic breakdown of the THI did not occur. The observed products of the partitioning of the THI by MurA were EP-UDP-GlcNAc and PEP, in ratios of 2-2.5:1. In an experiment with 1 μM MurA a $t_{1/2}$ for the THI of approximately 3 s was measured. From this data an approximate second order rate constant for the reaction of MurA and the THI of 2.3 X10^5 $M^{-1}s^{-1}$ was calculated.

Chapter 4   Discussion

4.1   Product Distribution of THI Breakdown

4.1.1 Observed Products in Breakdown

Under all the conditions used the major products of THI (1)

breakdown were UDP-GlcNAc, pyruvate and phosphate (2). These are

the products expected from the classic acetal hydrolysis mechanism. The

disappearance of 1 and the appearance of products obeyed first-order

kinetics. As well, no transient build-up of intermediates was observed by

HPLC. These results are consistent with slow dissociation of phosphate

followed by fast trapping of the oxocarbenium ion intermediate and fast

breakdown of the hemi-acetal intermediate (Figure 4.1-1).
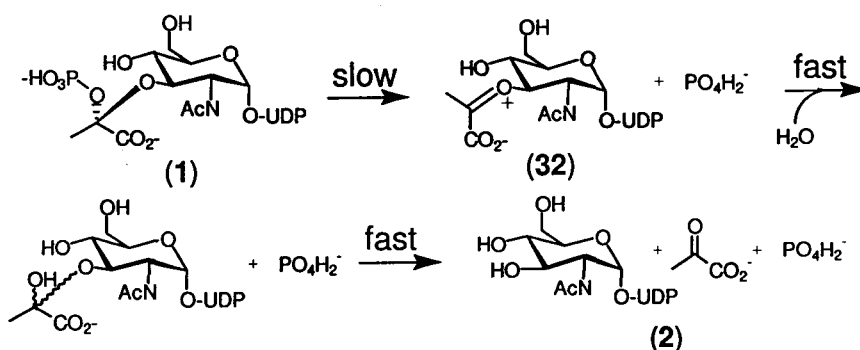
Figure 4.1-1 – Hydrolysis of the THI (1), showing the dissociation of phosphate as being the rate-limiting step.

Minor products of the breakdown of 1 were EP-UDP-GlcNAc (3)

and the MurA ketal (4). The plot of the product distribution versus pH

showed that the yield of 3 and 4 increased at higher pH, with pK_as at 6.2

and 6.1, respectively (Figure 3.7-4). The fact that the pH-dependence of **3**

and **4** formation were the same argues for a common rate-limiting step in

their formation. We have identified this step as dissociation of phosphate

with C-O bond cleavage to form an oxocarbenium ion intermediate (**32**)

(Figure 4.1-2). This would be followed by abstraction of a proton from **32**

to yield **3** or intramolecular nucleophillic attack by 4'-OH to form **4**.
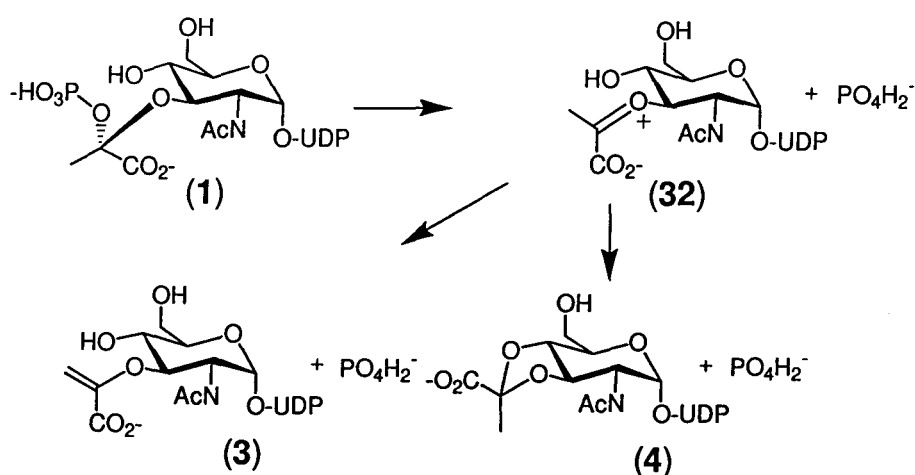
Figure 4.1-2 – Mechanism of the formation of EP-UDP-GlcNAc (**3**) and the MurA ketal (**4**) from the THI (**1**) via an oxocarbenium ion intermediate (**32**).

4.1.2 pH Dependence of Product Distribution

The variation of the product distribution was controlled by two pK_as

(Figure 3.7-4). The yield of all three products showed a pK_a at ~6.2. In

addition the yield of **2** and **4** showed pK_as of ~1.6. These pK_as are close

to values measured for phosphate monoesters, 0.7 to 1.4 and 5.7 to

7.2.[10;94] These phosphate pK_as are only observed in the product

distribution and not in the rate *versus* pH profile (Figure 3.7-3). Thus the

steps which determine the products of the breakdown of **1** must occur after the rate-limiting step. [66;95;96]

In order for the phosphate leaving group to have an influence on the product distribution, it cannot diffuse away immediately after C-O bond cleavage. The immediate product of C-O bond cleavage must therefore be an ion pair complex, similar to that observed with CMP-NeuAc hydrolysis.[33;97] The protonation state of the phosphate in the ion pair could affect the product distribution in one of two ways. (i) The phosphate could act as a general base catalyst in the formation of **3** and **4**. (ii) The increased negative charge on the phosphate at higher pH could form a stronger ion pair complex, thus allowing more time for the formation of **3** and **4**.
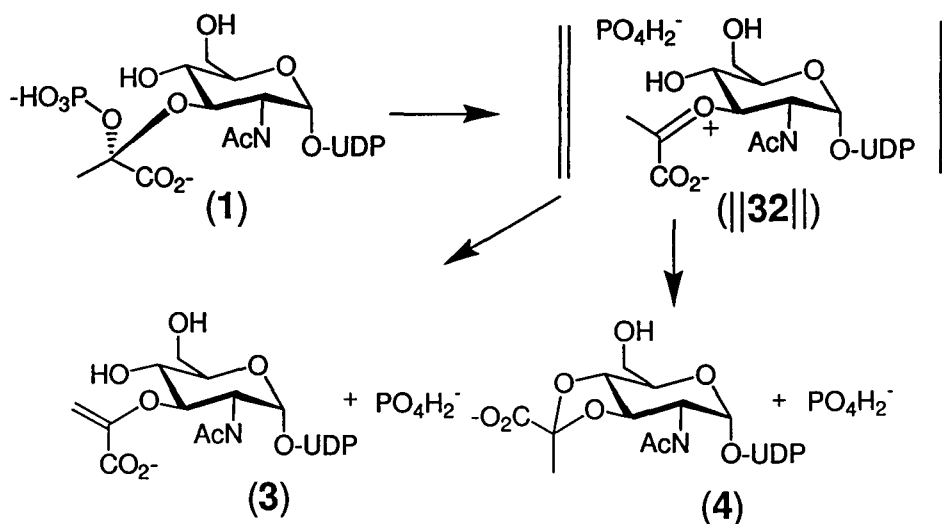
Figure 4.1-3 - Mechanism of the formation of EP-UDP-GlcNAc (**3**) and the MurA ketal (**4**) from the THI (**1**) via an ion pair complex (‖**32**‖).

90

Formation of **3** through general base catalysis by the phosphate within ‖**32**‖ is reasonable. General base catalysis of the formation of **4** seems less probable. For such catalysis to occur the phosphate would have to be on the same face of the oxocarbenium ion as the attacking 4'-OH. The phosphate would have to be in close proximity to the oxocarbenium ion to maintain electrostatic interactions, and close to the 4'-OH to allow for deprotonation of the 4'-OH. This would allow little room for the eventual nucleophillic attack of the 4'-OH on the oxocarbenium ion. It is also questionable as to whether general base catalysis would significantly affect the rate of **4** formation. Oxocarbenium ions are highly reactive towards nucleophillic attack, with diffusion often being the rate-limiting step.[32;33] The attacking nucleophile in **4** formation is an intramolecular one, thus diffusion is not limiting and the process would be very fast, with little need for general base catalysis.

Extension of the lifetime of ‖**32**‖ would result in an increase in the yield of **3** and **4** only if **2** could not form from ‖**32**‖. Instead **2** would have to form via attack of water on the subsequent solvent separated ion pair complex or on the free oxocarbenium (**32**). Although our data does not allow us to distinguish between these two possibilities, attack of water only on the free oxocarbenium ion was concluded for **31** hydrolysis.[33] Further support for the formation of **3** and **4** from ‖**32**‖ is that **8** formation was not reported in the hydrolysis of **7**. Hydrolysis of **7** proceeds with initial

formation of an oxocarbenium similar to **32** but does not form **8** without an

ion pair complex intermediate.

(7)   (8)
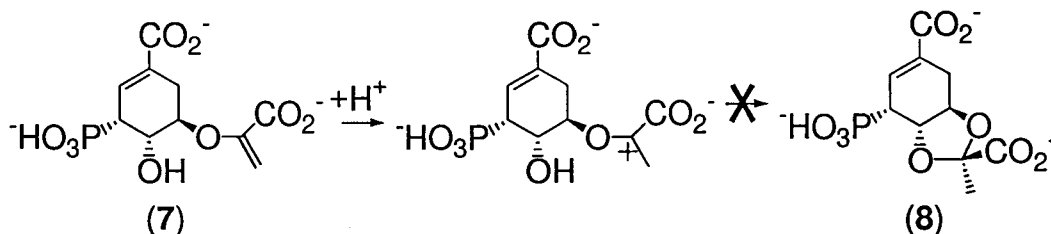
4.2 Mechanism of the Rate-Limiting Step of THI Breakdown

4.2.1 Absence of P-O Bond Cleavage

The lack of methyl phosphate formation when **1** was broken down

in methanol showed than P-O bond cleavage mechanisms did not

contribute significantly. Two possible mechanisms involving **1** breakdown

via P-O cleavage are given in Figure 4.2-1. The lack of observed P-O

cleavage shows that the pathway involving UDP-GlcNAc as the first group

to leave (Figure 4.2-1-upper) is unimportant. No experimental study of an

intermediate such as **33** has been reported to confirm that P-O bond

cleavage would result. However, given that compounds with poorer

leaving groups than pyruvate undergo P-O cleavage the breakdown of **33**

should proceed with a significant amount of P-O cleavage.[98] The

mechanism involving P-O cleavage directly from **1** (Figure 4.2-1-lower)

was also insignificant. For alkyl phosphates this mechanism is significant,

but depends very little on the identity of the leaving group (Section 1.3.2).

With **1**, P-O cleavage would occur at a similar rate to that of alkyl

phosphate and would be overshadowed by the greatly increased rate of

C-O cleavage. Thus C-O cleavage resulting in loss of phosphate is the

first step in **1** breakdown.
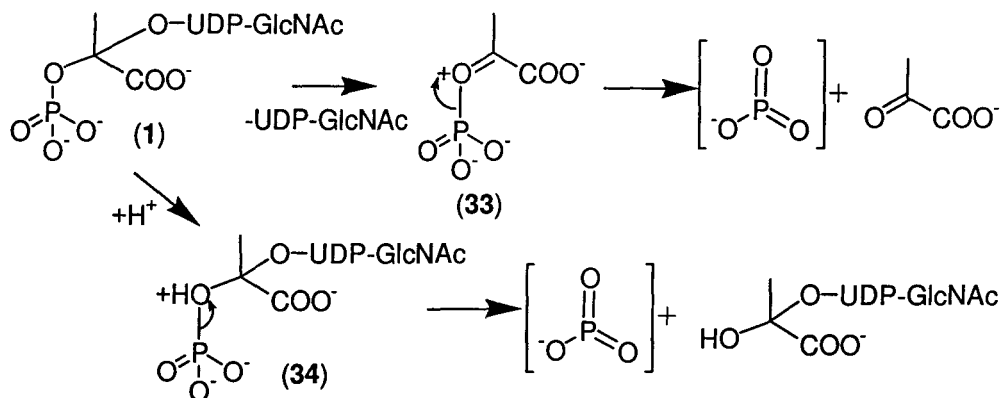
Figure 4.2-1 – Possible P-O cleavage mechanisms in the breakdown of **1**.

4.2.2 pH Dependence of Rate of THI Breakdown

In the range of pH 4 to 12 the rate of **1** breakdown increase linearly

with proton concentration, showing acid-catalysis. The rate *versus* pH

profile had a pK_a at 8.9 above which the rate increases 6-fold. The only

group present in **1** with a similar pK_a is the uridine ring (Figure 4.2-2).[99]

The effect of the uridine protonation on the rate of **1** breakdown is most

likely due to electrostatic stabilization of the oxocarbenium ion formation

by the negatively charged uridine ring above the pK_a. The magnitude of

the effect on the rate is similar to the field effects observed with glycosyl

phosphate hydrolysis (Section 1.3.3). As the pH was reduced below 4, a

plateau in the rate of hydrolysis was reached. A pK_a of 3.2 was fit to this

region of the rate *versus* pH profile. The pK_a of the carboxylate is

expected to be lower relative to acetate given the combined

electron-withdrawing effect of the phosphate and the ether oxygen. Thus

a pK_a slightly lower than the pK_as 2-phosphoglycolic acid (**35**) and

2-cyclohexyloxyacetic acid (**36**) (3.6 and 3.5, respectively) is expected and

observed.[94;100] The nature of the effect of the carboxylate will be

discussed below (Section 4.2.4).
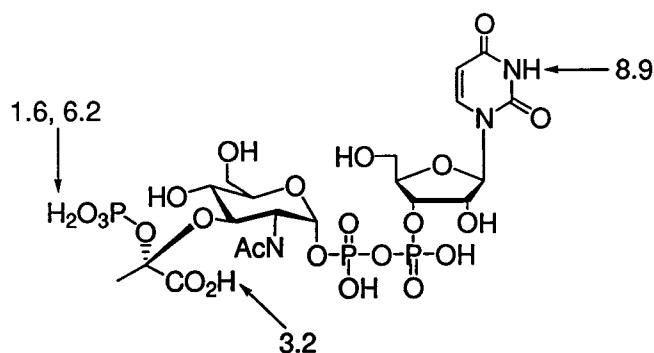
Figure 4.2-2 – Structure of **1** showing pK_as assigned from product distribution and rate *versus* pH profiles.

$\qquad\qquad$ (35) $\qquad\qquad\qquad\qquad$ (36)
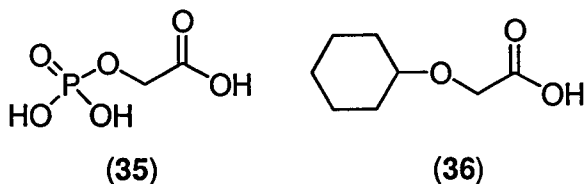
The pH *versus* rate profile for **1** breakdown has significant

differences from that of **29** and **31**. Whereas the profile for **1** shows

acid-catalysis from pH 4 to 12, the profiles for **29** and **31** show uncatalyzed

regions above pH 5 (Section 1.3.5). The mechanism of hydrolysis in

these uncatalyzed regions is spontaneous dissociation, involving anionic

leaving groups. The leaving groups for both **29** and **31** have pK_as $\approx$ 7.

For **1**, however the pK_a of the leaving group changes as the second

phosphate proton is removed with a pK_a of 6.2. This could make the **1**

phosphate an $\sim 10^6$-fold worse leaving group by increasing its pK_a from 6.2

to around 12. Thus, although the effects of this phosphate pK_a were not

seen in the rate *versus* pH profile, it could play a role in preventing the

spontaneous hydrolysis mechanism from taking over above pH 5.

(29)   (31)
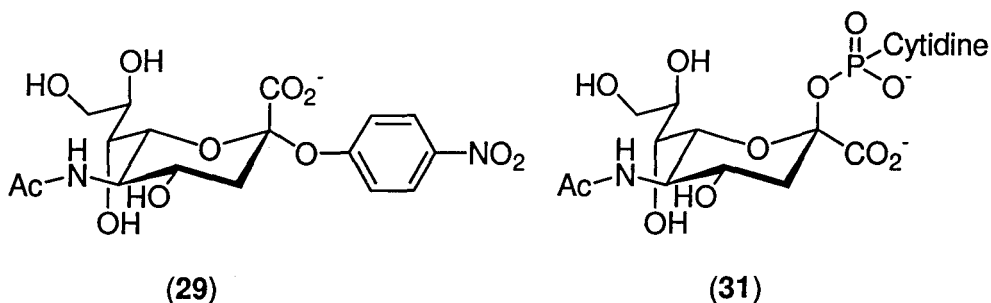
4.2.3 General Acid-catalysis

The SDKIE for **1** breakdown at pL 2.0 was 1.3 ± 0.4. At this pL the

only significant mechanism of breakdown is hydrolysis. The SDKIE was

typical of acetal hydrolyses where general acid-catalysis has been

shown(1.1 to 1.5).[29;42] In addition, it was consistent with the SDKIE of the

hydrolysis of **30b** (1.10 at pL 0) and **29** (1.36 and 1.31 at pL 1.0 and 2.8).

General acid-catalysis of **29** hydrolysis has also been verified by other

methods.[101] Because **1** has a similar oxocarbenium ion product and

comparable leaving group, it would be expected to hydrolyze with a similar

mechanism. The structure of **1** also fits several of the criteria required for

observation of general acid-catalysis: (i) a relatively stable carbocation

product and relatively good leaving group; (ii) significant steric bulk which

can be alleviated at the transition state (Section 1.3.1). Thus the

observation of general acid-catalysis for **1** is reasonable. The general acid

catalyst could be intermolecular, H_3O^+, or intramolecular, the α-carboxyl of

1 (see below).

30b
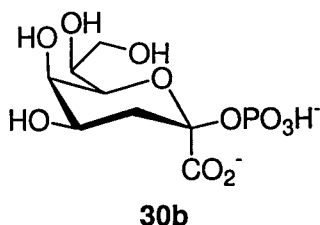
4.2.4 Role of the Carboxyl

The rate *versus* pH profile showed that the carboxyl plays an

important role in the breakdown of **1**. The plateau region could result from

one of two causes: (i) The carboxylate form could be more reactive than

the carboxylic acid form. In this case, general acid catalysis would be

intermolecular, catalyzed by H_3O^+. As the pH is lowered the plateau

region results from the opposing effects of decreasing carboxlyate

concentration and increasing proton concentration. (ii) The acid form could

be more reactive than the carboxylate form due to intramolecular general

acid-catalysis, where the plateau results from the maximum rate being

reached due to the fraction of carboxylic acid form reaching **1**. Regardless

of the reason, the size of the plateau region (1.5 pH units) indicates that

the more reactive form is at least 30-fold more reactive.

The effect of the carboxyl on the rate of **1** breakdown relative to hydrogen can be estimated by comparing the relative rates of **1** and **16f** breakdown. The rate constant for **1** breakdown at pH 7 and 25 °C is 1.4×10^{-4} s^{-1}. The rate constant for **16f** breakdown may be estimated as follows. The rate of **16a** hydrolysis at pH 0 and 25 °C is 4.1×10^{-5} s^{-1}.[30] Thus at pH 7 this acid-catalyzed rate would be 10^{7}-fold lower or 4.1×10^{-12} s^{-1}. **16f** would hydrolyze 2700-fold faster than **16a**, or approximately 1.1×10^{-8} s^{-1}.[65] Thus the rate of THI breakdown can be estimated to be 12700-fold faster than that of **16f** at pH 7 and 25 °C. There are differences remote from the site of reaction, which would have a small effect on relative rates.
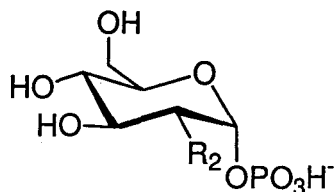
16a: R_2= OH
16f: R_2= H

Of this 12700-fold increased rate acceleration of **1** over **16f**, at least some could be accounted for by the change in the steric constraints surrounding the site of chemistry. Connected to C2 of **1** is the phosphate (sterically similar to a *t*-butyl group), a methyl group, and a secondary alcohol. All of these groups have equivalent groups in **16f**. However, in **1** the H of **16f** is replaced by the carboxyl. Given that the carboxyl branches

one atom away from C2, it would impart significant strain into **1**. A series

of benzaldehyde acetals (**37**) show hydrolysis rate dependant on the size

of the R group. For methyl, isopropyl, *t*-butyl R groups the relative rates of

hydrolysis where approximately 1:10:100.[67] This increase in rates is

smaller than our observed 12700-fold acceleration.
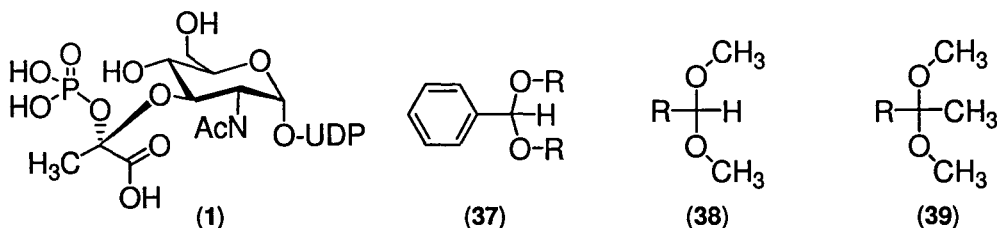
Another study comparing steric effects in acetals (**38**) to ketals (**39**),

showed R group steric effects are amplified in ketals. For example a

t-butyl R group in (**39**) has a six-fold greater increase on the activation

enthalpy of hydrolysis than the *t*-butyl R group in (**38**).[68] Thus the steric

acceleration of acetal hydrolysis by a given group is dependant on the

nature of the other groups present. In addition to steric effects on the rate

acceleration of **1** over **16f**, conformational effects related to the acyclic

nature of **1** and cyclic nature of **16f** also may play a role. The diethyl ketal

of acetone hydrolyses 8 times faster than the diethyl ketal of

cyclohexanone.[102] Thus steric and conformational effects can largely

account for the difference in rates between **1** and **16f**, although because

the steric effects are not simply additive, it is unclear exactly how much of

the rate acceleration can be accounted for.

If steric effects are largely responsible for the rate acceleration then the $\geq$ 30-fold difference in reactivity of the carboxylate and acid forms of **1** must be rationalized. If the carboxylate is the more reactive form, several effects may increase its reactivity. Electrostatic repulsion of the carboxylate and the negative phosphate leaving group would accelerate the rate. For comparison, in the hydrolysis of **29** the leaving group is neutral in the reactant and the difference in reactivity between the carboxyl forms is about 5-fold.[80] Of course this effect would only be present as long as the phosphate remained charge (pH < ~1.6).

The effect of the carboxylate could also be net inductive stabilization of the forming oxocarbenium ion relative to the acid. For the hydrolysis of α-carboxy-vinyl ethers, the carboxylate form was 1300-fold more reactive than the acid, through stabilization of the developing oxocarbenium ion.[76] The magnitude of this effect is dependant on the degree of oxocarbenium ion formation at the transition state. With vinyl ethers the transition state is late and the oxocarbenium ion almost fully formed. For **1** and **29** the transitions state may be earlier with less oxocarbenium ion formation and thus less relative stabilization by the carboxylate form.

Another mechanism by which the carboxylate could accelerate the rate is through nucleophilic assistance or electrostatic stabilization of the oxocarbenium ion during the displacement of the phosphate. Such

catalysis has been observed with other acetals.[74;75] Nucleophilic catalysis

would result in the formation of an α-lactone intermediate (40).

α-Lactones are generally very unstable, especially in aqueous solution,

where an open zwitterionic form (such as 32) is favoured.[103] Electrostatic

stabilization of the oxocarbenium ion intermediate would involve only

partial bond formation, thus a fully formed α-lactone would not result.

Although electrostatic stabilization seems more likely than nucleophilic

assistance, it still would involve significant strain and thus may not be

relevant.
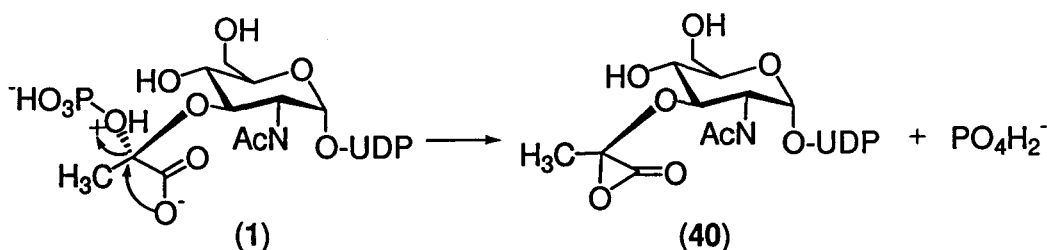
As described above, the reaction was general acid catalyzed. The

acid form of 1 being more reactive would indicate intramolecular general

acid-catalysis by the carboxylic acid. The structure of 1 differs significantly

from acetals that have been shown previously to undergo intramolecular

general acid-catalysis. Such acetals have the acid portion of the molecule

in the leaving group (e.g. 41, 42 and 43).[42;104;105] This results in a strong

intramolecular H-bond in the product (e.g. 44) that has been shown to be

important in driving the intramolecular general acid-catalyzed

mechanism.[105] 41, 42 and 43 also have their carboxyls held in a more

rigid rotational environment by the π-system of the leaving group ring, which would favour proton transfer. This is not present in the structure of 1. Intramolecular general acid-catalysis in 1 also would seem to contradict its absence the in hydrolysis of 29. Given that the structures of 1 and 29 are similar, with comparable leaving groups, the catalysis involved in their hydrolyses should be similar.

(41)   (42)   (43)   (44)
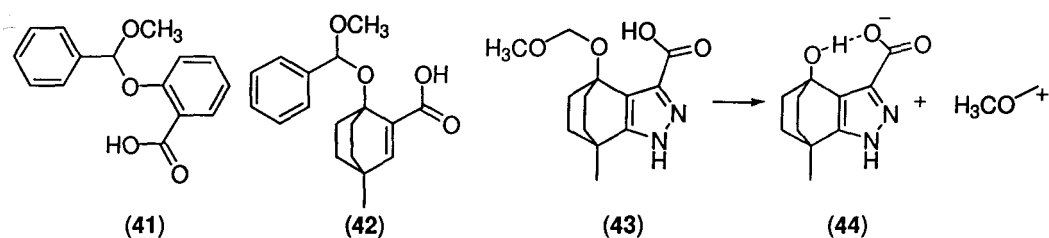
Ultimately, it is not possible to conclusively determine the role of the carboxyl from the experimental results. To be able to make more decisive arguments would require a closely related system where certain mechanisms could be eliminated. For example, comparison of the rate of 1 hydrolysis to that of 45 would allow better determination of the role of intramolecular general acid-catalysis, as would ^{18}O isotope effects at the carboxyl oxygens.

(1)   (45)
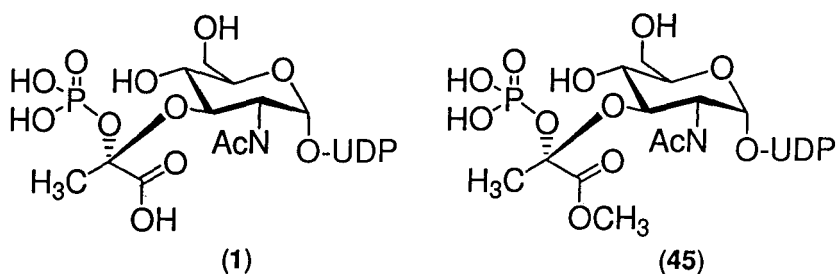
4.2.5 Site of Protonation

So far it has been shown that the first and rate-limiting step of **1**

breakdown is the general acid-catalyzed departure of the phosphate

leaving group. As discussed above the source of the proton in this step is

not clear. However the destination of the proton can be determined. As

discussed with *t*-butyl phosphate hydrolysis (Section 1.3.2), acid-catalysis

in the breakdown could occur in two ways: (i) protonation of the bridging

oxygen as in **46** or (ii) non-bridging oxygen protonation as in **47**.
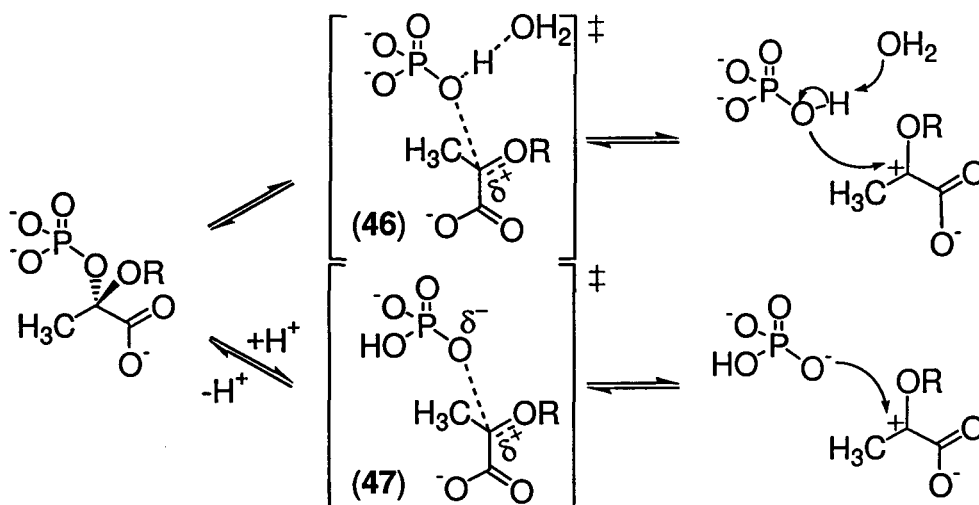
The rate *versus* pH profile does not show pK_as for the protonation

of the non-bridging oxygens of phosphate. This shows that the leaving

group ability of phosphate, which changes depending on its ionization

state, is not important in determining the rate. This observation is much

more consistent with **46** than **47**, because in **46** the developing negative

charge on the bridging oxygen from C-O cleavage is balanced by

simultaneous positive charge build up from protonation. In **47** the leaving

102

group ability is much more important since much more negative charge builds up on the bridging oxygen.

General acid-catalysis is also not consistent with **47**. For general acid-catalysis to occur, the site of the protonation must undergo a change in pK_a during the reaction, such that the protonation is unfavourable in the reactant, but favourable in the transition state. With **47**, the protonation by either possible proton source (H_3O^+ or **1**-COOH) is favourable in the reactant (pK_a 6.2) and the transition state (pK_a approaching 11.7).[95] For **46** general acid-catalysis is more reasonable as the pKa increases from $\approx$ -4 in the reactant towards 11.7 in the transition state.[29]

4.3   Effects of MurA on the Reaction Mechanism

4.3.1 Products of the Reaction

One important difference between the enzymatic and non-enzymatic breakdown of **1** is the change in the product distribution. The major product of the non-enzymatic reaction is **2**, whereas the only products of the enzymatic reaction are **3** and **48** (*i.e.* substrates). To prevent **2** formation MurA must prevent water from entering the active site. This may be the part of the function of the flexible loop that closes over the active site upon binding of MurAs substrates (Section 1.2.2). MurA may also significantly slow phosphate dissociation to prevent entry of water into the active site, just as extension of the lifetime of the ion pair complex increased the yields of **3** and **4**. MurA must also prevent the formation of

4. Hydrogen bonding of active site groups to the 4'-OH may prevent it from nucleophillic attack and thus **4** formation. MurA breakdown of **1** results in only a 2-2.5-fold excess of **3** over **48**. The complete absence of **48** in the non-enzymatic reaction shows that MurA must preferentially accelerate **48** production. Protonation of the leaving group oxygen, combined with electrostatic stabilization of the resulting cation would be an effective strategy.[22;29]

(2)

(3)

(4)

(48)
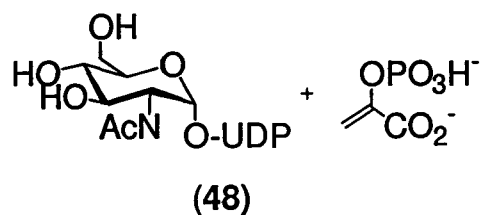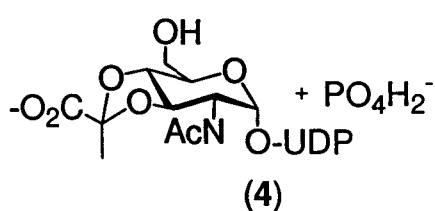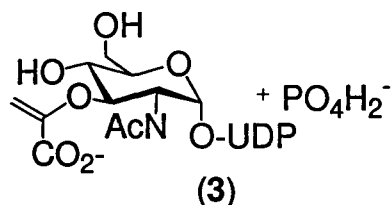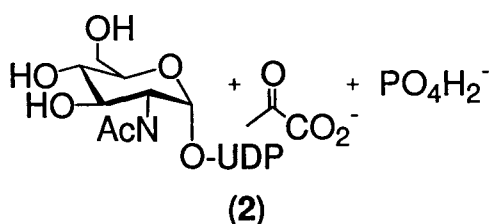
4.3.2 Increased Rate of Breakdown

Although the products of the MurA-catalyzed reaction are different than the non-enzymatic ones, the rate-limiting step of the non-enzymatic reaction, namely C-O cleavage, is still required in the MurA-catalyzed reaction. Thus, general acid-catalysis by the enzyme may be an important mechanism of rate acceleration. A recent study by our group identified this acid catalyst for the AroA reaction as lysine 22, with removal of the

lysine resulting in a 120-fold decreased rate.[22] This lysine is located such that it can protonate both leaving group oxygens (**49**).
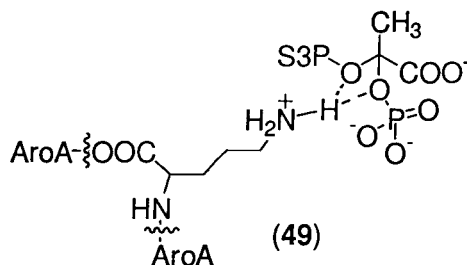
Electrostatic stabilization of an oxocarbenium ion intermediate or transition state may play an additional role in the MurA catalyzed breakdown. This type of catalysis is present in lyzozyme, which catalyzes a similar C-O cleavage.[42] The formation of the phosphothiolactyl (Figure 1.2-3) may be the result of electrostatic stabilization, followed occasional nucleophillic attack such as has been observed with vinyl ether hydrolysis.[106] Depending on the role of the carboxyl in **1** other catalytic strategies may also be used by MurA. If the carboxylate form of **1** is more reactive, the enzyme may utilize binding of only the carboxylate form. The combination of acid-catalysis by lysine 22 and exclusive binding of the carboxylate could allow for rates higher than in the plateau region in the rate *versus* pH profile.

4.3.3 Oxocarbenium Ion Intermediates

One feature of the non-enzymatic reaction that could not be demonstrated in the enzymatic reaction was the existence of an oxocarbeniun ion intermediate. Directly observing oxocarbenium ion

intermediates by NMR or indirectly via **4** production did not prove

successful. For the AroA reaction our group has shown that incubation of

the AroA reaction at equilibrium, with excess enzyme, produces **8**. The

presence of excess enzyme prevents production of **8** via release and

breakdown of **5**, as any released **5** is re-bound immediately. Thus **8**

production must occur on the enzyme from an oxocarbenium ion

intermediate.

The lack of evidence for the corresponding oxocarbenium ion

intermediate in the MurA reaction may be because the reaction is more

concerted, with a very short oxocarbenium ion intermediate lifetime. A

shorter lifetime could be caused by the presence of available nucleophiles

in the active site. For the glucosyl oxocarbenium ion it have been shown

that its lifetime is reduced in the presence of nucleophiles.[107]

(5)   (8)
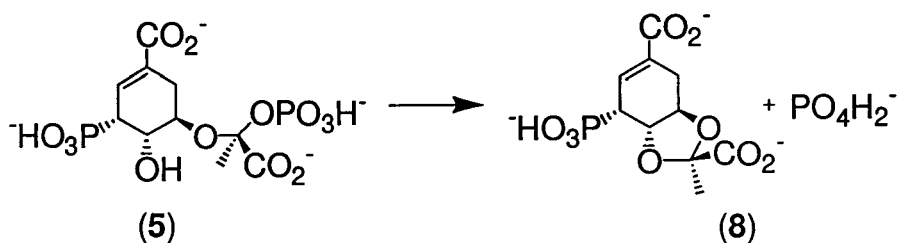
Future Work

Our ultimate goal is to understand the mechanism of MurA in atomic detail and use this knowledge for the design of inhibitors which will be effective antibiotics. To this end, the kinetic isotope effects (KIEs) of the enzyme catalyzed reaction will be measured at multiple sites within the substrates. These KIEs reflects the change in the vibrational environment of a labelled atom between the reactant and the TS. The understanding of the vibrational environments of the atoms around the reactive site, will allow use of computational methods to identify the transition state. The method used is Bond Order Vibrational Analysis and involves relating vibrational environments of the atoms to their bond strengths and then relating these bond strengths to bond lengths and angles which allow the structure of the transition state to be identified. Molecules which resemble the transition state will then be designed and once synthesized will serve as inhibitors of the enzyme. This method has been used previously with other enzymes to design competitive inhibitors with affinities of up to 10^6 times higher than that of the enzyme substrate.

Reference List

(1) Brown, E. D.; Vivas, E. I.; Walsh, C. T.; Kolter, R. *J.Bacteriol.* 1995, *177*, 4194-4197.

(2) Marquardt, J. L.; Brown, E. D.; Lane, W. S.; Haley, T. M.; Ichikawa, Y.; Wong, C. H.; Walsh, C. T. *Biochemistry* 1994, *33*, 10646-10651.

(3) Reddy, S. G.; Waddell, S. T.; Kuo, D. W.; Wong, K. K.; Pompliano, D. L. *J.Am.Chem.Soc.* 1999, *121*, 1175-1178.

(4) Lauer, B.; Submuth, R.; Kaiser, D.; Jung, G.; Bormann, C. *J.Antibiotics* 2000, *53*, 385-392.

(5) Kahan, F. M.; Kahan, J. S.; Cassidy, P. J.; Kropp, H. *Ann.N Y Acad.Sci.* 1974, *235*, 364-386.

(6) Kim, D. H.; Lees, W. J.; Kempsell, K. E.; Lane, W. S.; Duncan, K.; Walsh, C. T. *Biochemistry* 1996, 4923-4928.

(7) Sikorski, J. A.; Gruys, K. J. *Acc.Chem.Res.* 1997, *30*, 2-8.

(8) Sammons, R. D.; Gruys, K. J.; Anderson, K. S.; Johnson, K. A.; Sikorski, J. A. *Biochemistry* 1995, *34*, 6433-6440.

(9) Kim, D. H.; Lees, W. J.; Haley, T. M.; Walsh, C. T. *J.Am.Chem.Soc.* 1995, *117*, 1494-1502.

(10) Liang, P. H.; Lewis, J.; Anderson, K. S.; Kohen, A.; D'Souza, F. W.; Benenson, Y.; Baasov, T. *Biochemistry* 1998, *37*, 16390-16399.

(11) Kim, D. H.; Lees, W. J.; Walsh, C. T. *J.Am.Chem.Soc.* 1995, *117*, 6380-6381.

(12) Kim, D. H.; Tucker-Kellogg, G. W.; Lees, W. J.; Walsh, C. T. *Biochemistry* 1996, *35*, 5435-5440.

(13) Skarzynski, T.; Kim, D. H.; Lees, W. J.; Walsh, C. T.; Duncan, K. *Biochemistry* 1998 , *37*, 2572-2577.

(14) Anderson, K. S.; Sikorski, J. A.; Johnson, K. A. *Biochemistry* 1988, *27*, 7395-7406.

(15) Marquardt, J. L.; Brown, E. D.; Walsh, C. T.; Anderson, K. S. *J.Am.Chem.Soc.* 1993, *115*, 10398-10399.

(16) Brown, E. D.; Marquardt, J. L.; Lee, J. P.; Walsh, C. T.; Anderson, K. S. *Biochemistry* 1994, *33*, 10638-10645.

(17)　Schonbrunn, E.; Eschenburg, S.; Luger, K.; Kabsch, W.; Amrhein, N. *Proc.Natl.Acad.Sci.U.S.A* **2000**, *97*, 6345-6349.

(18)　Schonbrunn, E.; Svergun, D. I.; Amrhein, N.; Koch, M. H. *Eur.J.Biochem.* **1998**, *253*, 406-412.

(19)　Stallings, W. C.; Abdel-Mequid, S. S.; Lim, L. W.; Shieh, H. S.; Dayringer, H. E.; Leimgruber, N. K.; Stedeman, R. A.; Anderson, K. S.; Sikorski, J. A.; Padgette, S. R.; Kishore, G. M. *Proc.Natl.Acad.Sci.U.S.A* **2001**, 2944-2946.

(20)　Wanke, C.; Amrhein, N. *Eur.J.Biochem.* **1993**, *218*, 861-870.

(21)　Skarzynski, T.; Mistry, A.; Wonacott, A.; Hutchinson, S. E.; Kelly, V. A.; Duncan, K. *Structure.* **1996**, *4*, 1465-1474.

(22)　Mizyed, S.; Wright, J. E. I.; Byczynski, B.; Berti, P. J. *Biochemistry* **2003**, *42*, 6986-6995.

(23)　Anderson, K. S.; Sikorski, J. A. *J.Am.Chem.Soc.* **1988**, *110*, 6577-6579.

(24)　Byczynski, B.; Mizyed, S.; Berti, P. J. *J.Am.Chem.Soc.* **2003**, *In Press*.

(25)　Walker, M. C.; Jones, C. R.; Somerville, R. L.; Sikorski, J. A. *J.Am.Chem.Soc.* **1992**, *114*, 7601-7603.

(26)　Beau, J. M.; Schauer, R.; Haverkamp, J.; Kamerling, J. P.; Dorland, L.; Vliegenthart, J. F. *Eur.J.Biochem.* **1984**, *140*, 203-208.

(27)　Baasov, T.; Kohen, A. *J.Am.Chem.Soc.* **1995**, *117*, 6165-6174.

(28)　Anderson, K. S.; Johnson, K. A. *J.Biol.Chem.* **1990**, *265*, 5567-5572.

(29)　Cordes, E. H.; Bull, H. G. *Chem.Rev.* **1974**, *74*, 581-603.

(30)　Bunton, C. A.; Llewellyn, D. R.; Oldham, K. G.; Vernon, C. A. *J.Chem.Soc.* **1958**, 3588-3594.

(31)　Bunton, C. A.; Humeres, E. *J.Org.Chem.* **1969**, *34*, 572-576.

(32)　Richard, J. P.; Williams, K. B.; Amyes, T. L. *J.Am.Chem.Soc.* **2003**, *121*, 8403-8404.

(33)　Horenstein, B. A.; Bruner, M. *J.Am.Chem.Soc.* **1998**, *120*, 1357-1362.

(34)　Cordes, E. H. *Progr.Phys.Org.Chem.* **1967**, *4*, 1-44.

(35)　Wenthe, A. M.; Cordes, E. H. *J.Am.Chem.Soc.* **1965**, *87*, 3173-3180.

(36)　Ahtineva, A.; Lahti, M.; Pihlaja, K. *J.Org.Chem.* **1989**, *54*, 2011-2012.

(37)　Jia, Z. S.; Ottosson, H.; Zeng, X.; Thibblin, A. *J.Org.Chem.* **2002**, *67*, 182-187.

(38) Thibblin, A.; Saeki, Y. *J.Org.Chem.* **1997**, *62*, 1079-1082.

(39) Thibblin, A. *J.Chem.Soc.Perkin Trans.2* **1992**, 1195-1198.

(40) Zeng, X.; Thibblin, A. *J.Chem.Soc.Perkin Trans.2* **2001**, 1600-1607.

(41) Thibblin, A. *Spec.Pub.Royal Soc.Chem.* **1995**, *148*, 415-428.

(42) Fife, T. H. *Acc.Chem.Res.* **1972**, *5*, 264-272.

(43) Schowen, R. L. *Progr.Phys.Org.Chem.* **1972**, *9*, 275-332.

(44) Bruice, T. C.; Piszkiewicz, D. *J.Am.Chem.Soc.* **1967**, *89*, 3568-3576.

(45) Bunton, C. A.; Llewellyn, D. R.; Oldham, K. G.; Vernon, C. A. *J.Chem.Soc.* **1958**, 3574-3587.

(46) Kirby, A. J.; Varvoglis, G. A. *J.Am.Chem.Soc.* **1967**, *89*, 415-423.

(47) Kugel, L.; Halmann, M. *J.Org.Chem.* **1967**, *32*, 642-647.

(48) Lapidot, A.; Samuel, D.; Weiss-Broday, M. *J.Chem.Soc.* **1964**, 637-643.

(49) Herschlag, D.; Jencks, W. P. *J.Am.Chem.Soc.* **1989**, *111*, 7579-7586.

(50) Bianciotto, M.; Barthelat, J. C.; Vigroux, A. *J.Am.Chem.Soc.* **2002**, *24*, 7573-7587.

(51) Hu, C. H.; Brinck, T. *J.Phys.Chem.A* **1999**, *103*, 5379-5386.

(52) Bunton, C. A. *Acc.Chem.Res.* **1970**, 257-265.

(53) Batts, B. D. *J.Chem.Soc.B* **1966**, 551-555.

(54) Batts, B. D. *J.Chem.Soc.B* **1966**, 547-551.

(55) Garrison, A. W.; Boozer, C. E. *J.Am.Chem.Soc.* **1968**, *90*, 3486-3494.

(56) Modro, T. A.; Lawry, M. A.; Murphy, E. *J.Org.Chem.* **1978**, *43*, 5000-5006.

(57) Florián, J.; Warshel, A. *Phos.Sulf.Silic.* **1999**, *144-146*, 525-528.

(58) Bunton, C. A.; Kellerman, D.; Oldham, K. G.; Vernon, C. A. *J.Chem.Soc.B* **1966**, 292-294.

(59) Chandrasekhar, S. *Res.Chem.Intermed.* **1992**, *17*, 173-209.

(60) Richard, J. P.; Jencks, W. P. *J.Am.Chem.Soc.* **1984**, *106*, 1373-1383.

(61) Richard, J. P.; Jencks, W. P. *J.Am.Chem.Soc.* **1984**, *106*, 1396-1401.

(62) Young, P. R.; Jencks, W. P. *J.Am.Chem.Soc.* **1977**, *92*, 8238-8248.

(63)   Banait, N. S.; Jencks, W. P. *J.Am.Chem.Soc.* **1991**, *113*, 7951-7958.

(64)   Withers, S. G.; MacMlennan, D. J.; Street, I. P. *Carb.Res.* **1986**, *154*, 127-144.

(65)   Withers, S. G.; Percival, M. D.; Street, I. P. *Carb.Res.* **1989**, *187*, 43-66.

(66)   O'Connor, J. V.; Barker, R. *Carb.Res.* **1979**, *73*, 227-234.

(67)   Belarmino, A. T. N.; Froehner, S.; Zanette, D. *J.Org.Chem.* **2003**, *68*, 706-717.

(68)   Wiberg, K. B.; Squires, R. R. *J.Am.Chem.Soc.* **1981**, *103*, 4473-4478.

(69)   Jenson, J. L.; Martinez, A. B.; Shimazu, C. L. *J.Org.Chem.* **1983**, *48*, 4175-4179.

(70)   Chou, D. T. H.; Watson, J. N.; Scholte, A. A.; Borgford, T. J.; Bennet, A. J.
       J.Am.Chem.Soc. **2000**, *122*, 8357-8364.

(71)   Kresge, A. J.; Sagatys, D. S.; Chen, H. L. *J.Am.Chem.Soc.* **1977**, *99*, 7228-7233.

(72)   Pascal, R. *J.Phys.Org.Chem.* **2002**, *15*, 566-569.

(73)   Barber, S. E.; Dean, K. E. S.; Kirby, A. J. *Can.J.Chem.* **1999**, *77*, 792-801.

(74)   Kirby, A. J.; Strömberg, R. *Chem.Comm.* **1994**, 709-710.

(75)   Fife, T. H.; Przystas, T. J. *J.Am.Chem.Soc.* **1980**, *102*, 292-299.

(76)   Kresge, A. J.; Leibovitch, M.; Sikorski, J. A. *J.Am.Chem.Soc.* **1992**, *114*, 2618-
       2622.

(77)   Chiang, Y.; Kresge, A. J.; Young, C. I. *Can.J.Chem.* **1978**, *56*, 461-464.

(78)   Kirby, A. J.; Williams, N. H. *Chem.Comm.* **1991**, 1643-1644.

(79)   Huang, X.; Surry, C.; Hiebert, T.; Bennet, A. J. *J.Am.Chem.Soc.* **1995**, *117*,
       10614-10621.

(80)   Ashwell, M.; Guo, X.; Sinnott, M. L. *J.Am.Chem.Soc.* **1992**, *114*, 10158-10166.

(81)   Lin, C. H.; Murray, B. W.; Ollmann, I. R.; Wong, C. H. *Biochemistry* **1997**, *36*,
       780-785.

(82)   Ruano, M. J.; Cabezas, J. A.; Hueso, P. *Comp.Biochem.Phys.Part B* **1999**, *123*,
       301-306.

(83)   Comb, D. G.; Watson, D. R.; Roseman, S. *J.Biol.Chem.* **1966**, *241*, 5637-5642.

(84)   Roossien, F. F.; Brink, J.; Robillard, G. T. *Biochim.Biophys.Acta* **1983**, *760*, 185-
       187.

(85)   Xu, Y.; McGuire, M.; Dunaway-Mariano, D.; Martin, B. M. *Biochemistry* **1995**, *34*,
       2195-2202.

(86)   Salomaa, P.; Schaleger, L. L.; Long, F. A. *J.Am.Chem.Soc.* **1964**, *86*, 1-7.

(87)   Lanzetta, P. A.; Alvarez, L. J.; Reinach, P. S.; Candia, O. A. *Anal.Biochem.* **1979**, *100*, 95-97.

(88)   Meyerson, S.; Kuhn, E. S.; Ramirez, F.; Marecek, J. F. *J.Am.Chem.Soc.* **1982**, *104*, 7231-7239.

(89)   Ramirez, F.; Marecek, J. F.; Szamosi, J. *J.Org.Chem.* **1980**, *45*, 4748-4752.

(90)   Leo, G. C.; Sikorski, J. A.; Sammons, R. D. *J.Am.Chem.Soc.* **1990**, *112*, 1653-1654.

(91)   Anderson, K. S.; Sammons, R. D.; Leo, G. C.; Sikorski, J. A.; Benesi, A. J.; Johnson, K. A. *Biochemistry* **1990**, *29*, 1460-1465.

(92)   Laali, K. K.; Okazaki, T.; Coombs, M. M. *J.Org.Chem.* **2000**, *65*, 7399-7405.

(93)   Edelhoch, H. *Biochemistry* **1967**, *6*, 1948-1954.

(94)   Hartman, F. C.; LaMuraglia, G. M.; Tomozawa, Y.; Wolfenden, R. *Biochemistry* **1975**, *14*, 5274-5279.

(95)   Saha, A.; Saha, N.; Ji, L.; Zhao, J.; Gregan, F.; Sajadi, S. A. A.; Song, B.; Sigel, H. J. *Biol.Inorg.Chem.* **1996**, *1*, 231-238.

(96)   Massoud, S. S.; Sigel, H. *Inorg.Chem.* **1988**, *27*, 1447-1453.

(97)   Horenstein, B. A.; Bruner, M. *J.Am.Chem.Soc.* **1996**, *118*, 10371-10379.

(98)   Fife, T. H.; Pujari, M. P. *J.Am.Chem.Soc.* **1990**, *112*, 5551-5557.

(99)   Privat, E. J.; Sowers, L. C. *Mutat.Res.* **1996**, 151-156.

(100) Charton, M. J. *J.Org.Chem.* **1964**, *29*, 1222-1225.

(101) Ashwell, M.; Sinnott, M. L.; Zhang, Y. *J.Org.Chem.* **1994**, *59*, 7539-7540.

(102) Kreevoy, M. M.; Morgan, C. R.; Taft, R. W., Jr. *J.Chem.Soc.* **1960**, *82*, 3064-3066.

(103) Lew, C. S. Q.; Wagner, B. D.; Angelini, M. P.; Lee-Ruff, E.; Lusztyk, J.; Johnston, L. J. *J.Am.Chem.Soc.* **1996**, *118*, 12066-12073.

(104) Brown, C. J.; Kirby, A. J. *J.Chem.Soc.Perkin Trans.2* **1997**, 1081-1094.

(105) Hartwell, E.; Hodgson, D. R. W.; Kirby, A. J. *J.Am.Chem.Soc.* **2000**, *122*, 9326-9327.

(106) Kirby, A. J.; Williams, N. H. *Chem.Comm.* **1991**, 1644-1645.

(107) Bennet, A. J.; Kitos, T. E. *J.Chem.Soc.Perkin Trans.2* **2002**, *7*, 1207-1222.

Appendix A - MS and NMR

2601: THI

pb08 63 (5.380) Sb (5,1.00); Sm (Mn, 2x0.30); Cm (53:65)

Scan ES-
2.32e4
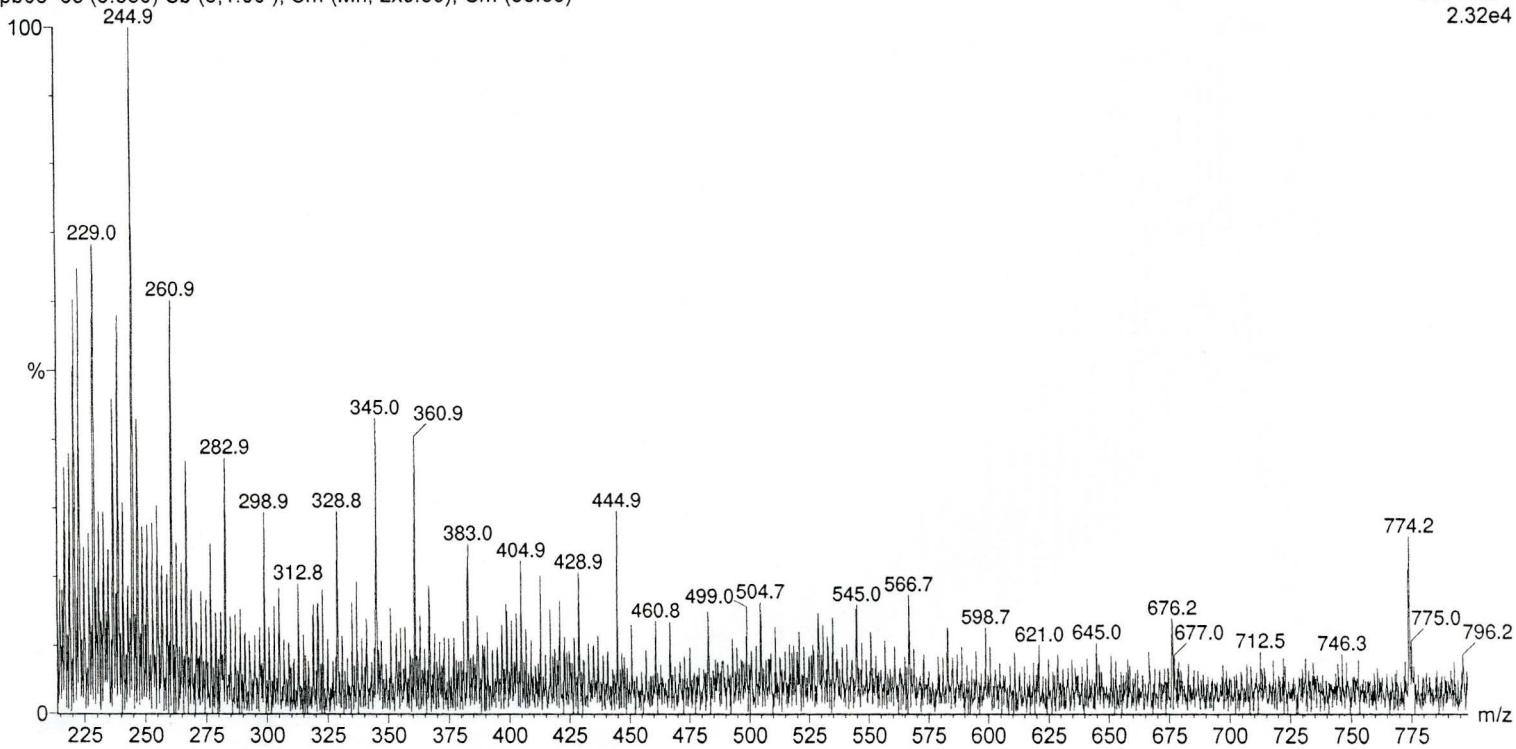
Figure A-1 - Electrospray mass spectrum with quadrupole detection in the anion mode of HPLC purified THI. The peak at m/z 774.2 is that expected of the monoanion of the THI.

MurA 10 uM ACN/H2O

SM20 68 (3.438) Cm (66:82)

Scan ES+
8.15e7
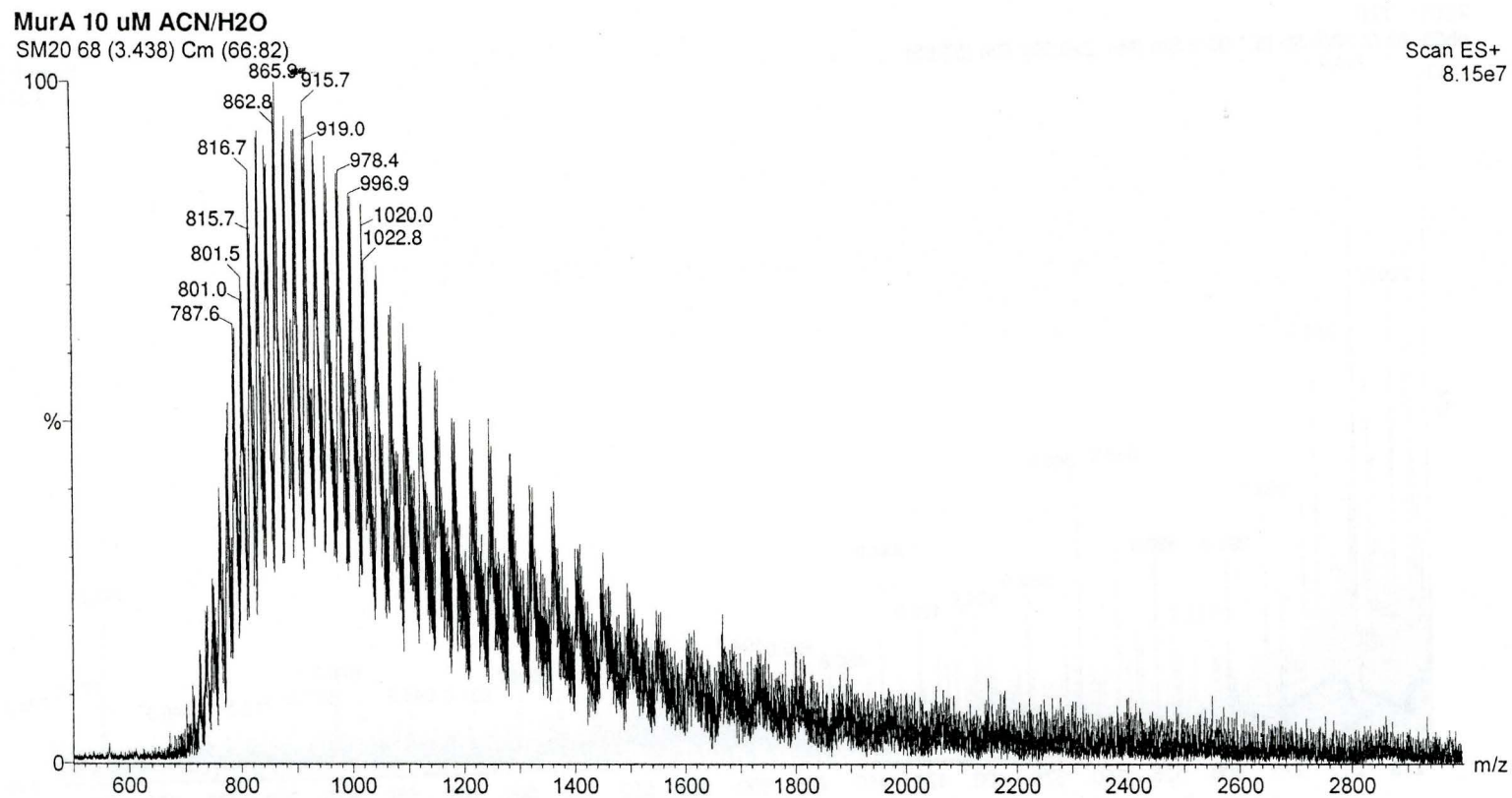
Figure A-2 - Electrospray mass spectrum with quadrupole detection in the cation mode of purified 10 μM MurA in acetonitrile/water (1:1) with 1% formic acid. Observed peaks are for multiply charged forms of MurA. For example the peaks at m/z 865.9 and 915.7 are the +52 and +49 charged forms of MurA, respectively.

MurA 10 uM ACN/H2O

SM20 68 (3.438) M1 [Ev-143821,It18] (Gs,1.500,706:2058,1.00,L10,R10); Sb (10,20.00); Cm (66:82)

Scan ES+
4.64e8
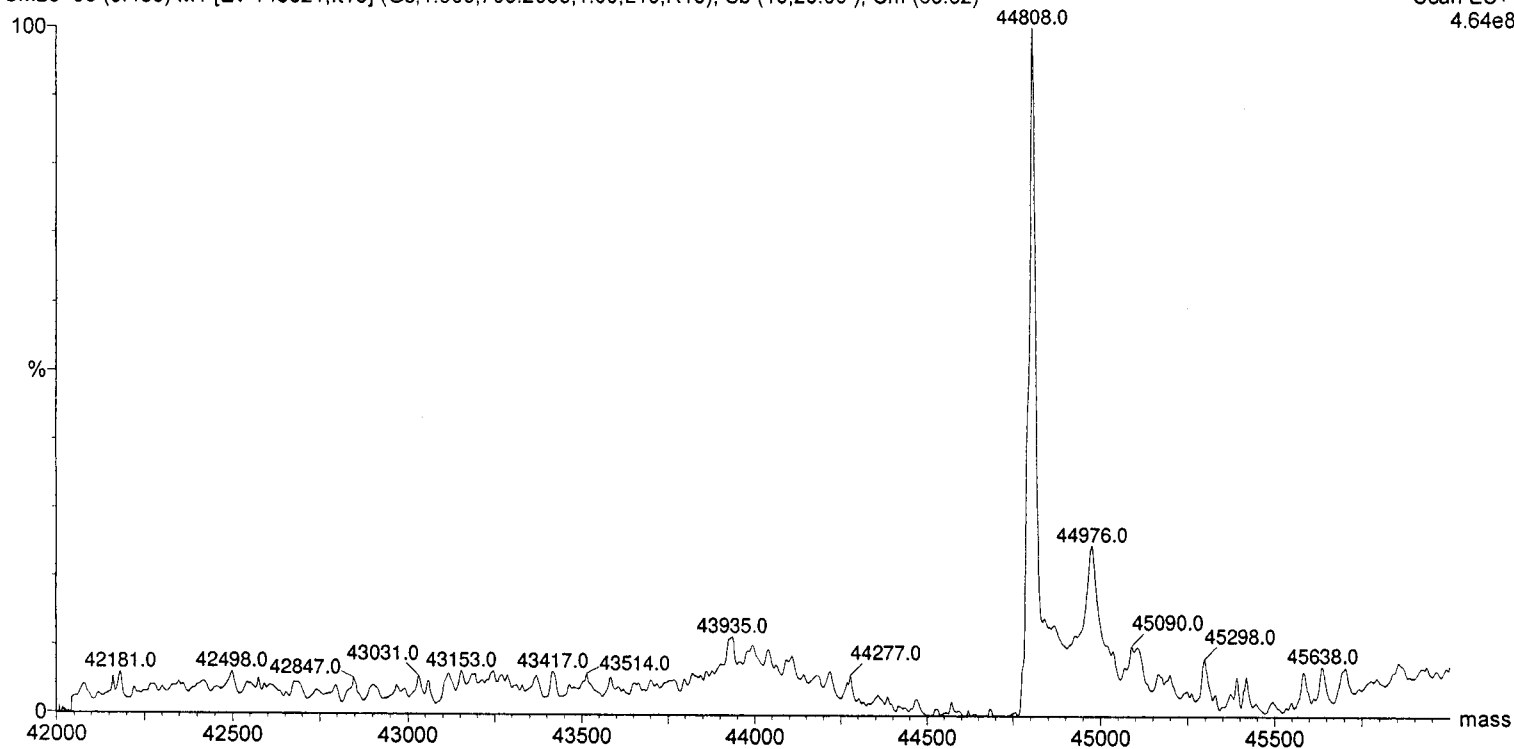
Figure A-3 – Mass spectrum calculated from Figure A-2, using MaxEnt (Micromass). Peak at m/z 44808 ± 20 Da is the calculated mass of the singly charged form of the purified MurA. The expected mass of MurA from the published amino acid sequence is 44818 Da.

13C3PEP. Triply labelled 13C PEP
13C NMR in D2O
300 MHz
June 23rd, 2002.
acquired by Jason Lee

ppm

172.469
171.459

150.859
149.843
148.797

113.232

100.518
99.456

60.560

0.467

Current Data Parameters
NAME   bart13C3PEP
EXPNO   2
PROCNO   1

F2 - Acquisition Parameters
Date_   20020623
Time   10.14
INSTRUM   av300
PROBHD   10 mm BBO BB-1
PULPROG   zgpg30
TD   32768
SOLVENT   CDCl3
NS   1379
DS   2
SWH   18832.393 Hz
FIDRES   0.574719 Hz
AQ   0.8700404 sec
RG   10321.3
DW   26.550 usec
DE   10.00 usec
TE   300.0 K
DI   0.50000000 sec
d11   0.03000000 sec
d12   0.00002000 sec

============ CHANNEL f1 ============
NUC1   13C
P1   10.70 usec
PL1   -3.00 dB
SFO1   75.4756758 MHz

============ CHANNEL f2 ============
CPDPRG2   waltz16
NUC2   1H
PCPD2   80.00 usec
PL2   120.00 dB
PL12   20.00 dB
PL13   20.00 dB
SFO2   300.1316746 MHz

F2 - Processing parameters
SI   32768
SF   75.4677504 MHz
WDW   EM
SSB   0
LB   5.00 Hz
GB   0
PC   1.40

1D NMR plot parameters
CX   20.00 cm
F1P   210.000 ppm
F1   15848.23 Hz
F2P   -5.000 ppm
F2   -377.34 Hz
PPMCM   10.75000 ppm/cm
HZCM   811.27832 Hz/cm

ppm   175   150   125   100   75   50   25   0

Figure A-4 — ^{13}C-NMR spectrum of 4 μmol ^{13}C$_3$ PEP after 1379 scans on 300 MHz spectrometer. The assigned peaks are C1 (172.5 ppm, doublet), C2 (149.8 ppm, doublet of doublets), C3 (100.5 ppm, doublet).

Sample 1
Selective 1-D TOCSY at 1.35 ppm
Spin lock: 100 ms
1H NMR in D2O (28-5-2002)
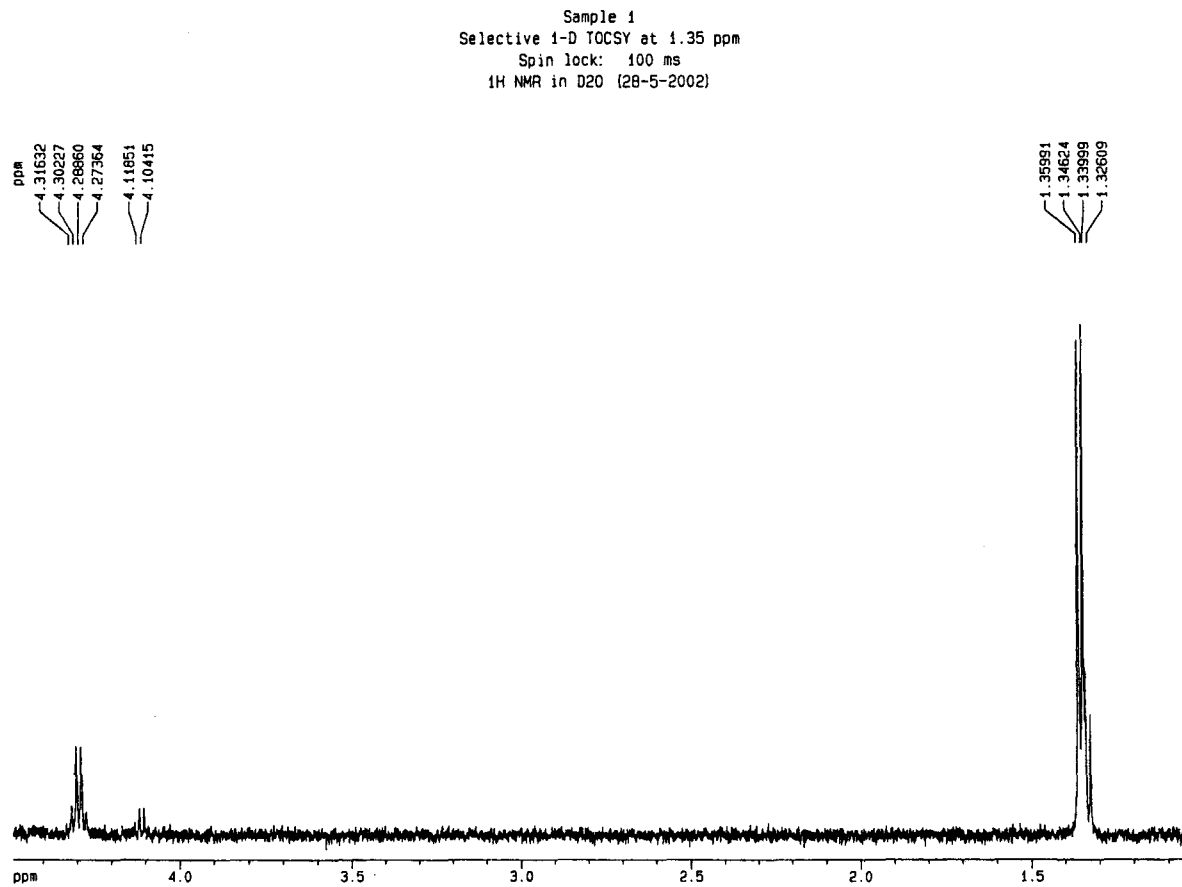
Figure A-5 – 1-D TOCSY experiment of UDP-MurNAc sample run on 500 MHz spectrometer in 160 scans. Irradiation of the signal at 1.35 ppm results in through bond magnetization transfer to the signal at 4.29 ppm.
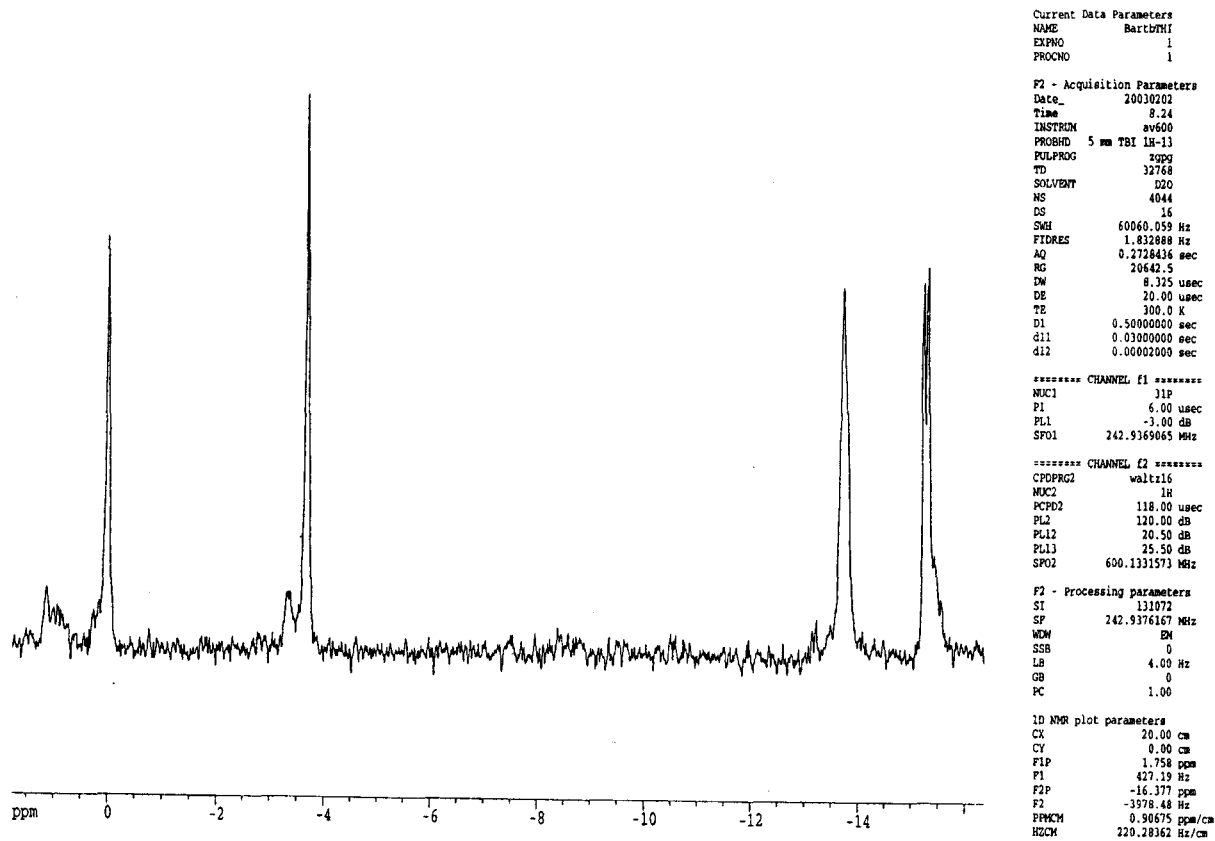
Figure A-6 – ^{31}P-NMR spectrum of 1.7 μmol $^{13}C_3$ THI after 4044 scans on 600 MHz spectrometer. The assigned peaks are inorganic phosphate (0 ppm); and the three phosphate groups in the THI P1 (-3.5 ppm), P2 and P3 (-13.5 and -15.5 ppm) (see Figure 3.6-1)

Figure A-7 - ^{13}C-NMR spectrum of 1.7 µmol $^{13}C_3$ THI after 12541 scans on 600 MHz spectrometer. The assigned peaks are C1 (175.4 ppm, doublet), C2 (100.7 ppm, doublet of doublets of doublets), C3 (24.5 ppm, doublet). Other peaks are singlets and therefore do not result from $^{13}C_3$ labelled material.

13C Ketal in D2O   150ul in Shigemi Tube
bartb 10 AV 600 28 February 2003

BRUKER

Current Data Parameters
NAME   bartb
EXPNO   10
PROCNO   1

F2 - Acquisition Parameters
Date_   20030228
Time   15.27
INSTRUM   av600
PROBHD   5 mm TBI 1H-13
PULPROG   zgpg30
TD   32768
SOLVENT   D2O
NS   156418
DS   16
SWH   36231.883 Hz
FIDRES   1.105709 Hz
AQ   0.4522622 sec
RG   20642.5
DW   13.800 usec
DE   20.00 usec
TE   300.0 K
D1   0.50000000 sec
d11   0.03000000 sec
d12   0.00002000 sec

======== CHANNEL f1 ========
NUC1   13C
P1   13.80 usec
PL1   -3.00 dB
SFO1   150.9193844 MHz

======== CHANNEL f2 ========
CPDPRG2   waltz16
NUC2   1H
PCPD2   118.00 usec
PL2   120.00 dB
PL12   20.50 dB
PL13   25.50 dB
SFO2   600.1331573 MHz

F2 - Processing parameters
SI   65536
SF   150.9028850 MHz
WDW   EM
SSB   0
LB   4.00 Hz
GB   0
PC   1.00

180 170 160 150 140 130 120 110 100 90 80 70 60 50 40 30 ppm

Figure A-8 - ^{13}C-NMR spectrum of 25 nmol $^{13}C_3$ MurA ketal purified from breakdown of 1.7 µmol $^{13}C_3$ THI after 156418 scans on 600 MHz spectrometer run in a Shigemi tube (150 µL total). The sample of MurA Ketal was shown to contain approximately a two fold excess of UDP-GlcNAc and an equivalent of EP-UDP-GlcNAc. The assigned peaks are MurA ketal C1 (176.4 ppm, weak), C3 (22.0 ppm, doublet); EP-UDP-GlcNAc C1 (170.1 ppm, doublet), C2 (155.2 ppm, doublet of doublets), C3 (94.1 ppm, doublet of doublets). The broad peak at ~112 ppm is due to the probe glue.
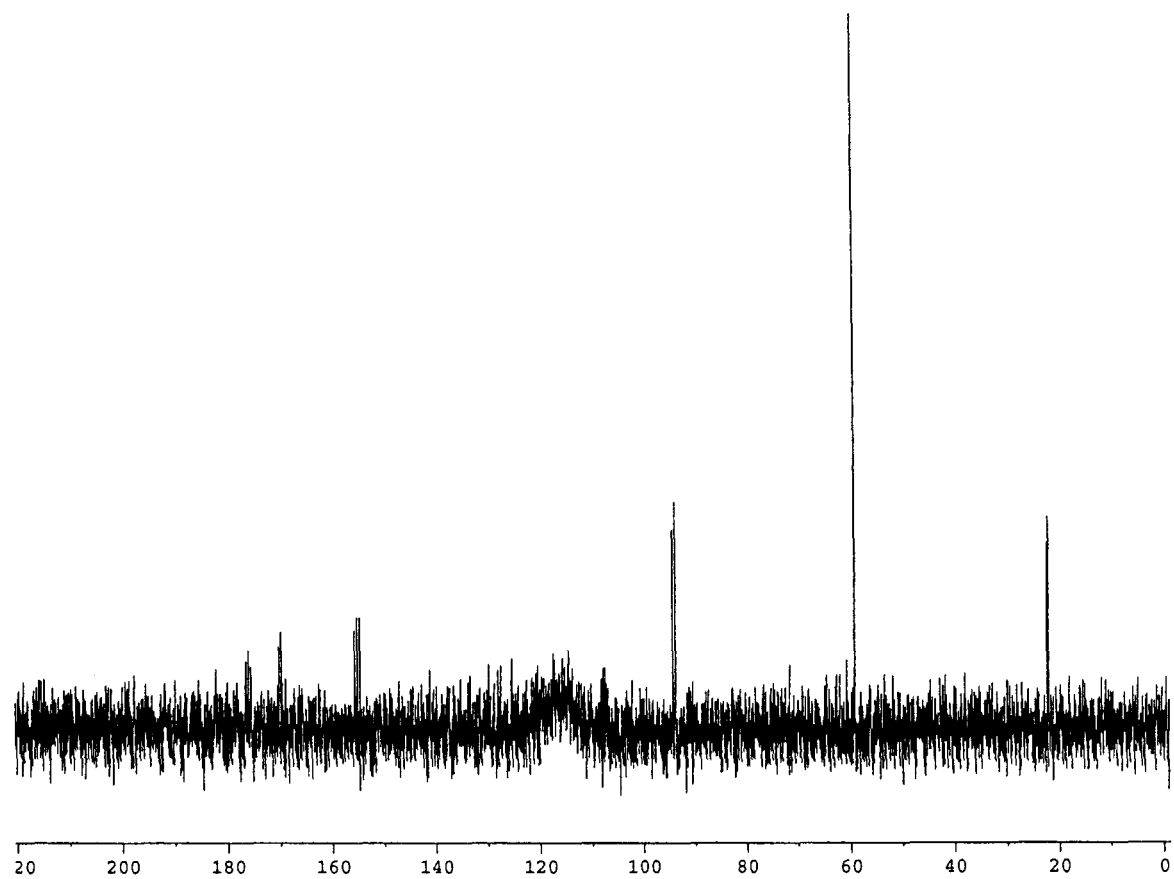
Figure A-9 - ^{13}C-NMR spectrum of ^{13}C$_3$ MurA ketal adjusted for the signal for the probe glue using trapezoidal multiplication to remove signal (112 ppm) due to the probe glue from the FID. Weak signal for the MurA ketal C2 (107.8 ppm, doublet of doublets) can be barely distinguished from background.

13C Ketal in D2O   150ul in Shigemi Tube
bartb 10 A V 600 28 February 2003

108.264
108.156
107.863
107.713
107.418
107.159
106.863

BRUKER

Current Data Parameters
NAME   bartb
EXPNO   10
PROCNO   1

F2 – Acquisition Parameters
Date_   20030228
Time   15.27
INSTRUM   av600
PROBHD 5 mm TBI 1H-13
PULPROG   zgpg30
TD   32768
SOLVENT   D2O
NS   156418
DS   16
SWH   36231.883 Hz
FIDRES   1.105709 Hz
AQ   0.4522622 sec
RG   20642.5
DW   13.800 usec
DE   20.00 usec
TE   300.0 K
D1   0.50000000 sec
d11   0.03000000 sec
d12   0.00002000 sec

========= CHANNEL f1 =========
NUC1   13C
P1   13.80 usec
PL1   -3.00 dB
SFO1   150.9193844 MHz

========= CHANNEL f2 =========
CPDPRG2   waltz16
NUC2   1H
PCPD2   118.00 usec
PL2   120.00 dB
PL12   20.50 dB
PL13   25.50 dB
SFO2   600.1331573 MHz

F2 – Processing parameters
SI   65536
SF   150.9028850 MHz
WDW   EM
SSB   0
LB   4.00 Hz
GB   0
PC   1.00

109.5   109.0   108.5   108.0   107.5   107.0   106.5   106.0   ppm

Figure A-10 – Expansion of region near weak signal from MurA ketal C2 from ^{13}C-NMR spectrum of ^{13}C$_3$ MurA ketal adjusted for the signal for the probe glue using trapezoidal multiplication to remove signal (112 ppm) due to the probe glue from the FID. Weak signal for the MurA ketal C2 (107.8 ppm, doublet of doublets) can be barely distinguished from background.

123
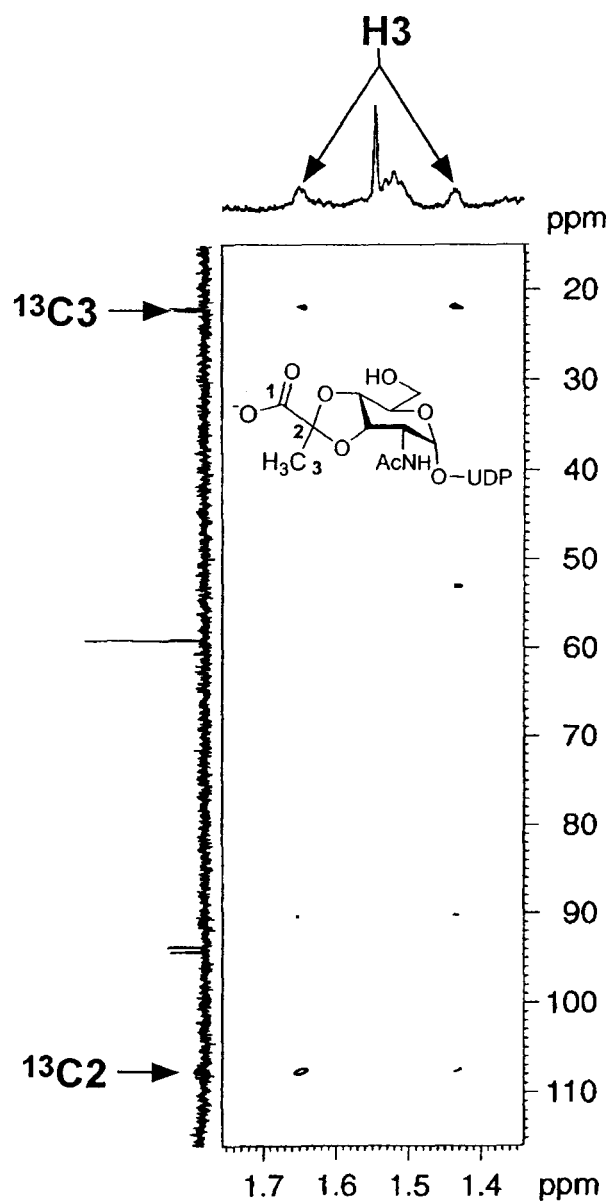
Figure A-11 - HMBC spectrum collected in 128 increments with 256 scans per increment and a delay time of 1 s between scans. The data were linear-predicted in F_1 to 1024 points before Fourier transformation. The spectra were collected without ^{13}C decoupling, so correlations are seen to the ^{13}C satellites of the methyl signal in the ^1H spectrum. The assigned correlation are for H-3 (1.54 ppm, doublet) and both C2 (107.8 ppm) and C3 (22.0 ppm)
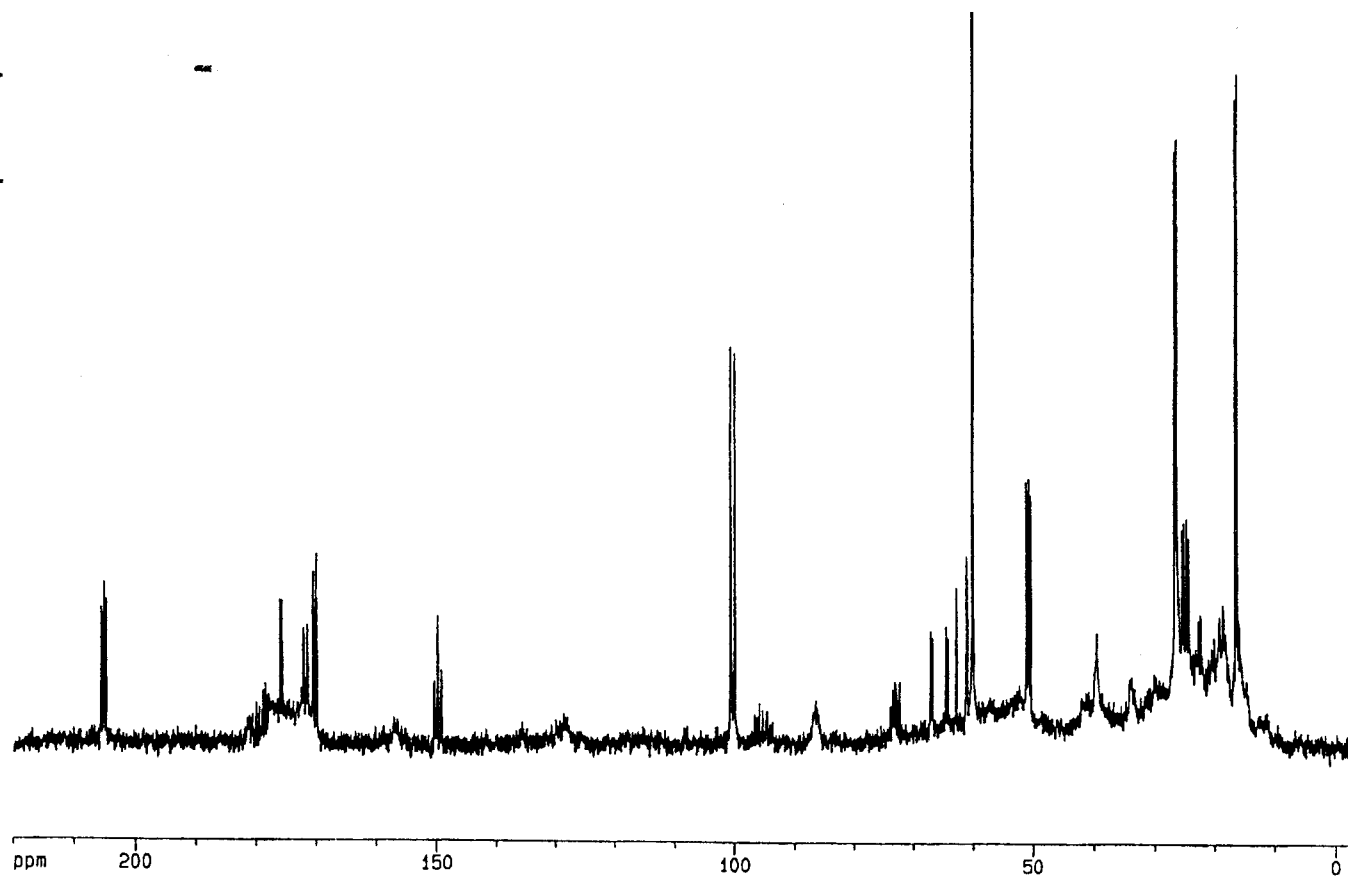
Figure A-12 - ^{13}C-NMR spectrum of MurA reaction at equilibrium after 59519 scans on the 500 MHz spectrometer. The assigned peaks are PEP C1 (171.8 ppm), C2 (149.9 ppm), C3 (100.3 ppm); EP-UDP-GlcNAc C3 (95.0 ppm); THI C1 (179.8 ppm), C2 (96.2 ppm), C3 (24.6 ppm); pyruvate C1 (170.3 ppm), C2 (205.2 ppm), C3 (26.6 ppm); UDP-MurNAc C1 (178.8 ppm), C2 (50.8 ppm), C3 (16.4 ppm).

Appendix B – THI Breakdown Data

Table B-1 – Rates and product distributions of the breakdown of the THI at various pH in H_2O and D_2O.

pH Profile		Data From January 2003		
		Percent Products		
pH	Rate (s^{-1})	UDP-GlcNAc	MurA ketal	EP-UDP-GlcNAc
1	7.08E-01	99.7%	0.3%	N.Q.[§§]
1.5	6.56E-01	99.4%	0.6%	N.Q.
2.02	6.47E-01	99.2%	0.8%	N.Q.
2.5	6.37E-01	98.9%	1.1%	N.Q.
3.03	4.32E-01	98.6%	1.2%	0.2%
3.49	2.85E-01	98.1%	1.6%	0.3%
4.05	1.74E-01	98.2%	1.6%	0.2%
4.41	7.00E-02	98.5%	1.3%	0.2%
5.04	1.83E-02	98.2%	1.6%	0.2%
5.5	7.72E-03	97.8%	1.9%	0.4%
6.02	6.30E-04	94.8%	3.7%	1.5%
6.53	2.83E-04	93.5%	4.5%	2.0%
7.02	1.40E-04	91.9%	5.6%	2.5%
7.52	7.49E-05	91.5%	5.8%	2.6%
8.03	4.34E-05	90.2%	6.7%	3.1%
8.53	1.00E-05	91.5%	5.7%	2.8%
9.03	9.36E-06	90.5%	6.4%	3.1%
9.46	3.78E-06	90.2%	6.5%	3.4%
SDKIE		Data From February 2003		
pL	Rate (s^{-1})	Solvent		
2.05	0.361	D_2O		
2.05	0.450	D_2O		
2.05	0.467	D_2O		
2.02	0.647	H_2O		
2.02	0.504	H_2O		
2.02	0.426	H_2O		
2.02	0.546	H_2O		

_____

[§§]   N.Q. – not quantitable

pH Profile			Data From June 2002	
5	1.84E-02	98.4%	1.5%	N.D.
6.5	4.08E-04	93.9%	3.9%	2.1%
7.5	5.18E-05	94.3%	5.6%	N.D
8.5	4.03E-06	91.8%	4.5%	3.5%
9.5	3.00e-06	90.3%	5.3%	4.3%
10.3	5.56E-07	84.3%	6.0%	9.6%
12	7.80E-08	N.D.	N.D.	N.D

Table B-2 – Fitted values from equation 4 (double ionization) for pH dependences of the rate and product distribution.

Rate vs. pH			
pK_{a2}	3.2 ± 0.1		
$pK_{a4}{}^{b}$	8.9 ± 0.3		
k_{max} (s^{-1})	0.72 ± 0.12		
k_{mid} (s^{-1})	$1.6\ (\pm 0.8) \times 10^{-5}$		
k_{min} (s^{-1})	$7\ (\pm 3) \times 10^{-8a\dagger\dagger\dagger}$		
Product Distribution vs. pH			
	UDP-GlcNAc	MurA ketal	EP-UDP-GlcNAc
pK_{a1}	1.7 ± 0.3	1.5 ± 0.1	N.D.
pK_{a3}	6.2 ± 0.1	6.1 ± 0.1	6.2 ± 0.2
$f(X)_{low}$	$1^{\ddagger\ddagger\ddagger}$	$0^{\ddagger\ddagger\ddagger}$	$0^{\ddagger\ddagger\ddagger}$
$f(X)_{mid}$	0.986 ± 0.001	0.012 ± 0.001	$0^{\ddagger\ddagger\ddagger}$
$f(X.)_{high}$	0.907 ± 0.002	0.062 ± 0.003	0.030 ± 0.006

...   N.D. – not determined

†††   The numerical value of k_{min} was almost completely defined by single k_i at the highest pH measured.

‡‡‡   Value fixed in fitted curves.